RADIATION PATTERN SHAPING OF A TWO-ELEMENT, CONCENTRIC RING TRANSDUCER USING PHASE AND AMPLITUDE SHADING

Albert Hampden Proctor Shaw

NAVAL POSTGRADUATE SCHOOL
Monterey, California

THESIS

RADIATION PATTERN SHAPING OF A TWO-ELEMENT, CONCENTRIC RING TRANSDUCER USING PHASE AND AMPLITUDE SHADING

by

Albert Hampden Proctor Shaw

December 1975

Thesis Advisor: O. B. Wilson

Approved for public release; distribution unlimited.

SECURITY CLASSIFICATION OF THIS PAGE (When Data Entered)

REPORT DOCUMENTATION PAGE		READ INSTRUCTIONS BEFORE COMPLETING FORM
1. REPORT NUMBER	2. GOVT ACCESSION NO.	3. RECIPIENT'S CATALOG NUMBER
4. TITLE (and Subtitle) Radiation Pattern Shaping of a Two-Element, Concentric Ring Transducer Using Phase and Amplitude Shading		5. TYPE OF REPORT & PERIOD COVERED Master's Thesis; December 1975
		6. PERFORMING ORG. REPORT NUMBER
7. AUTHOR(s) Albert Hampden Proctor Shaw		8. CONTRACT OR GRANT NUMBER(s)
9. PERFORMING ORGANIZATION NAME AND ADDRESS Naval Postgraduate School Monterey, California 93940		10. PROGRAM ELEMENT, PROJECT, TASK AREA & WORK UNIT NUMBERS
11. CONTROLLING OFFICE NAME AND ADDRESS Naval Postgraduate School Monterey, California 93940		12. REPORT DATE December 1975
		13. NUMBER OF PAGES 98
14. MONITORING AGENCY NAME & ADDRESS(if different from Controlling Office) Naval Postgraduate School Monterey, California 93940		15. SECURITY CLASS. (of this report) Unclassified
		15a. DECLASSIFICATION/DOWNGRADING SCHEDULE

16. DISTRIBUTION STATEMENT (of this Report)

Approved for public release; distribution unlimited.

17. DISTRIBUTION STATEMENT (of the abstract entered in Block 20, if different from Report)

18. SUPPLEMENTARY NOTES

19. KEY WORDS (Continue on reverse side if necessary and identify by block number)

Radiation Pattern Shaping
Phase and Amplitude Shading
Concentric Ring Transducer

20. ABSTRACT (Continue on reverse side if necessary and identify by block number)

A high-frequency transducer which gives usefully uniform radiation into a half space is required for use as a target locator in an underwater acoustic range. Phase and amplitude shading of a two-element transducer consisting of a central circular piston and a concentric annular ring has been proposed to meet the requirement. A transducer resonant at 74 kHz but scaled in terms of wave length to 25 kHz in the transverse

dimension has been constructed and tested at both frequencies. Exceptionally wide radiation patterns with major lobe widths of the order of 150 degrees (10dB down) were obtained. At the scaled frequency computer model predictions based on simple theory agreed well with the measured radiation patterns. At the resonant frequency, however, predicted secondary lobe details were not found in the patterns. These discrepancies have been attributed to the non-uniform motion of the radiating surfaces due to mutual coupling effects through the transducer structure and the transmission medium. In spite of these minor problems associated with the prototype transducer, promising results have been obtained and have shown the design concept to be a valid and viable one.

Radiation Pattern Shaping of a Two-Element, Concentric Ring Transducer Using Phase and Amplitude Shading

by

Albert Hampden Proctor Shaw
Lieutenant Commander, Canadian Forces
B.Sc.E.E., University of Manitoba, 1964
B.Sc.E.A., Naval Postgraduate School, 1975

Submitted in partial fulfillment of the
requirements for the degree of

MASTER OF SCIENCE IN ENGINEERING ACOUSTICS

from the

NAVAL POSTGRADUATE SCHOOL
December 1975

ABSTRACT

A high-frequency transducer which gives usefully uniform radiation into a half space is required for use as a target locator in an underwater acoustic range. Phase and amplitude shading of a two-element transducer consisting of a central circular piston and a concentric annular ring has been proposed to meet the requirement. A transducer resonant at 74 kHz but scaled in terms of wave length to 25 kHz in the transverse dimension has been constructed and tested at both frequencies. Exceptionally wide radiation patterns with major lobe widths of the order of 150 degrees (10dB down) were obtained. At the scaled frequency computer model predictions based on simple theory agreed well with the measured radiation patterns. At the resonant frequency, however, predicted secondary lobe details were not found in the patterns. These discrepancies have been attributed to the non-uniform motion of the radiating surfaces due to mutual coupling effects through the transducer structure and the transmission medium. In spite of these minor problems associated with the prototype transducer, promising results have been obtained and have shown the design concept to be a valid and viable one.

TABLE OF CONTENTS

LIST OF TABLES

LIST OF ILLUSTRATIONS

LIST OF ILLUSTRATIONS (continued)

LIST OF ILLUSTRATIONS (continued)

ACKNOWLEDGEMENT

The author is indebted to his wife, Gloria Jean, for her unfailing support and tolerance shown during the period of this study and for her assistance in typing the draft manuscript. Appreciation is also expressed to Lieutenant Winfield Scott Slocum, IV, and to Mr. Robert Moeller for their assistance in constructing the transducer. The technical and financial support provided by the Naval Torpedo Station Keyport, Washington, is gratefully acknowledged.

I. INTRODUCTION

Target-mounted sound sources are commonly used in conjunction with fixed ocean bottom hydrophone arrays to obtain target position on underwater ranges. The use of an essentially non-directional source on the target is desirable in order to insonify a large volume of water. This ensures that in the case of a long base line, range-range system sufficient numbers of hydrophones are insonified and in the case of a short base line, range-bearing system, at least one array will receive an adequate sound level from any point in the range.

Consideration of the geometry involved in tracking an underwater vehicle with ocean floor mounted hydrophones reveals that the slant range from the vehicle to the receivers may be an order of magnitude greater than the distance from the vehicle to the ocean bottom. This would suggest that more acoustic energy from a source mounted on the underbody of a target should be directed obliquely with a relative minimum transmitted vertically downward. For example, given a target 200 meters above the bottom in an acoustic range where the distance between hydrophone arrays is 2000 meters, the maximum slant range, r, from the vehicle to the array would be 1020 meters. Assuming a sound frequency of 75 kHz, for which the absorption coefficient in sea water, a, is about 0.03 dB per meter, the transmission loss, TL, to the array may be calculated [Ref. 1].

$$TL = 20 \log r + ar$$

The transmission loss at the maximum range would be 91 dB and at the minimum range of 200 m approximately 52 dB. In order that roughly equivalent energy be received by the array under these extremes of position, the directional properties of the target-mounted sound source must be such to compensate for this 40 dB difference in transmission loss. This requirement, modified by consideration of the pitch and roll motions of the vehicle and the undesirable effects of surface reflections, has led to the practical specification that the source radiate uniformly within a conical volume approximately 150° wide centered on the axis of the transducer oriented vertically downward. A typical pattern specification is shown in Fig. 1.

In the past the requirement for such a broad radiation pattern has been met quite satisfactorily by a pop-out transducer utilizing a spherical piezoelectric ceramic element. The beam pattern shown in Fig. 2 was obtained from such a source. At low speeds, the hydrodynamics of the test vehicles is not greatly affected by the protruding pop-out transducer. However, the performance of high-speed vehicles is seriously affected and a requirement exists for a flush-mounted, broad-beam, high-frequency source transducer.

Some appreciation of the magnitude of the problem may be gained by considering the specification in Fig. 1. If one attempts to use a circular piston to meet this requirement, one finds that the required directivity, D, is approximately 4. Directivity may be related to frequency and piston radius [Ref. 1].

$$D = \frac{(ka)^2}{1-J_1(2ka)/ka} \qquad 1.1$$

At 75 kHz, this results in a piston diameter of approximately 1.28 centimeters. Note also that the sound pressure level required at one meter is 93 dB re 1 microbar. This corresponds to a sound pressure, p, of approximately 4.5×10^4 microbars on the axis at one meter. This pressure along the axis and a directivity ratio of 4 requires an acoustical power of 35 watts and, assuming uniform radiation over the surface of the piston, a required intensity, I, at the piston surface of approximately 2.75×10^5 watts/m^2. Relating this intensity to pressure at the piston face [Ref. 1],

$$P_{rms} = \sqrt{\rho_o c I} \qquad 1.2$$

where $\rho_o c$ is the specific acoustic impedance, leads to a requirement for an rms pressure in excess of six atmospheres. At such high intensities and pressure levels, cavitation and

Other undesirable physical phenomena would occur. Thus a solution to the problem utilizing a small single-piston transducer appears to have some important limitations and, therefore, an alternative approach should be sought.

The intent of this study has been to develop a flush mount transducer concept capable of generating broad beam patterns at high frequencies, to build and test the proposed transducer, and to determine whether a conventional computer model may be used to predict the directional properties of the transducer.

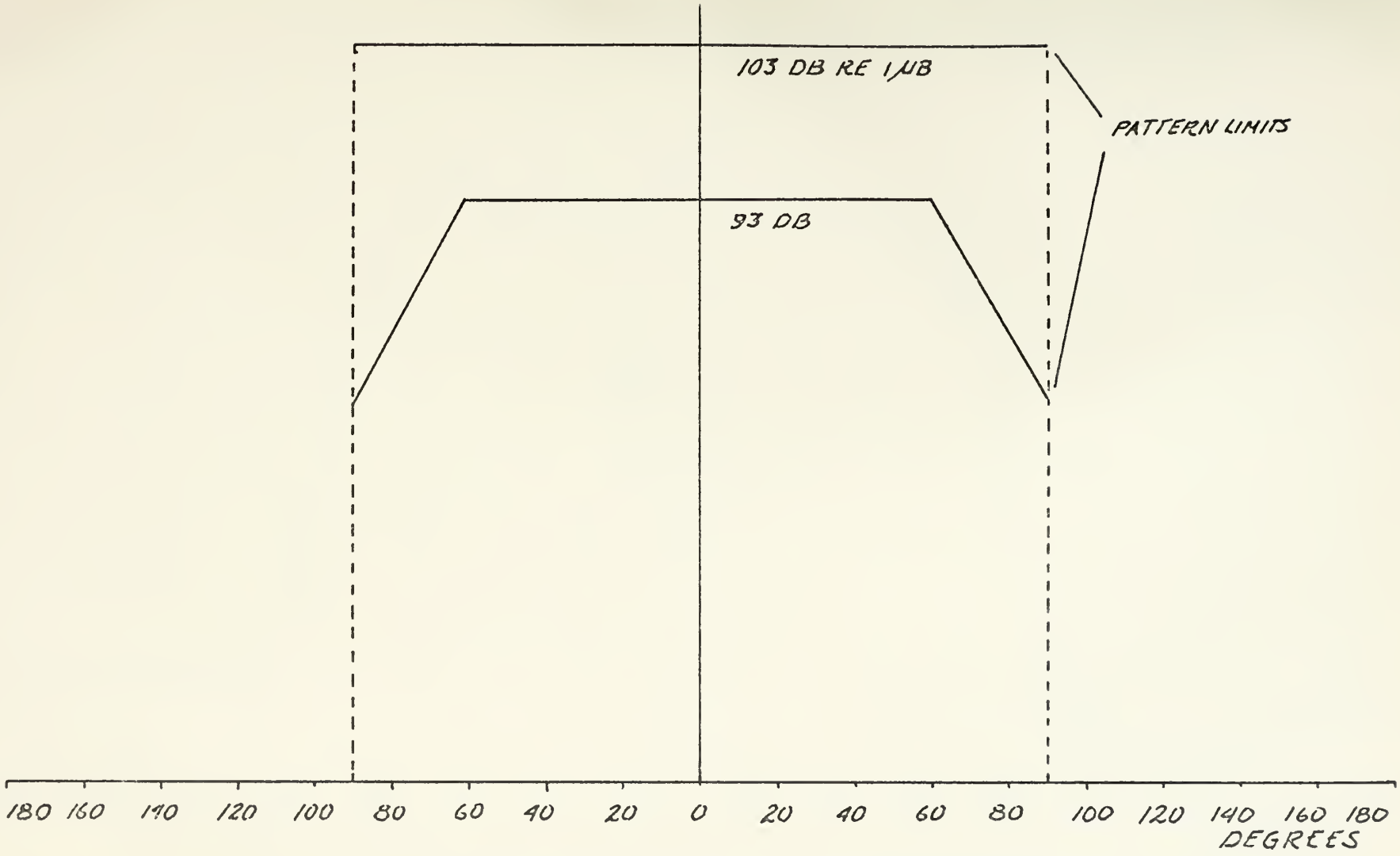

FIG 1 RADIATION PATTERN SPECIFICATION

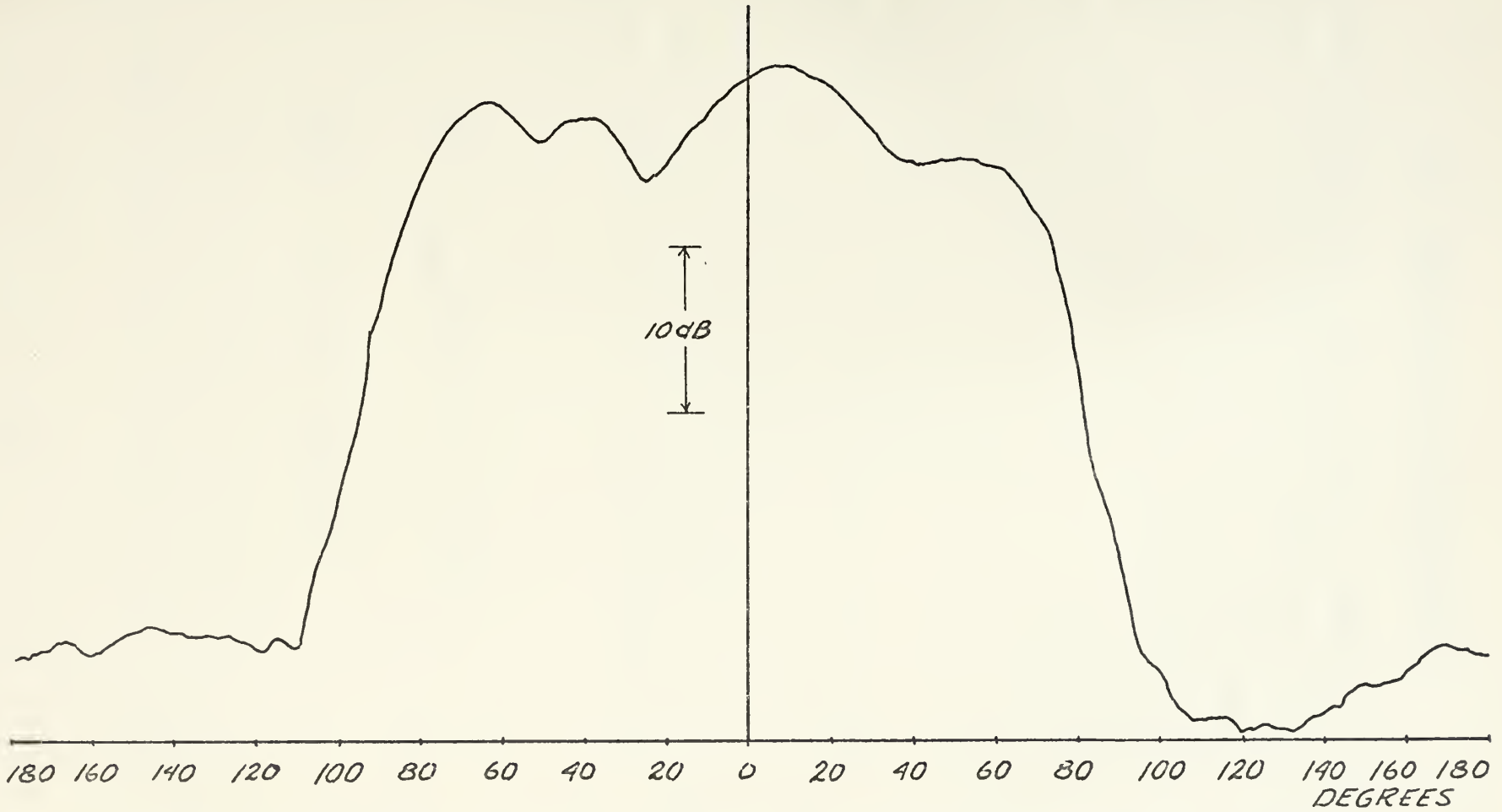

FIG 2 BEAM PATTERN OF PRESENTLY USED TRANSDUCER - 75KHZ

II. THEORETICAL CONSIDERATIONS

Fourier diffraction theory [Ref. 2] suggests a means of achieving a desirable beam pattern while still maintaining a flush profile for the transducer face. This theory relates a spatial distribution function of pressure amplitude to a spatial frequency function which in turn is related to a radiation pattern function. Thus from a known aperture excitation the radiation pattern may be determined uniquely. Similarly, given a desirable radiation pattern a corresponding aperture function may be found.

Consider an ideal, one-dimensional piston driven uniformly. The aperture excitation of this piston may be represented by the spatial function A(x) shown in Fig. 3a. This spatial amplitude function and the resultant spatial frequency function B(s) are a Fourier transform pair defined by:

$$B(s) = \int_{\text{Aperture}} A(x) \exp(-j\pi sx)dx \qquad 2.1$$

and

$$A(x) = \int B(s) \exp(j2\pi xs)ds \qquad 2.2$$

Further, as spatial frequency, s, is defined in terms of angular position from the x = 0 axis, θ, and wavelength, λ, by

$$s = \frac{\theta}{\lambda} \qquad 2.3$$

there exists a one-to-one relationship between B(s) and the radiation pattern B(θ). From Equation 2.1,

$$B(\theta) = \int_{\text{Aperture}} A(x) \exp\left(-j2\pi\frac{\theta}{\lambda}x\right)dx \qquad 2.4$$

As an example, for the piston excitation function in Fig. 3a, the resultant radiation pattern function, B(θ) is of the form:

$$\frac{\text{Sin } \frac{\pi\Delta\theta}{\lambda}}{\frac{\pi\Delta\theta}{\lambda}}$$

as shown in Fig. 3b.

If one considers two aperture excitation functions superimposed on each other, linearity of superposition permits expression of the resultant beam pattern as the sum of the individual beam patterns. For example, let the aperture function of a two-element transducer be that represented by Fig. 4a. This function may be decomposed into the sum of the two spatial functions shown in Fig. 4b. The beam patterns of these two functions are obtained by Fourier transformation and are shown in Fig. 4c. The resultant beam pattern, which is the sum of these two, is shown in Fig. 4d and is seen tc be, in one dimension, exactly the sort of pattern required. Pressure on the axis may be controlled by amplitude shading and the shape

of the main side lobes controlled by the dimensions of the two radiating elements.

The extension to a two-dimensional aperture may be made by means of the two dimensional Fourier transformation,

$$B(\theta,\phi) = \iint_{\text{Aperture}} A(x)\, A(y)\, e^{-j2\pi\frac{\phi}{\lambda}y}\, dxdy \qquad 2.5$$

For the case of a circular piston of radius a, moving uniformly with a velocity $Uoe^{j\omega t}$, in an infinite baffle, evaluation of this integral leads to the familiar far-field pressure amplitude [Ref. 1]:

$$p = \frac{\rho_o c U_o k a^2}{2r} \left| \frac{2J_1(k a \sin\theta}{k a \sin\theta} \right| \qquad 2.6$$

where θ = angle from the normal to the piston,

k = propagation constant

$\rho_o c$ = acoustic impedance

r = range

Normalizing this expression to the axis pressure and relating to a reference pressure of unity results in the usual beam pattern relation:

$$SPL(\theta) = 20 \log \left[\frac{2J_1(k a \sin\theta)}{k a \sin\theta}\right] \qquad 2.7$$

Now, considering a transducer in which an inner circular piston of radius a_i, is driven with uniform motion, U_i, and an outer annulus of radii a_o and a_{oi} (where $a_o > a_{oi}$) is driven with uniform motion U_o, the normalized beam pattern function may be found by superposition to be:

$$SPL(\theta) = 20 \log \left[a_o^2 U_o \frac{2J_1(ka_o \sin\theta)}{ka_o \sin\theta} - a_{oi}^2 U_o \frac{2J_1(ka_{oi} \sin\theta)}{ka_{oi} \sin\theta} \right.$$

$$\left. \pm a_i^2 U_i \frac{2J_1(ka_i \sin\theta)}{ka_i \sin\theta} \right] \qquad 2.8$$

where the plus sign is used for relative motion in phase and the minus sign for relative motion 180 degrees out of phase.

Appendix A contains a computer program utilizing Equation 2.8 which may be used to predict the normalized sound pressure levels as a function of angle for a two-element transducer, of the type previously described, operating in a plane infinite baffle. In this project, this program has been used to develop a transducer configuration to meet the requirements of the underwater range sound source. Johnson [Ref. 3] developed what would appear to be a more realistic model for predicting the radiation pattern of a transducer of similar geometry operating in a finite cylindrical baffle. While his program was developed specifically for this problem, it has the disadvantage of

requiring significantly more computer time and for this reason has not been used as a design tool.

Having obtained a viable theoretical basis on which to proceed, the thrust of this project has been an attempt to validate the concept of transducer radiation pattern shaping using phase and amplitude shading. A transducer using two coaxially mounted circular radiators, one a circular piston and the other a concentric annulus, has been built and beam patterns obtained for several amplitude shading ratios. Phase shading has been limited to driving the radiators electrically in phase and 180 degrees out of phase. The second objective has been to determine the accuracy with which the simplified program model predicts the beam patterns obtained. Remembering the model assumptions of uniform motion and plane infinite baffling, discrepancies between the model predictions and those measured were to be expected. Motion of the radiating faces would be expected to be affected by mutual coupling both through the medium and the transducer structure. These problems have been studied and are reported on in the following chapters.

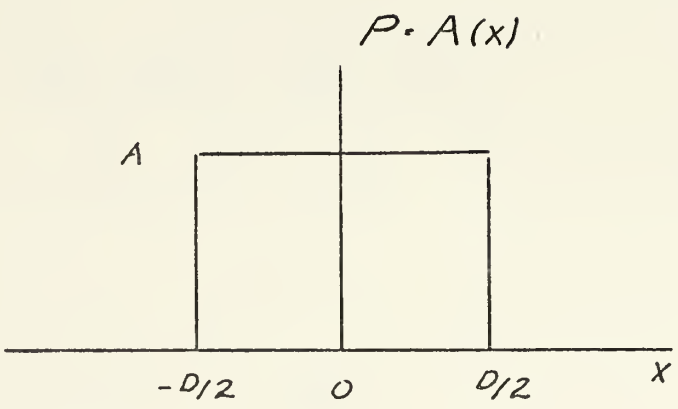

FIG 3a. APERTURE FUNCTION

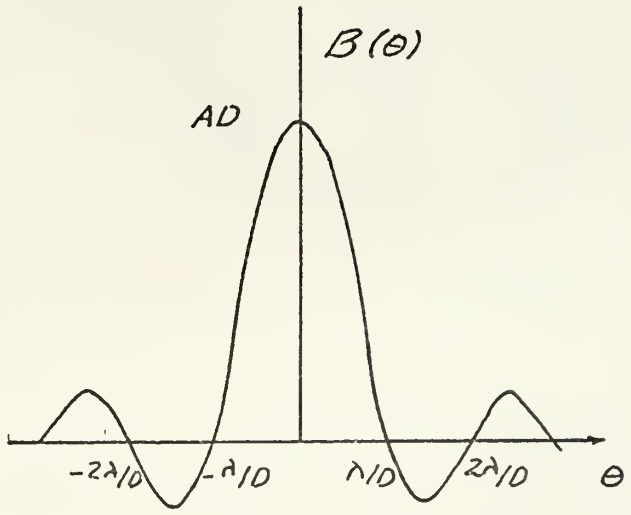

FIG 3b. BEAM PATTERN FUNCTION

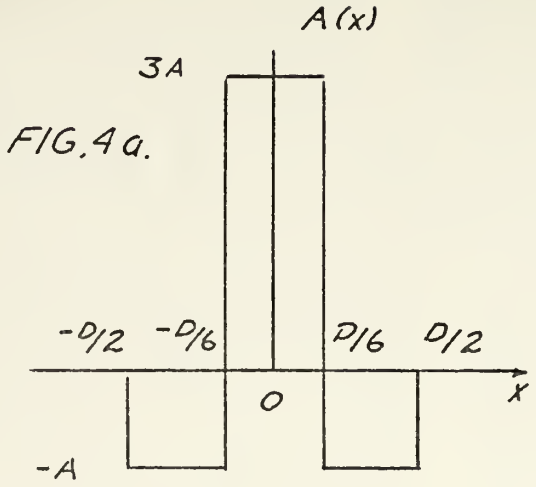

FIG. 4a.

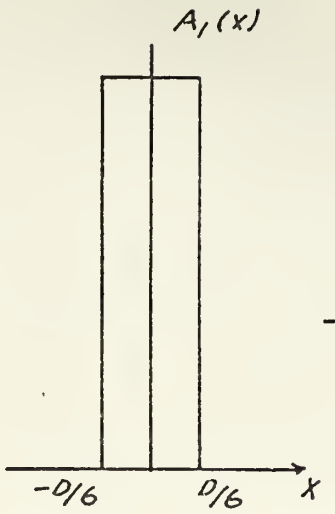

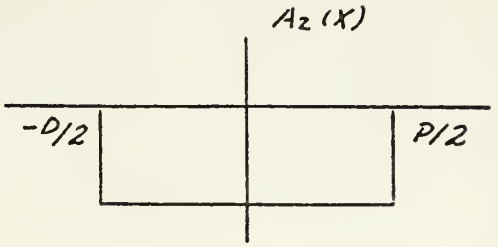

FIG. 4b.

FIG. 4d

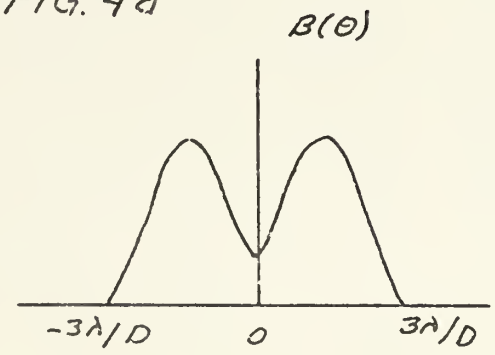

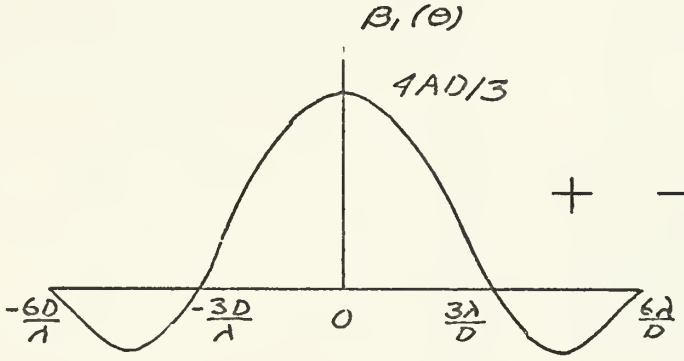

FIG. 4c.

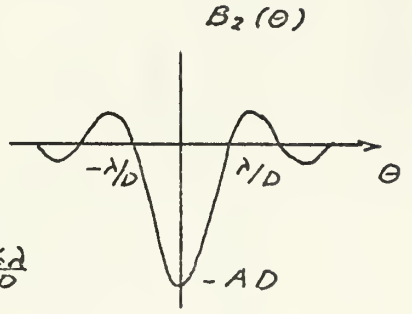

FIG. 4. BEAM PATTERN SUPERPOSITION

III. EXPERIMENTAL PROCEDURES

A. TRANSDUCER DESIGN AND CONSTRUCTION

The objective of this experiment was the construction of a transducer which could be used to verify both the concept of, and the program model for, radiation pattern shaping by phase and amplitude shading. The transducer configuration chosen was that of the model described in the previous chapter.

Initially it was hoped to build a transducer resonant at 75 kHz with a transverse dimension of the order of one and a half wave lengths. This dimension was selected as a reasonable compromise to minimize flexural motions and still meet the high acoustical power requirements. However, material availability precluded this approach and it was decided to construct a transducer scaled dimensionally in the transverse direction to 25 kHz (λ = 6 cm). Scaling was justified in that the "ka" term in Equation 2.8 was kept constant.

A number of one quarter inch long, one inch diameter piezoelectric ceramic disks was available. These were found to have a first longitudinal half wave resonance at approximately 312 kHz. Since this frequency was much higher than desired it was decided to operate in a quarter wave length resonant mode. Even with mass loading it did not appear to be feasible to design for a resonant

frequency of 25 kHz so a compromise was reached which designed for a longitudinal resonant frequency of approximately 70 to 80 kHz.

The geometry selected for the radiating faces was also a compromise. It was decided that the inner piston should be driven by a single ceramic disk and the outer annulus by six disks. While a minimum radiating area was desirable, the physical requirement for clamping bolts to hold the joints with the piezoelectric ceramics in compression and the one inch diameter of the disks necessitated relatively large radiating faces. There was also a requirement that the mass loading of each ceramic element be approximately the same so that common resonant frequencies would result. The end product was the configuration shown in Fig. 5.

The transducer elements were constructed as shown in Fig. 6. Each ceramic disk was sandwiched between engraved printed circuit board material which allowed for a good electrical contact and a good mechanical coupling through the non-conductive fiberglass. The metal radiating faces were then applied and the whole secured in compression to the aluminum cannister shaped housing shown in Fig. 7. Counter-sunk screwheads in the radiating faces were filled with silver epoxy to give a plane conducting surface. Three cable ways were drilled through the housing to allow cable connections to be made in the water-tight area between the housing and the aluminum backing plate, Fig. 8. Ceramic elements driving the outer annulus were connected in

parallel. The ceramic disk driving the inner piston was connected independently allowing for separate control of each radiating face. Shielded two-connector cables for each radiating face were passed through separate water-proof cable glands. A valve was fitted to the backing plate to allow for oil filling and air evacuation.

On completion of assembly the radiating faces were covered with a 1/32 inch neoprene sheet shown in Fig. 9a and attached with the securing ring in Fig. 7. The transducer was checked for water-tight integrity and then charged with oil. Air evacuation was accomplished under a vacuum. The assembled transducer is shown in Fig. 9b.

B. ELECTRICAL ADMITTANCE MEASUREMENTS

On completion of the transducer building phase, electrical admittance measurements were taken at the terminals of the inner and outer transducer elements to determine their behavior when driven electrically in and out of phase. Data were obtained in water and in air to determine the effects of radiation loading.

To obtain the admittance curves in a convenient manner the following items of test equipment were used:

Hewlett Packard 3590A Wave Analyzer

Hewlett Packard 3594 Sweeping Local Oscillator

Hewlett Packard 467A Power Amplifier

Hewlett Packard 400E Voltmeter

FIG 5 RADIATING FACES

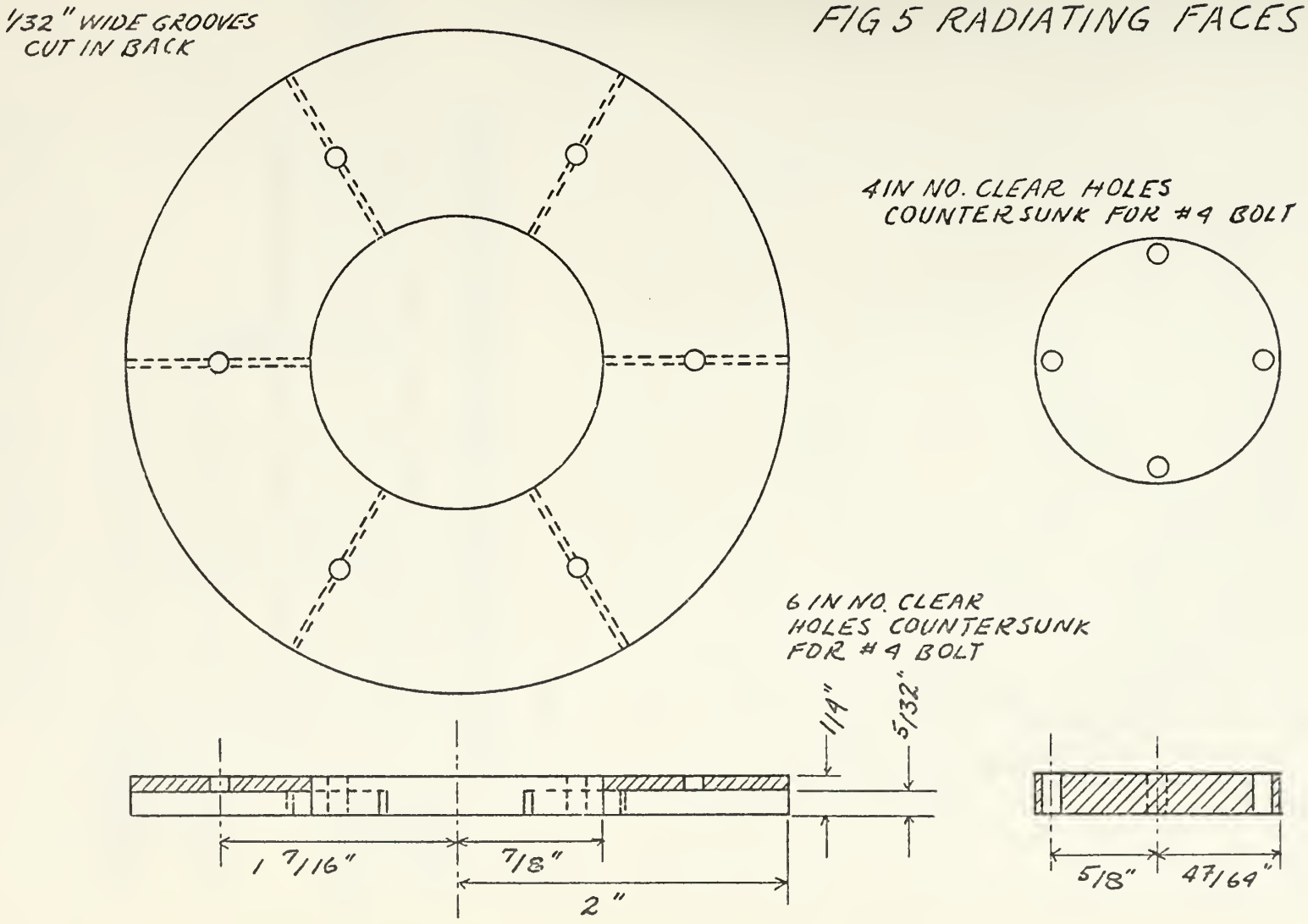

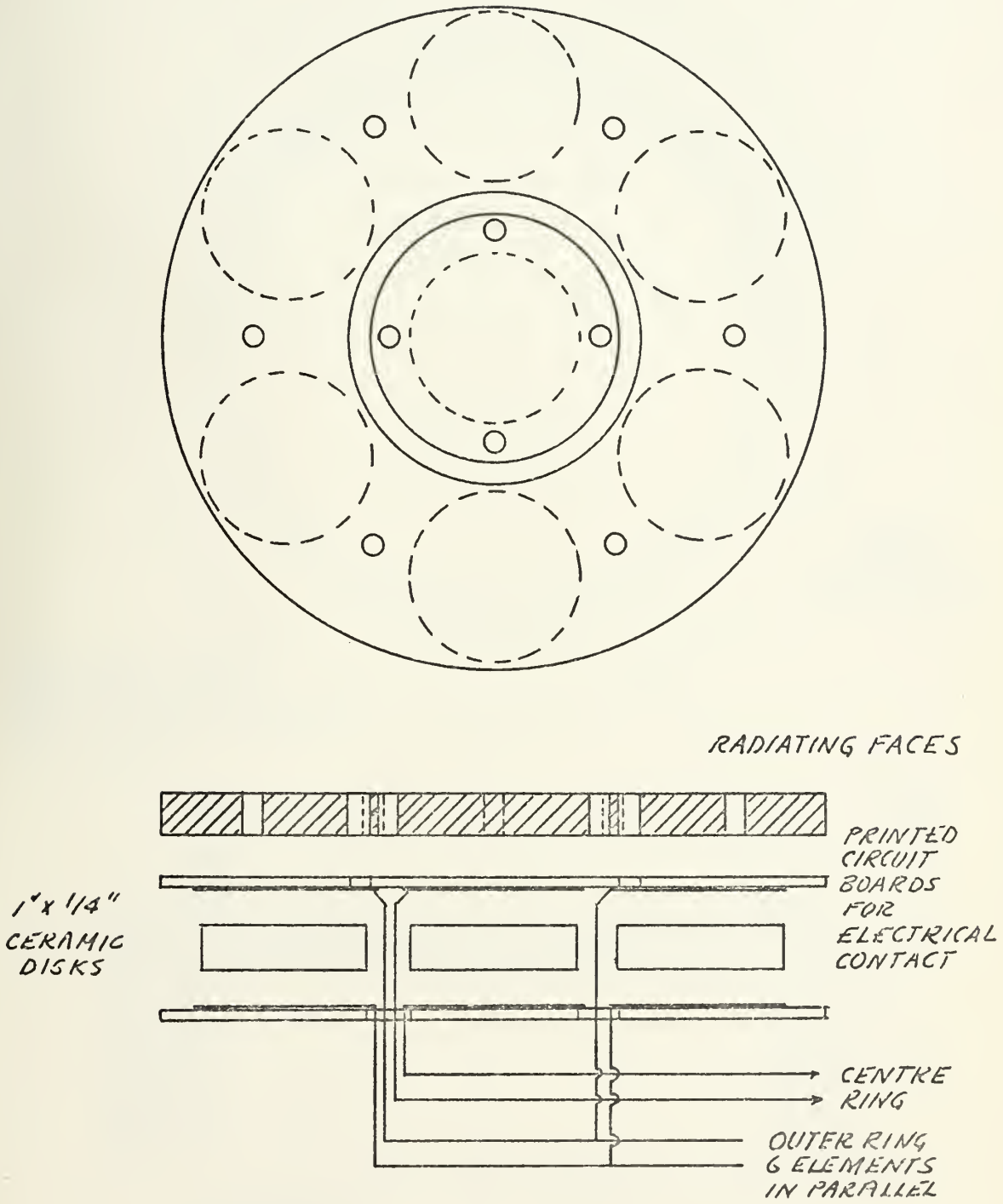

FIG 6 TRANSDUCER ELEMENTS EXPANDED VIEW

FIG 7 TRANSDUCER HOUSING

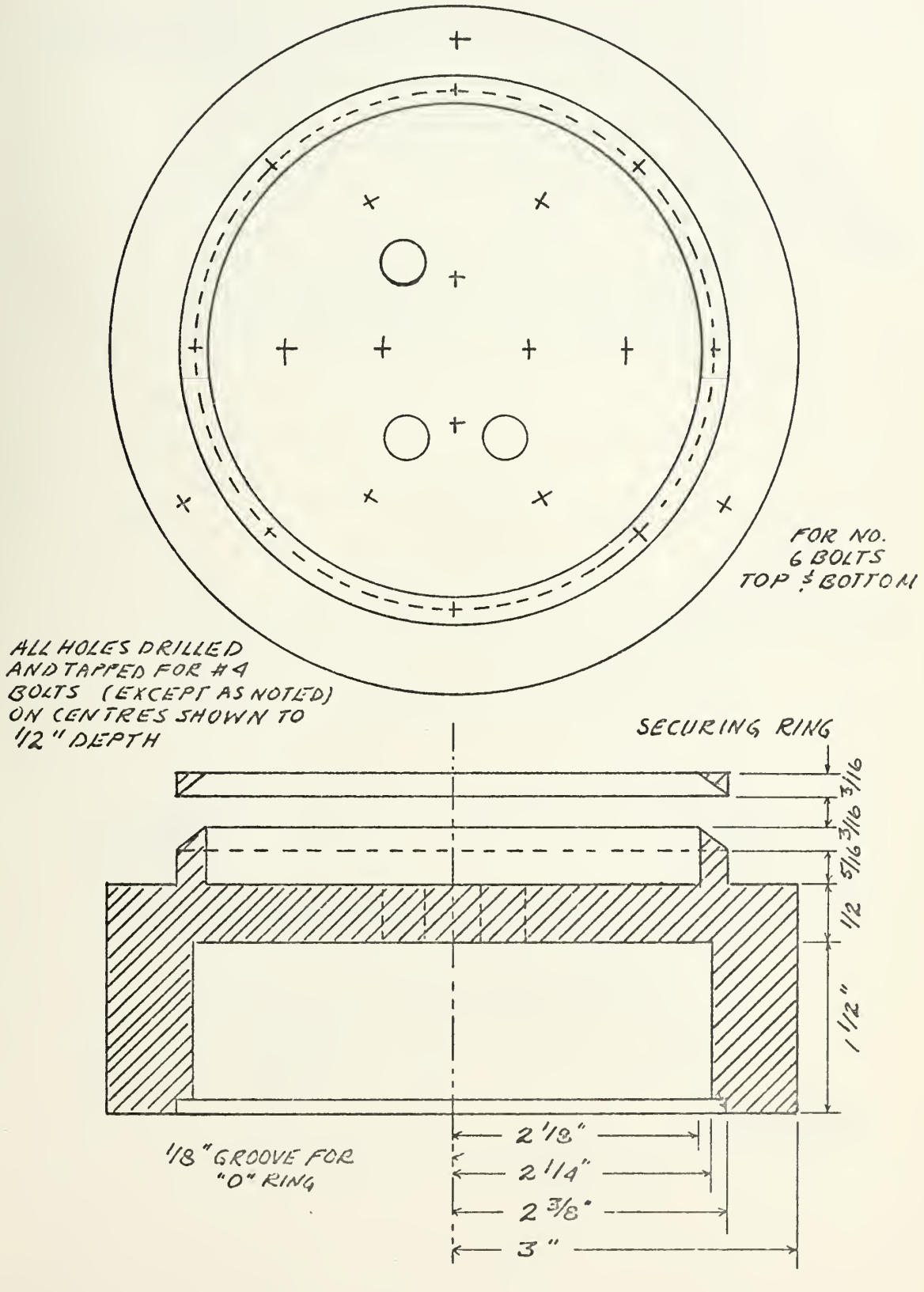

FIG 8 BACKING PLATE

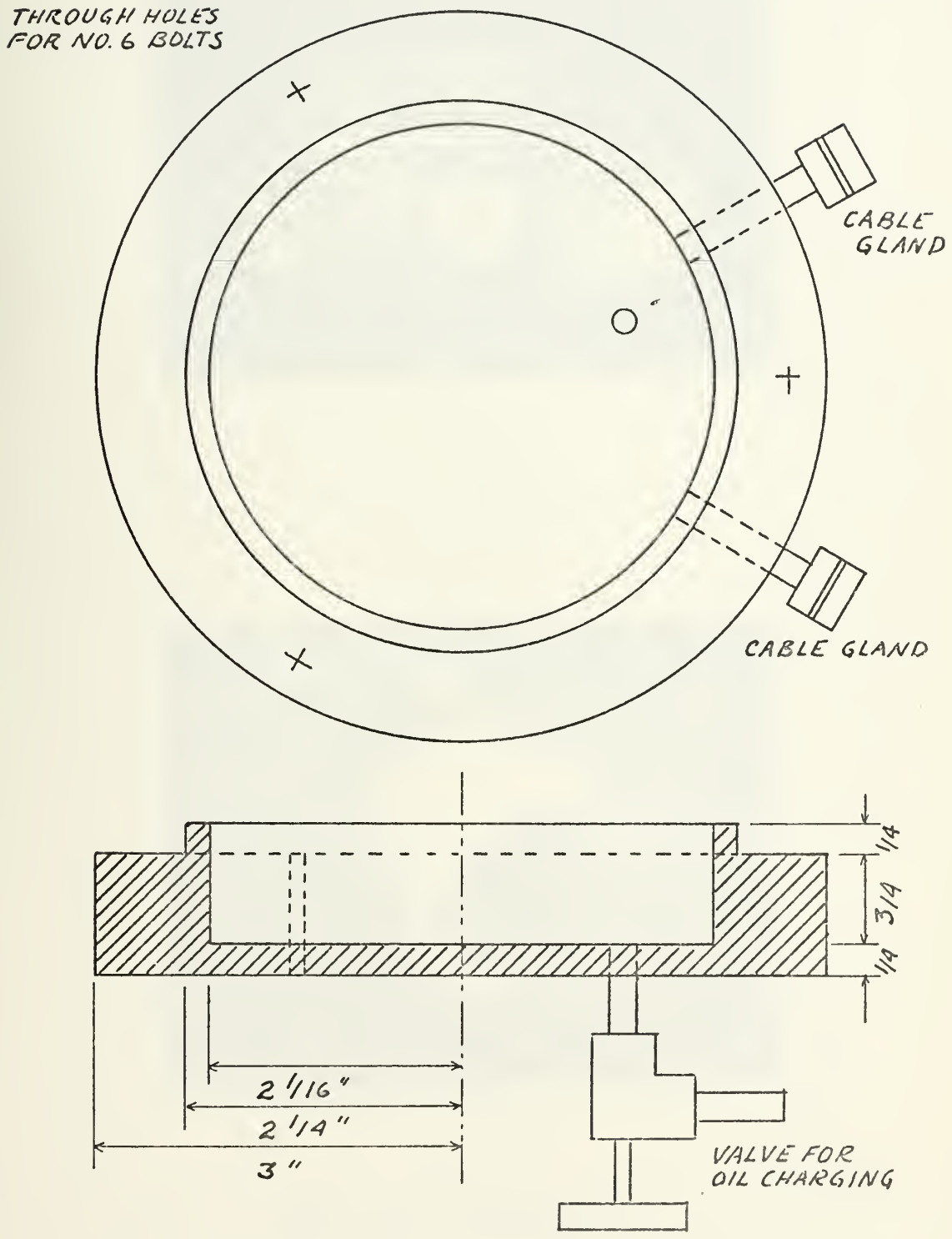

FIG. 9a. TRANSDUCER

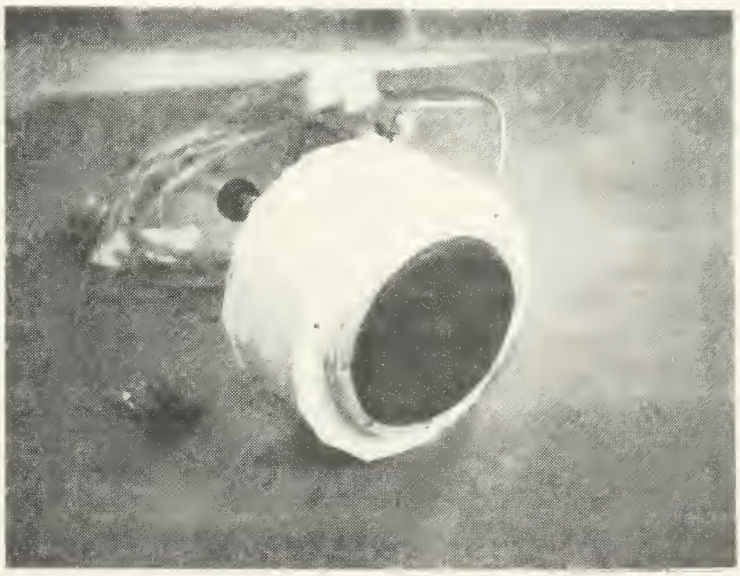

FIG. 9b. TRANSDUCER

Dranetz Type 100C Impedance/Admittance Meter

Varian F100 Recorder

The equipment was set up as shown in Fig. 10.

Admittance data as a function of frequency were obtained under differing phase and loading conditions. The results are shown in Figs. 11 through 19. The primary resonances obtained are summarized in Table I.

TABLE I

RESONANT FREQUENCIES

Phase Shading (Degrees)	Outer Ring (kHz)	Inner Ring (kHz)
180	56.2	56.3
180	63.4	62.3
180	69.3	68.2
180	74.2	74.0
180	77.0	78.6
180	99.6	99.5
0	56.1	55.2
0	63.5	65.3
0	69.5	69.4
0	74.3	74.0
0	76.9	76.6
0	99.7	104.5

The number of resonances obtained for each experimental situation was indicative of the mechanical complexity of the system. Subsequent measurements of displacement determined that only the resonances at 56, 63 and 74 kHz were strong longitudinal resonances; the remainder are assumed to have been radial modes.

Radiation loading was found to have no effect on the resonant frequency values although admittance values for the longitudinal resonances were changed. This was as expected due to the damping effect of the transmission medium. Phase reversal of the inner ring had little effect on the outer ring but the converse was not true. At 74 kHz a negative resistance was measured at the inner ring when the outer ring was driven 180° out of phase whereas a large positive resistance had been noted with zero phase shading. This led to the conclusion that the dynamic properties of the outer annulus were largely responsible for those of the transducer as a whole.

On the basis of these data, it was decided to use 74 kHz as the resonant frequency for subsequent measurements. While 25 kHz was to be used as the modeled frequency, the admittance measurements show it to be a good value for studying the off-resonance properties of the transducer as well.

FIG 10 ADMITTANCE MEASUREMENTS

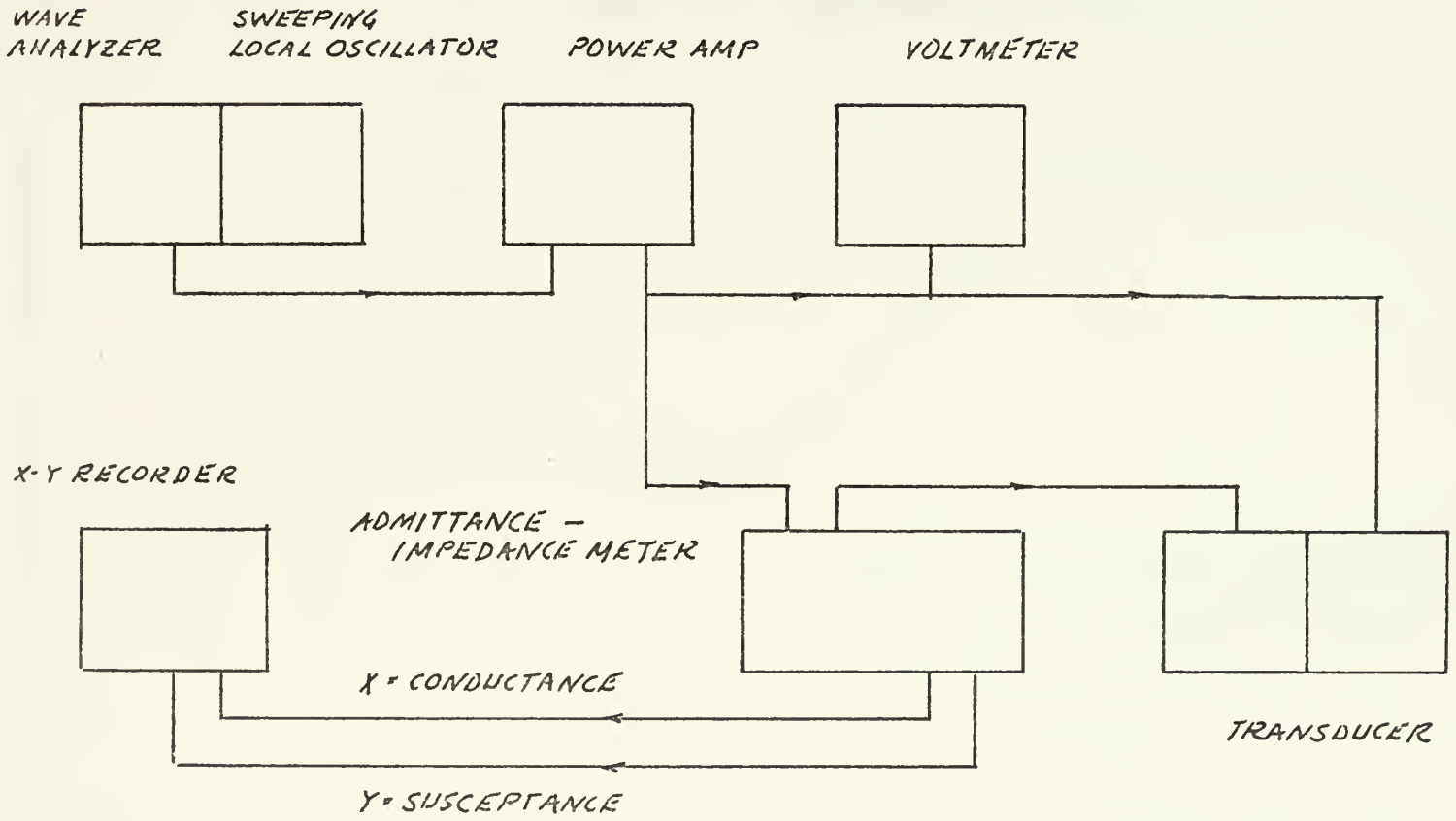

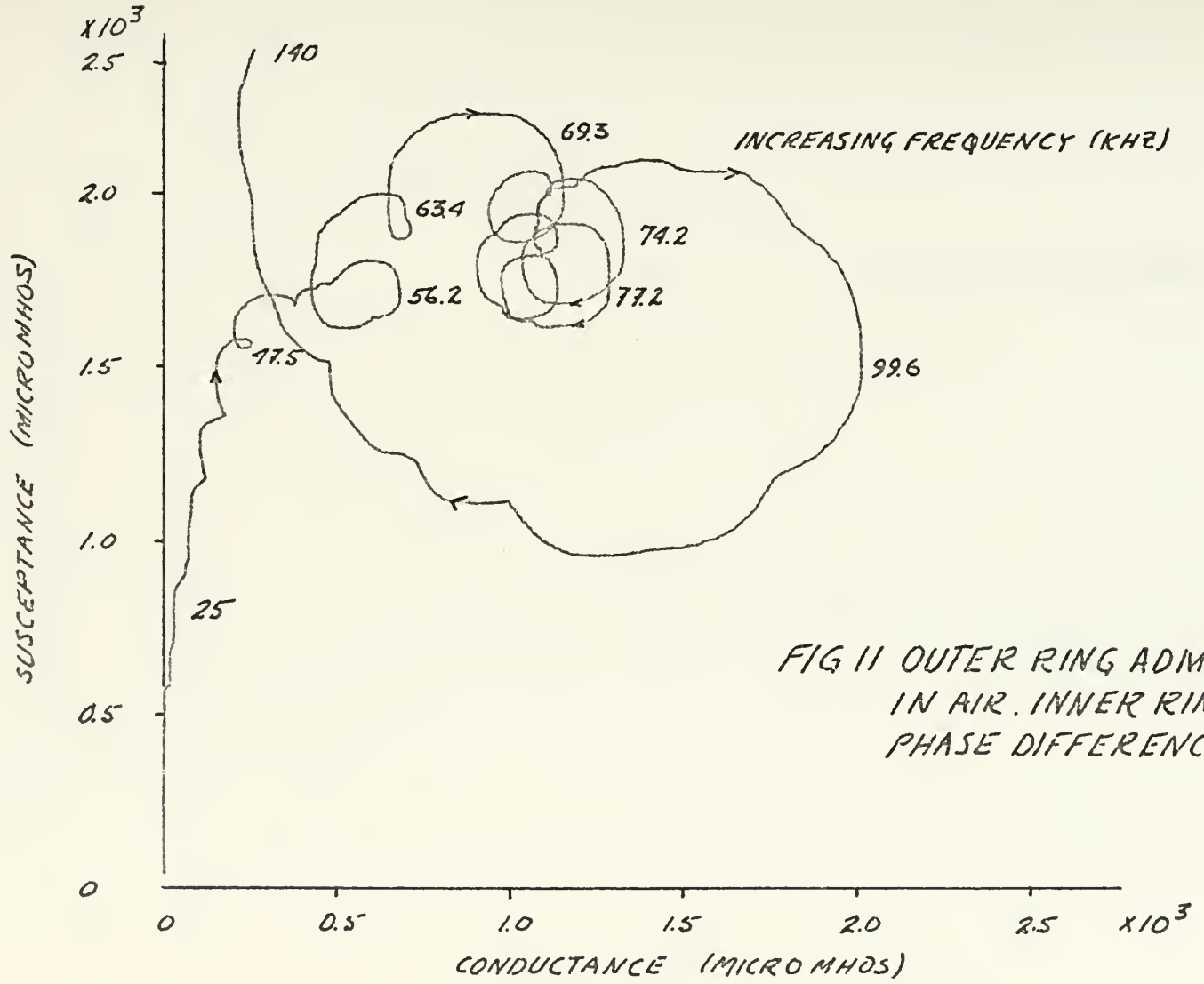

FIG 11 OUTER RING ADMITTANCE IN AIR. INNER RING 180° PHASE DIFFERENCE

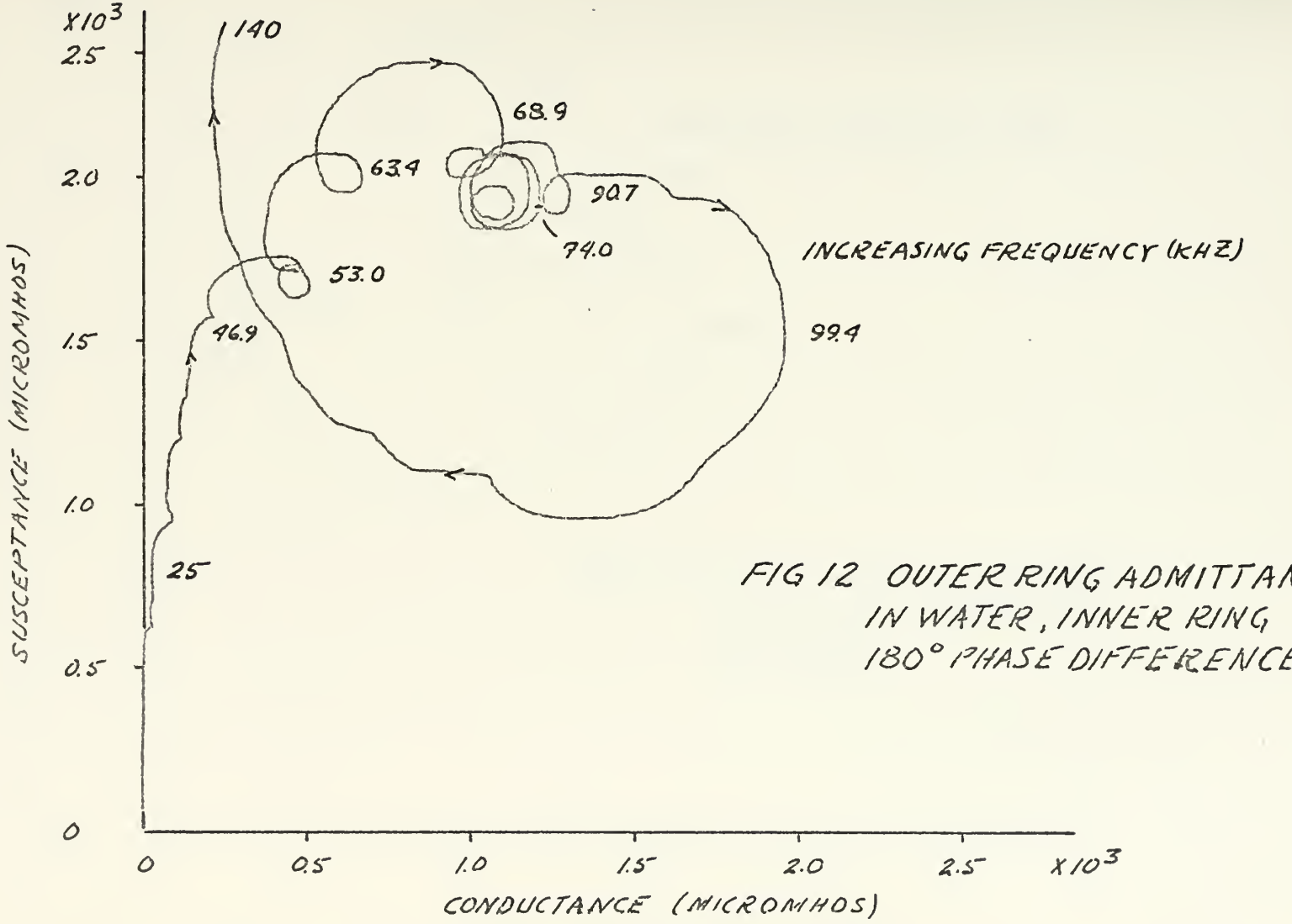

FIG 12 OUTER RING ADMITTANCE
IN WATER, INNER RING
180° PHASE DIFFERENCE

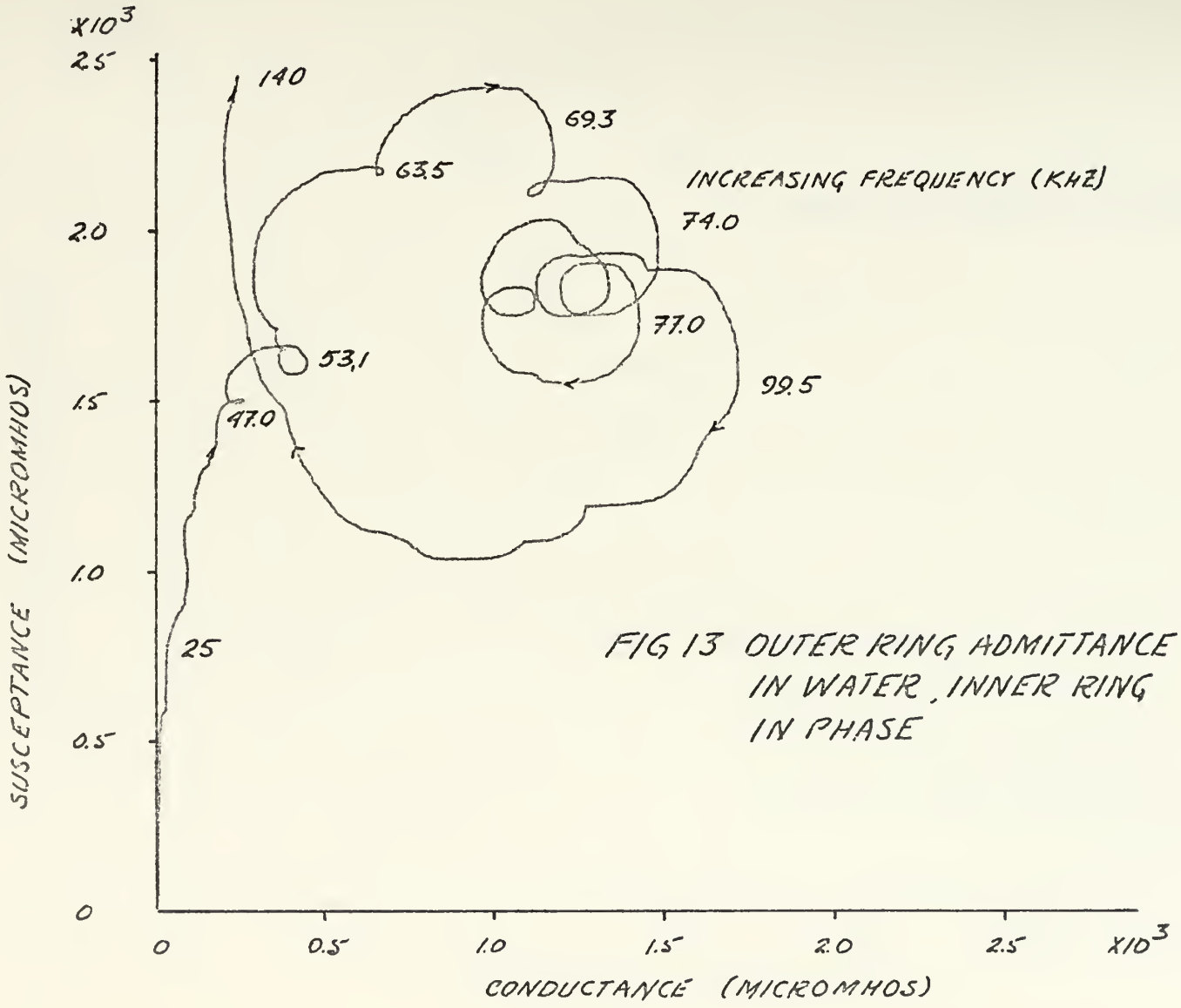

FIG 13 OUTER RING ADMITTANCE IN WATER, INNER RING IN PHASE

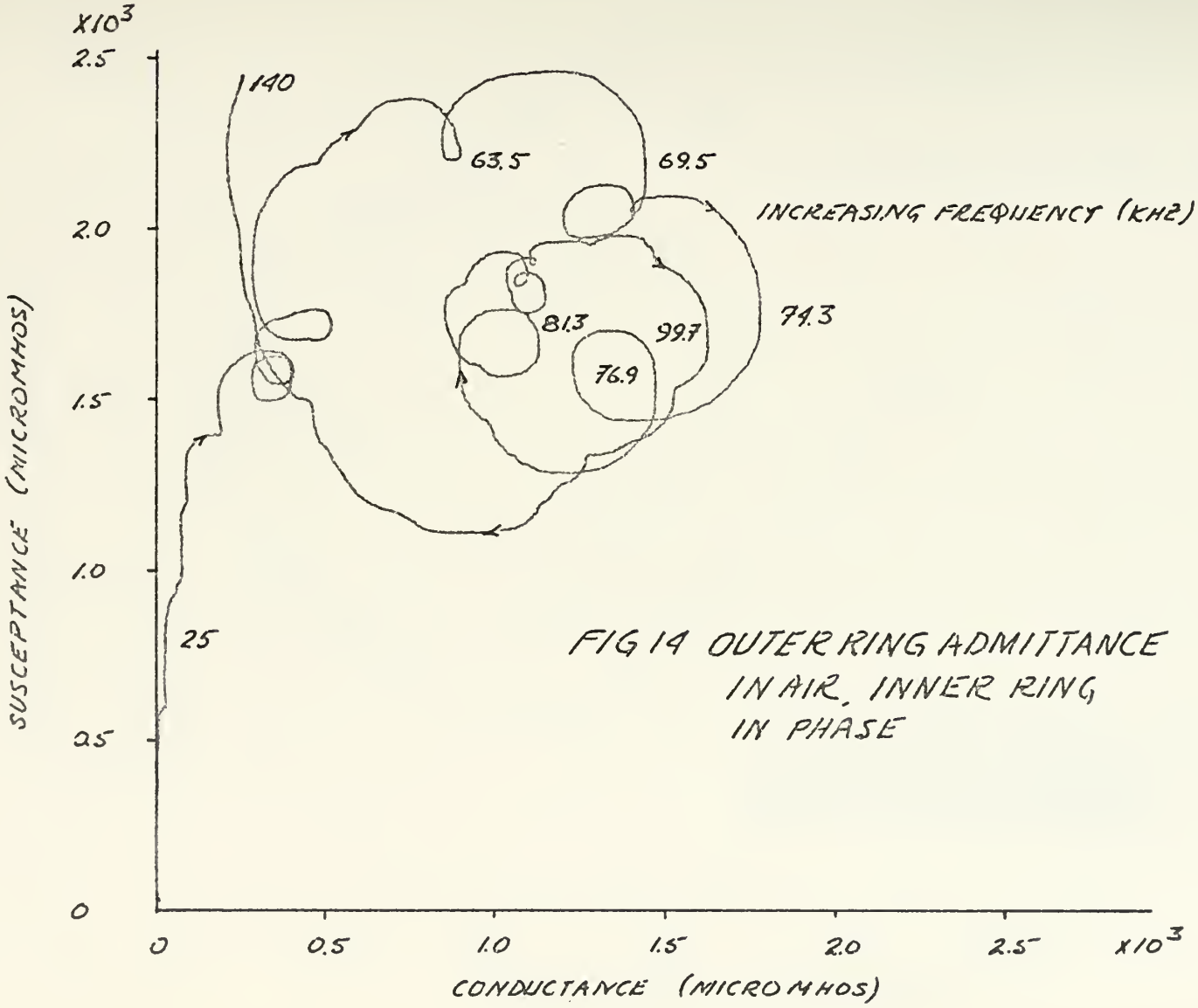

FIG 14 OUTER RING ADMITTANCE
IN AIR, INNER RING
IN PHASE

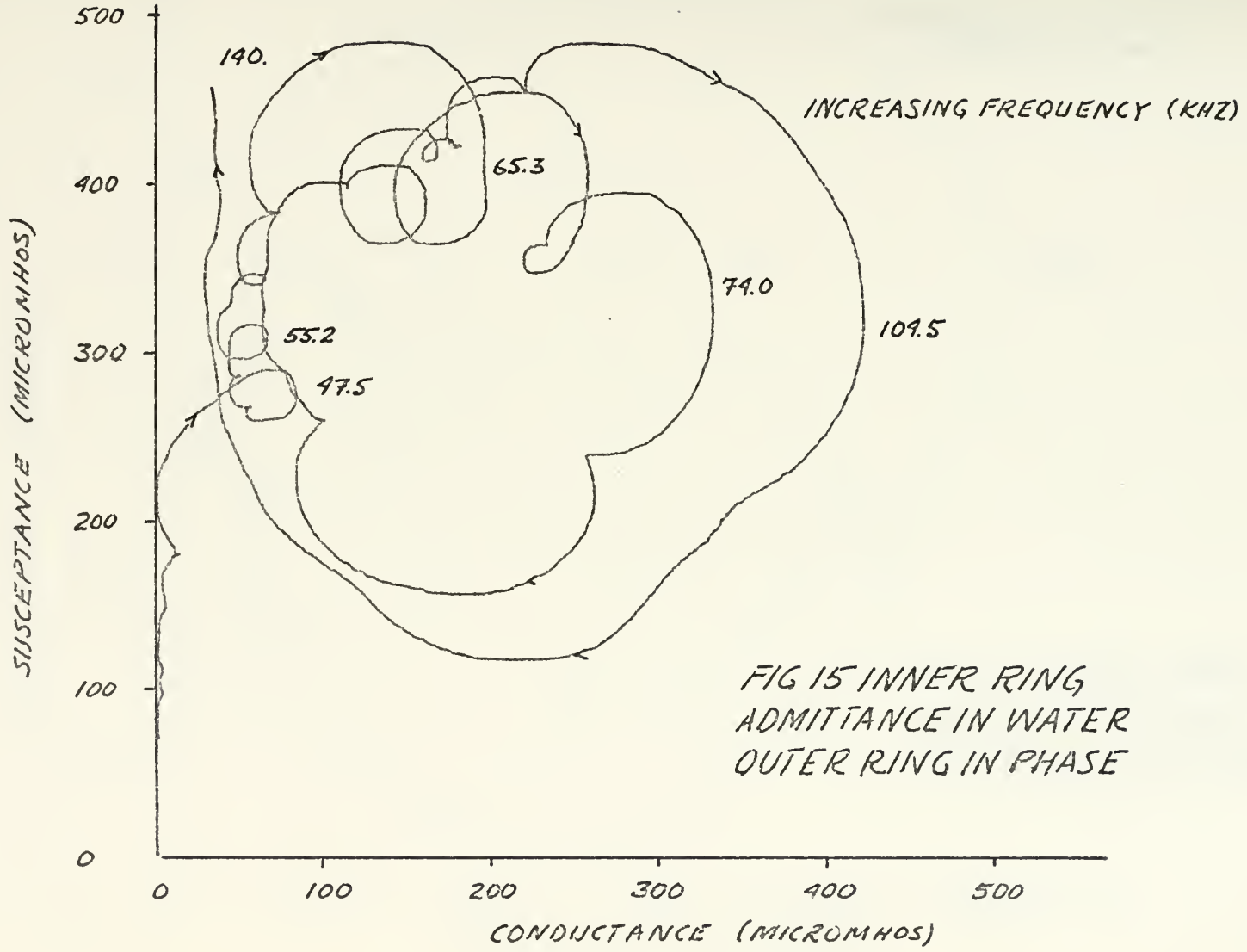

FIG 15 INNER RING
ADMITTANCE IN WATER
OUTER RING IN PHASE

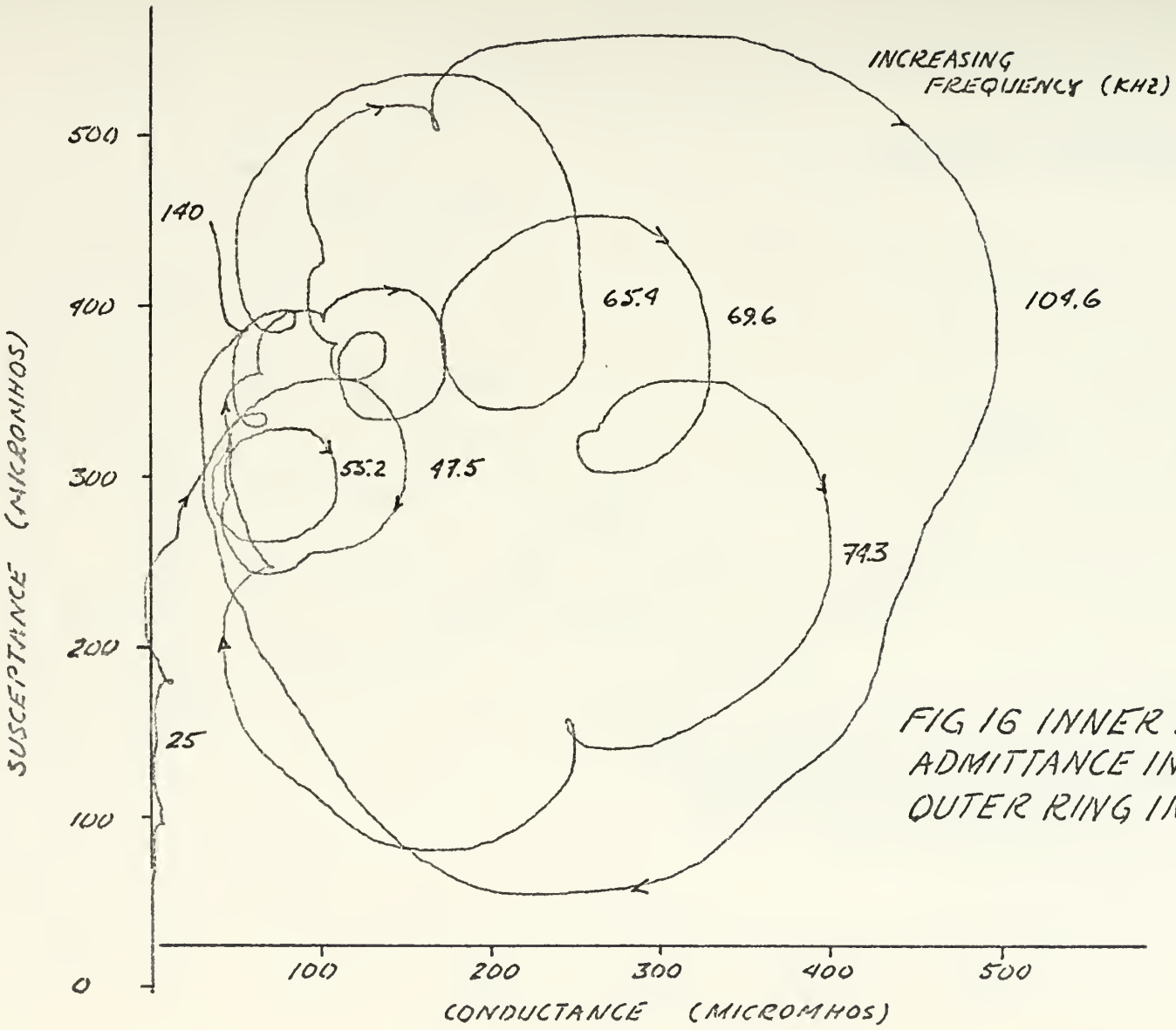

FIG 16 INNER RING ADMITTANCE IN AIR OUTER RING IN PHASE

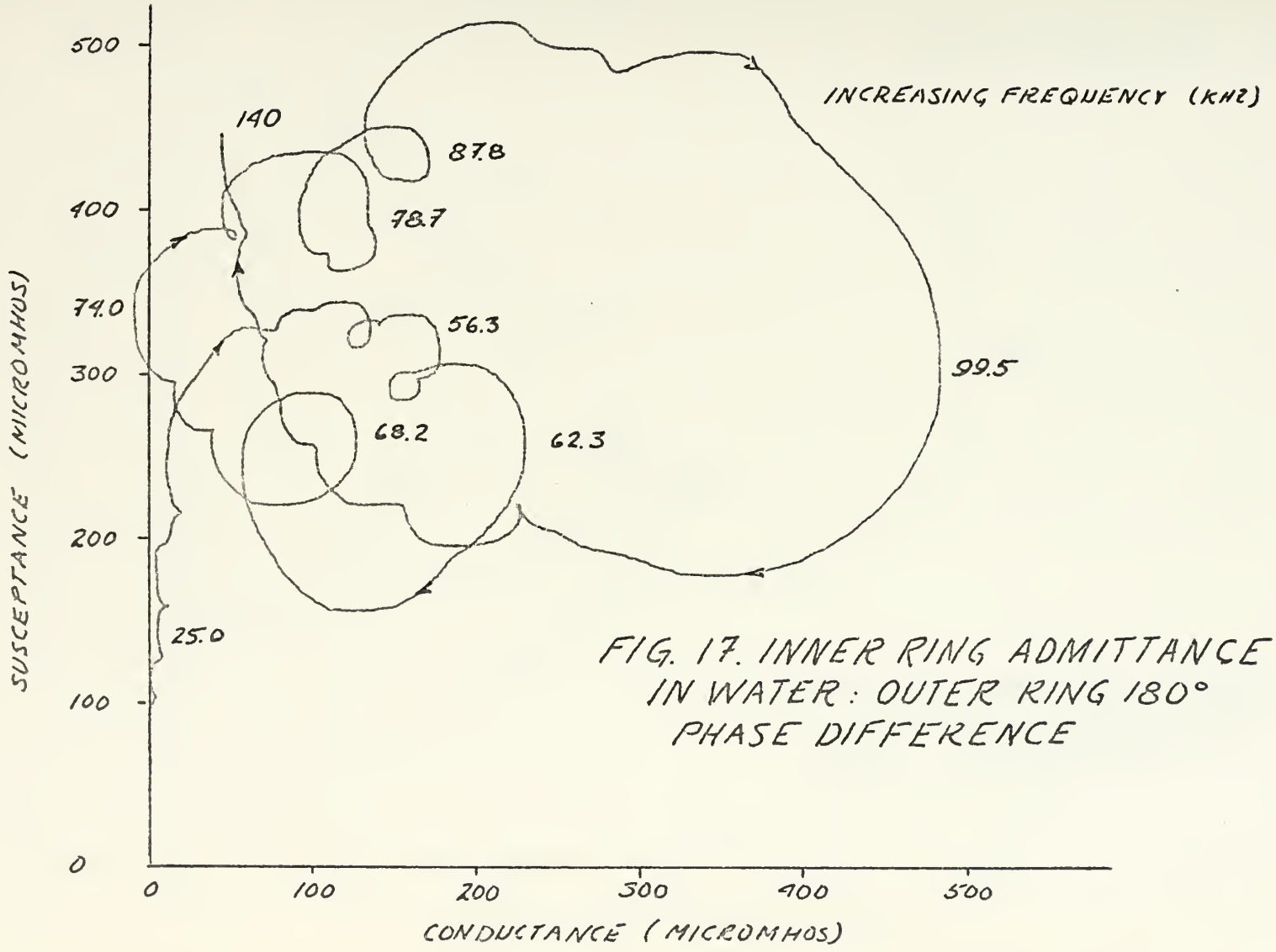

FIG. 17. INNER RING ADMITTANCE IN WATER: OUTER RING 180° PHASE DIFFERENCE

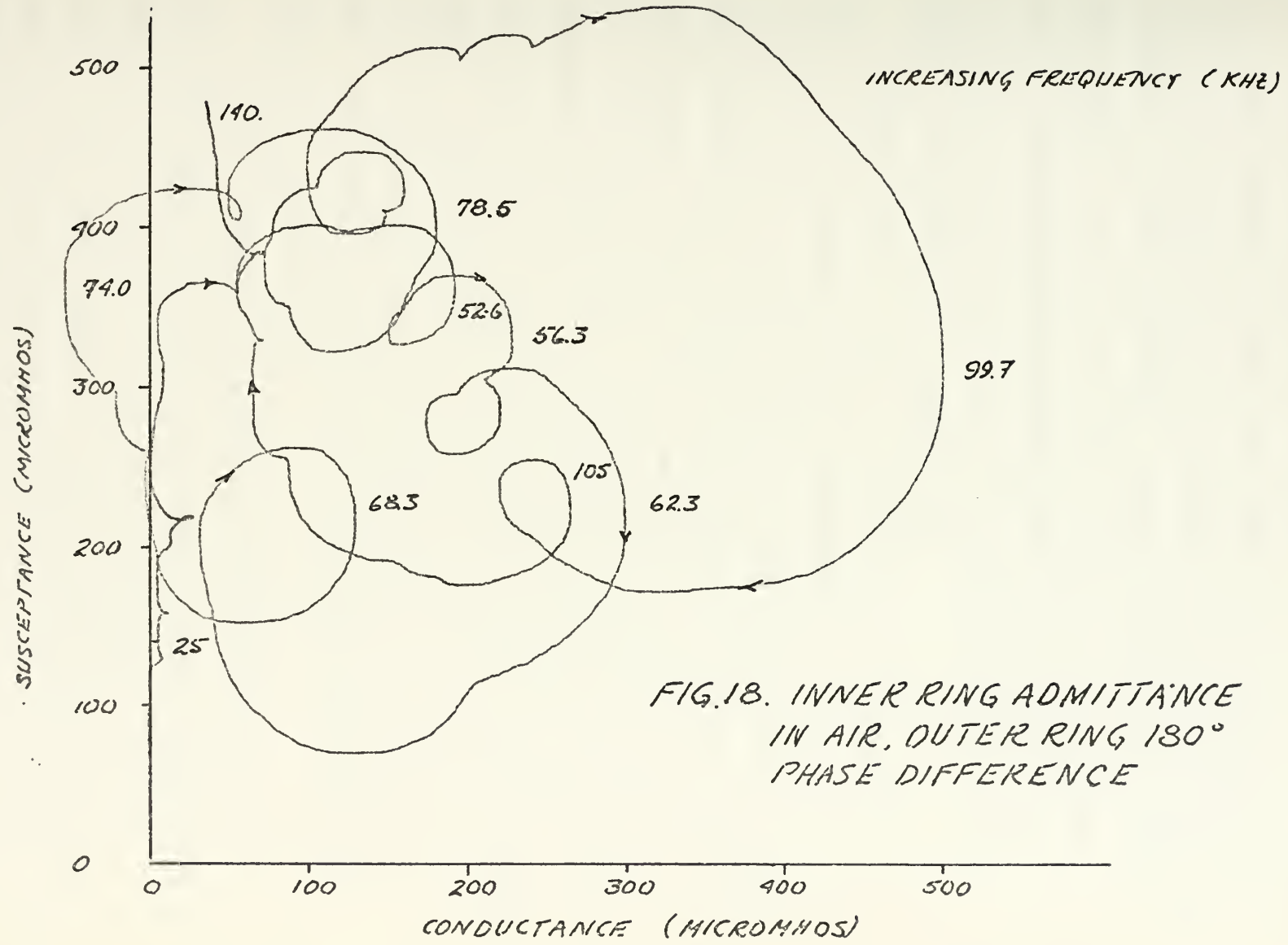

FIG. 18. INNER RING ADMITTANCE IN AIR, OUTER RING 180° PHASE DIFFERENCE

C. RADIATION PATTERN MEASUREMENTS

The objective of this experiment was to measure the radiation patterns of the transducer at the frequencies of interest, 74 kHz and 25 kHz. Phase and amplitude shading were applied and the resultant changes in the patterns noted. The measured patterns were compared with those predicted by the simple theory in order to validate the model's usefulness as a design tool.

Several special items of apparatus were required to facilitate radiation pattern measurements. A 13-inch diameter plane circular baffle of half-inch aluminum plate was manufactured initially but during testing was found to be radiating strongly due to mechanical coupling with the transducer housing. A modified octagonal baffle of maximum dimension 12 inches was made using half-inch balsa wood sheet sandwiched between 1/16 inch thick aluminum plates. When mounting the baffle to the transducer no metal-to-metal contact was allowed and it was found that this arrangement apparently did effectively decouple the transducer and the baffle.

To allow for rapid plotting of the beam patterns an automated mechanical method for rotating the transducer and baffle was required. A fractional-horsepower motor was used to drive the assembly through a gear train with an electrical potentiometer which produced a D.C. voltage proportional to angular position. This arrangement is

sketched in Fig. 19. The D.C. signal was applied to the x axis of a standard plotter to generate the abscissa of the beam patterns.

The following standard items of test equipment were also used:

Hewlett Packard 204C Oscillator

General Radio 1192B Frequency Counter

General Radio 1396A Tone Burst Generator

40 dB Gate

Harrison 6205B D.C. Power Supply

Hewlett Packard 407A Power Amplifier

Krohn Hite DCA 50R Power Amplifier

LC10 Hydrophone

Hewlett Packard 465 Voltage Amplifier

Krohn Hite 3202R Band Pass Filter

Hewlett Packard 450A Voltage Amplifier

Envelope Detector

PAR 160 Boxcar Integrator

Hewlett Packard 7561A Logarithmic Converter

Hewlett Packard 7035B X-4 Recorder

Tektronix RM45A Dual Trace Oscilloscope

The equipment was connected as shown in Fig. 20. The transducer and hydrophone were located in the anechoic tank with the hydrophone in the far field.

Beam patterns were taken using a pulsed mode of operation in order to minimize the effects of standing

waves in the tank and to eliminate the effects of surface reflections. In the pulsed mode, the direct path pulse was readily identifiable so that the Boxcar Integrator could be gated to generate a D.C. voltage proportional to the average amplitude of that pulse only. This output was fed to a calibrated logarithmic converter which then generated the ordinate of the beam pattern in decibels.

Data were taken at 25 kHz using a 0.64 millisecond burst with a pulse repetition frequency of approximately 150 Hz, and at 74 kHz using a 0.21 millisecond burst with a pulse repetition frequency of approximately 50 Hz. The transducer and baffle were rotated at six degrees per second.

The back faces of the transducer and baffle were coated with a foamed polyurethane material to reduce radiation from these surfaces. At 25 kHz, high driving voltages (a base voltage of 30 volts peak to peak compared to 10 volts peak to peak at 74 kHz) were used to improve the signal-to-noise ratio. A drop in the ambient noise level due to shut-down of machinery in the testing lab and some water infusion into the pressure release material combined to give pattern structure in the back hemisphere of the 25 kHz patterns.

The radiation patterns under varying phase and amplitude shadings are reproduced in Figs. 21 through 24 for the 74 kHz data and in Figs. 28 through 31 in the 25 kHz case.

The patterns in Figs. 25 through 27 and 32 and 33 were taken to determine the frequency dependency of the patterns. For the patterns obtained at 25 kHz and 74 kHz the model predictions are also plotted on the respective figures.

The results clearly show the effects on the radiation patterns of phase and amplitude shading. While the position of the lobes apparently was determined primarily by the geometry, the relative amplitudes of the main lobe and secondary lobes could be shaped at will. Phase shading of 180 degrees lowered the relative amplitude of the central lobe. Increasing the ratio of voltage to the inner radiator to that of the outer radiator further lowered the central lobe, although a limit was reached after which the central lobe fused with the side lobes to give a uniform wide main beam. This performance is essentially consistent with that predicted by the theory. The pattern obtained at the scaled frequency of 25 kHz, using a voltage ratio of 3:1 and 180-degree phase shading is especially noteworthy in that, in spite of a non-optimum geometry, it closely fits the requirements of the radiation pattern specified in Fig. 1.

Unfortunately the results also clearly showed that the model predictions were inadequate in the secondary lobes, especially at the higher frequencies, and in the main lobe at the higher amplitude shadings. Some discrepancy was anticipated in the secondary lobes due to the suspected non-uniform motion of the radiating faces, so these results

were not too surprising. However, since the design concept appeared to be promising, it was decided to investigate further the operation of the transducer to try and explain the lack of agreement between the model and the physical results. The remaining experimental phases were directed toward this end.

The details of the radiation patterns were observed to be quite frequency-dependent even within a band width of ten percent. This was not unexpected but did reinforce the belief that a production transducer would have to be mechanically simple in order to insure that the resultant pattern at the operating frequency could be reliably reproduced.

D. THREE PORT EQUIVALENT NETWORK MEASUREMENTS

Since it was expected that mutual coupling between the elements, both through the transmission medium and through the transducer structure itself, would affect the motion of the radiators, the first step in testing the computer model assumptions was to obtain some measure of the extent of these effects. The transducer was considered to be a three port linear passive network with two electrical ports and one acoustical port. The procedure in this experiment was to drive one electrical port and measure the effect at the other, both in air with the acoustical port unloaded and in water with it loaded.

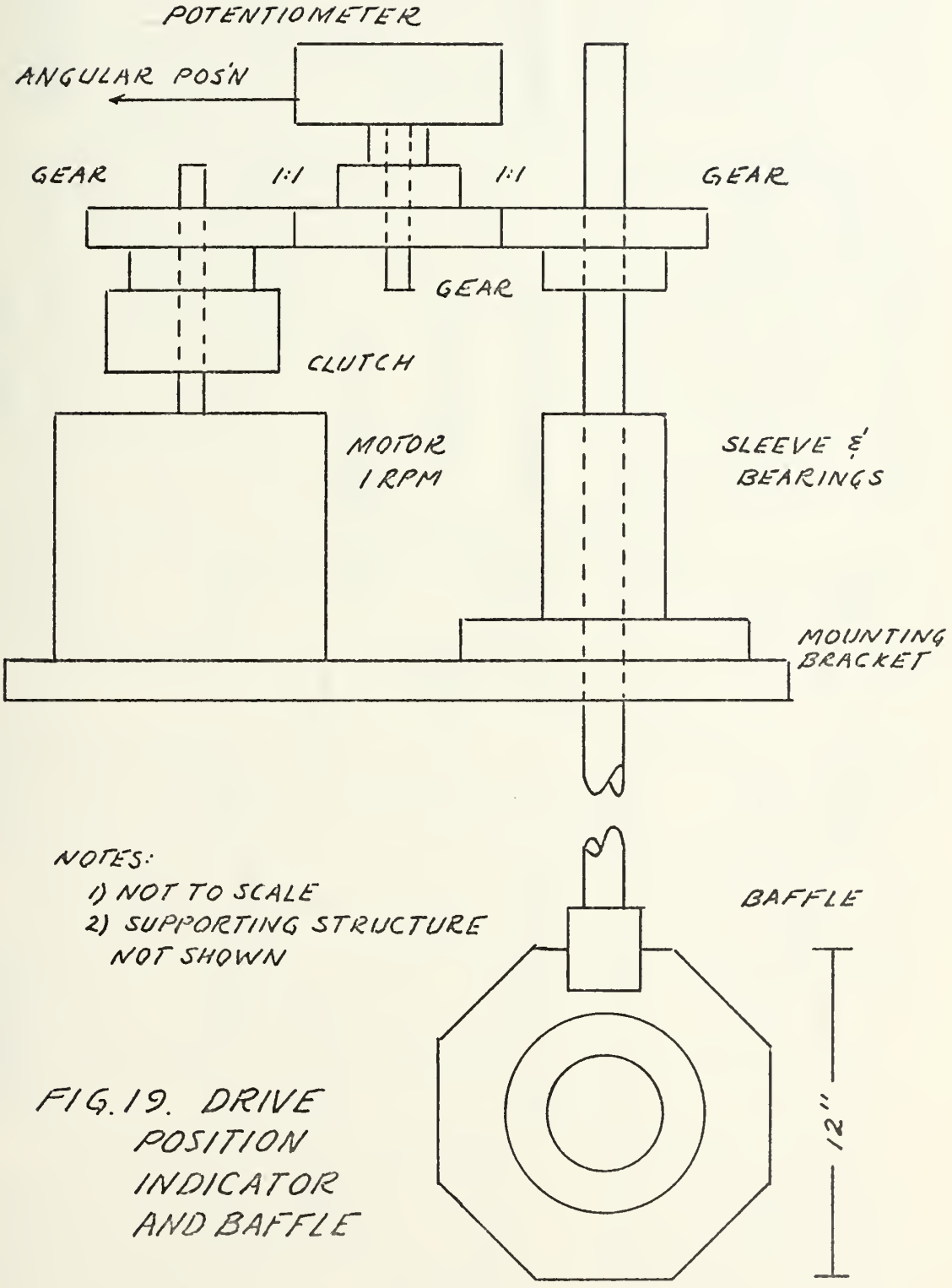

FIG. 19. DRIVE POSITION INDICATOR AND BAFFLE

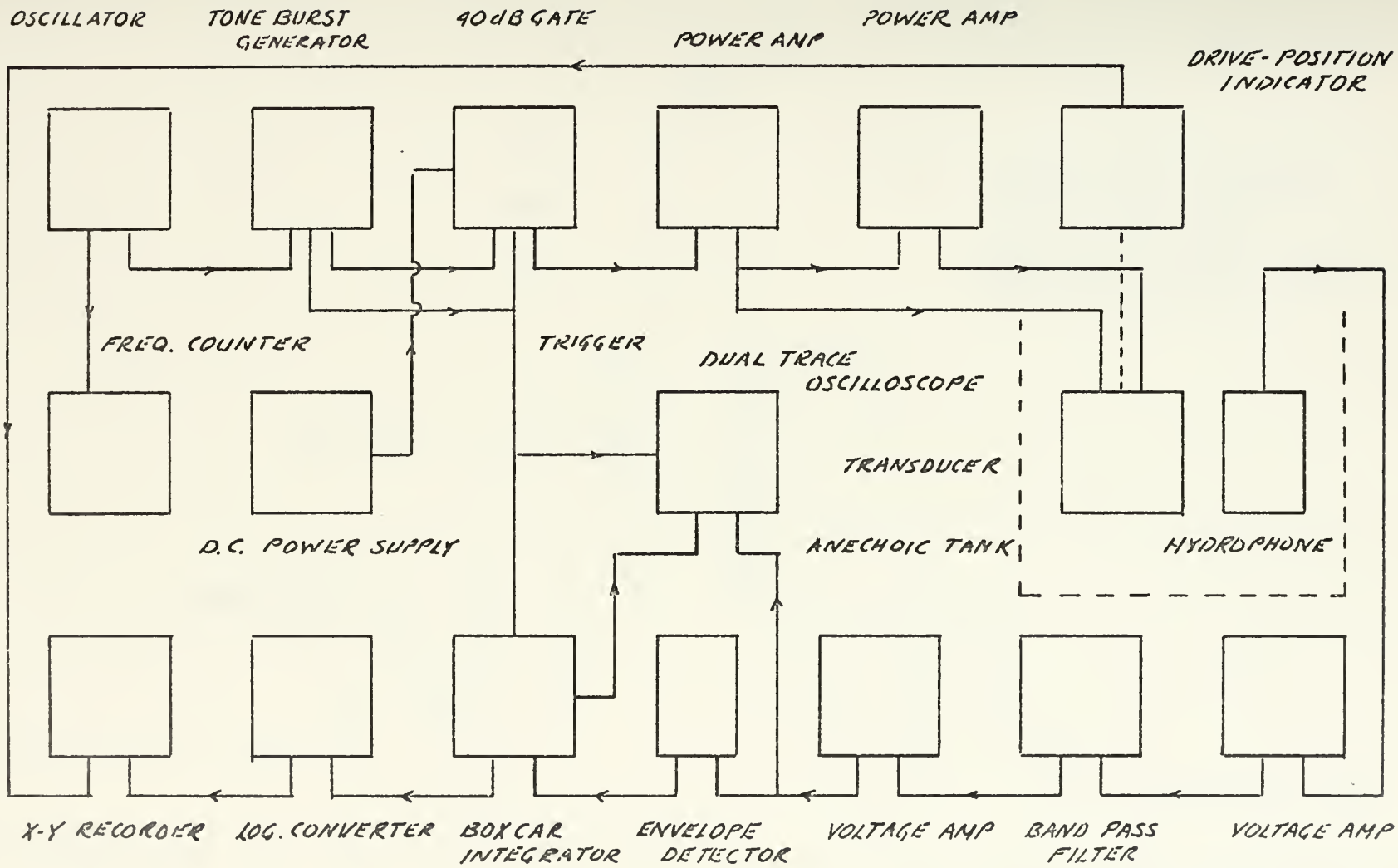

FIG. 20. BEAM PATTERN MEASUREMENTS

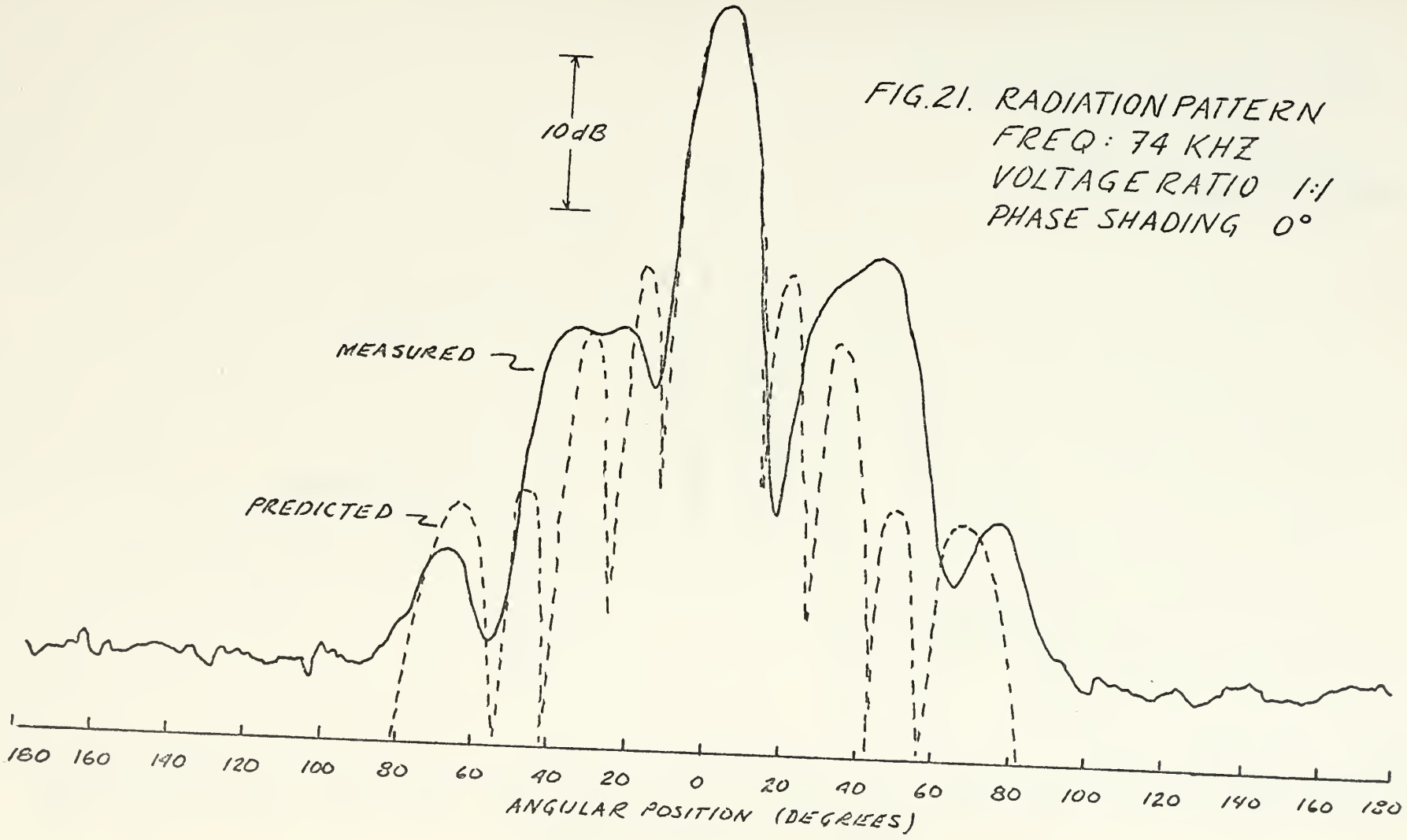

FIG. 21. RADIATION PATTERN
FREQ: 74 KHZ
VOLTAGE RATIO 1:1
PHASE SHADING 0°

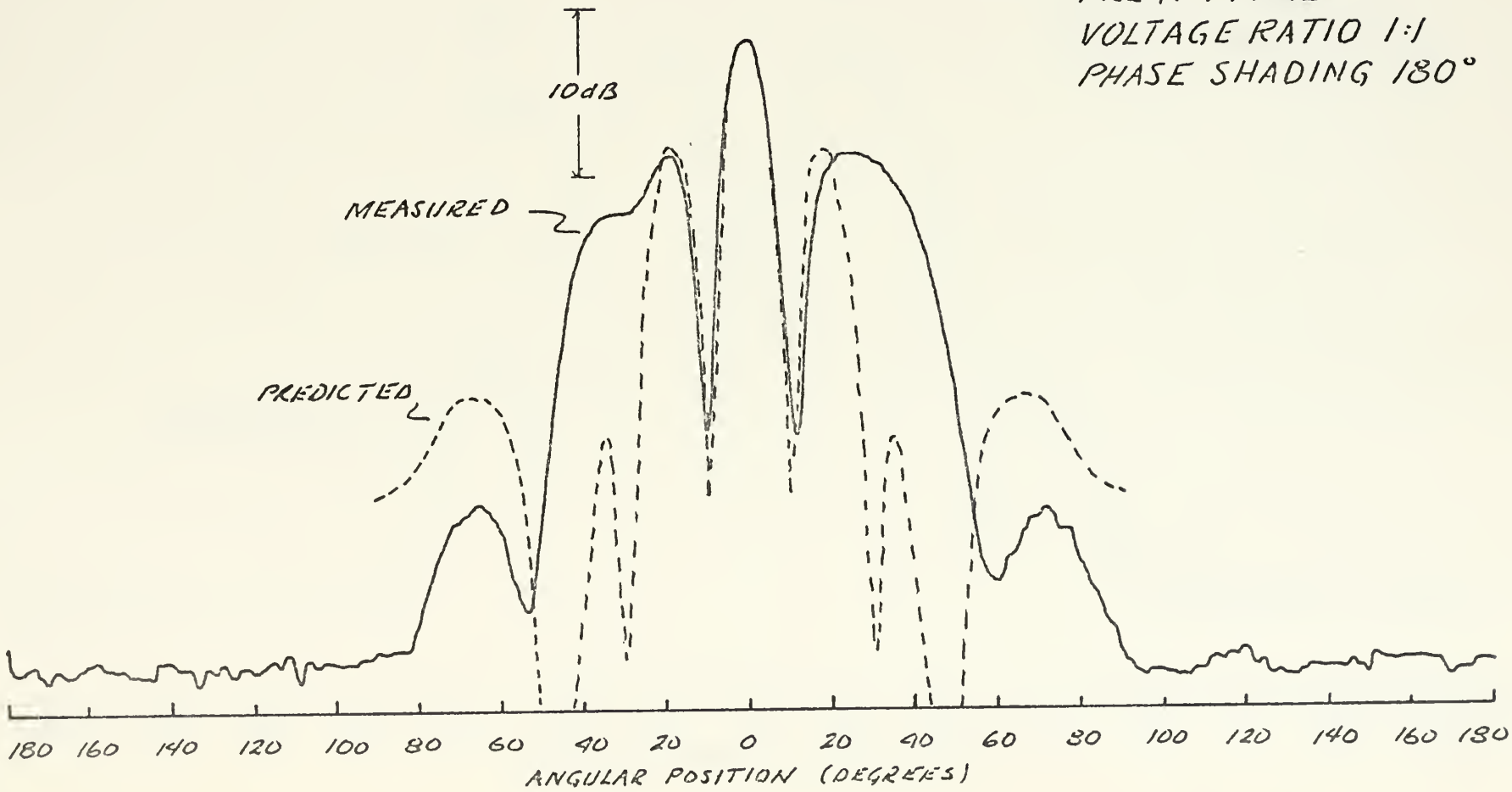

FIG. 22. RADIATION PATTERN
FREQ. 74 KHZ
VOLTAGE RATIO 1:1
PHASE SHADING 180°

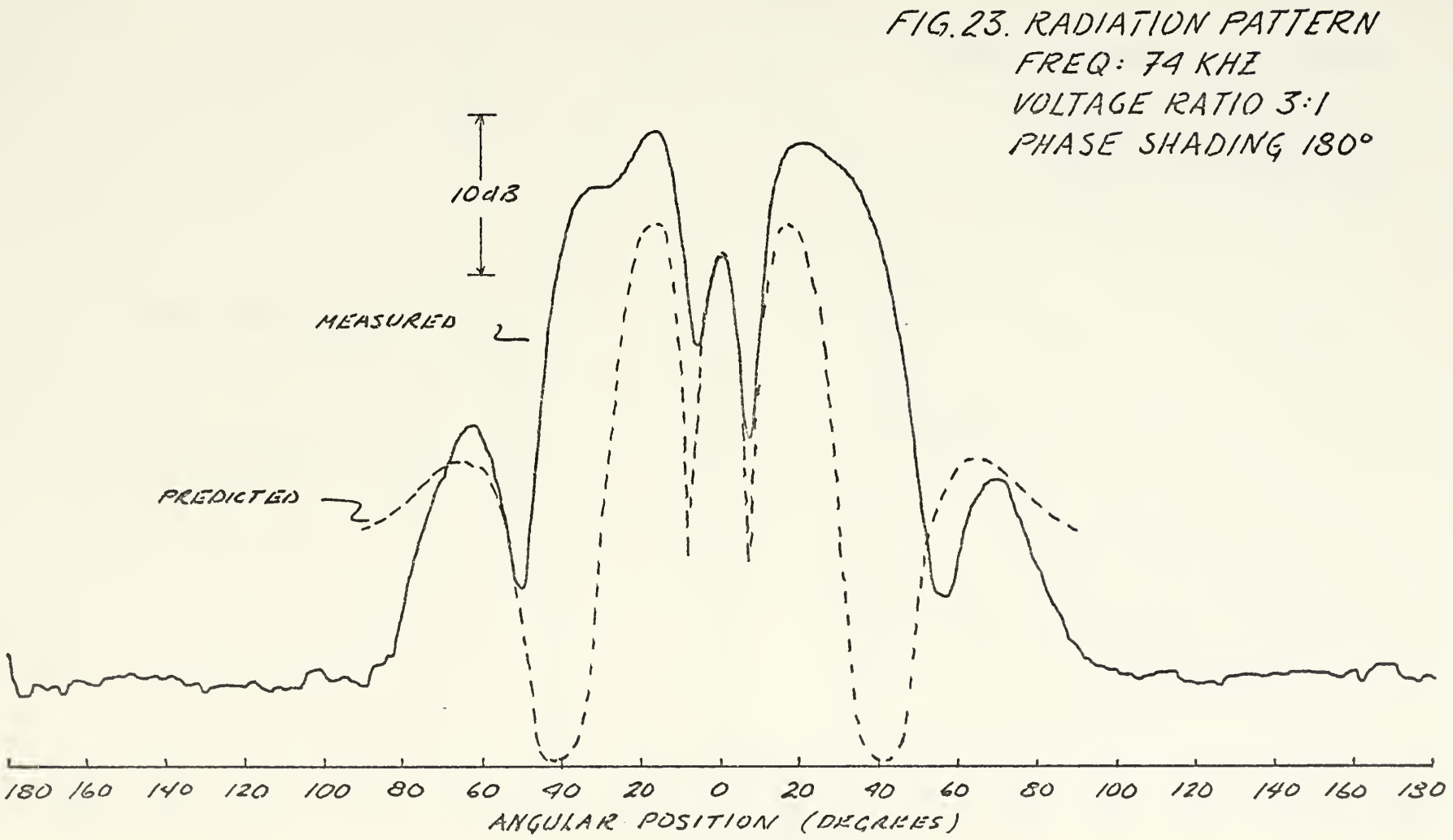

FIG. 23. RADIATION PATTERN
FREQ: 74 KHZ
VOLTAGE RATIO 3:1
PHASE SHADING 180°

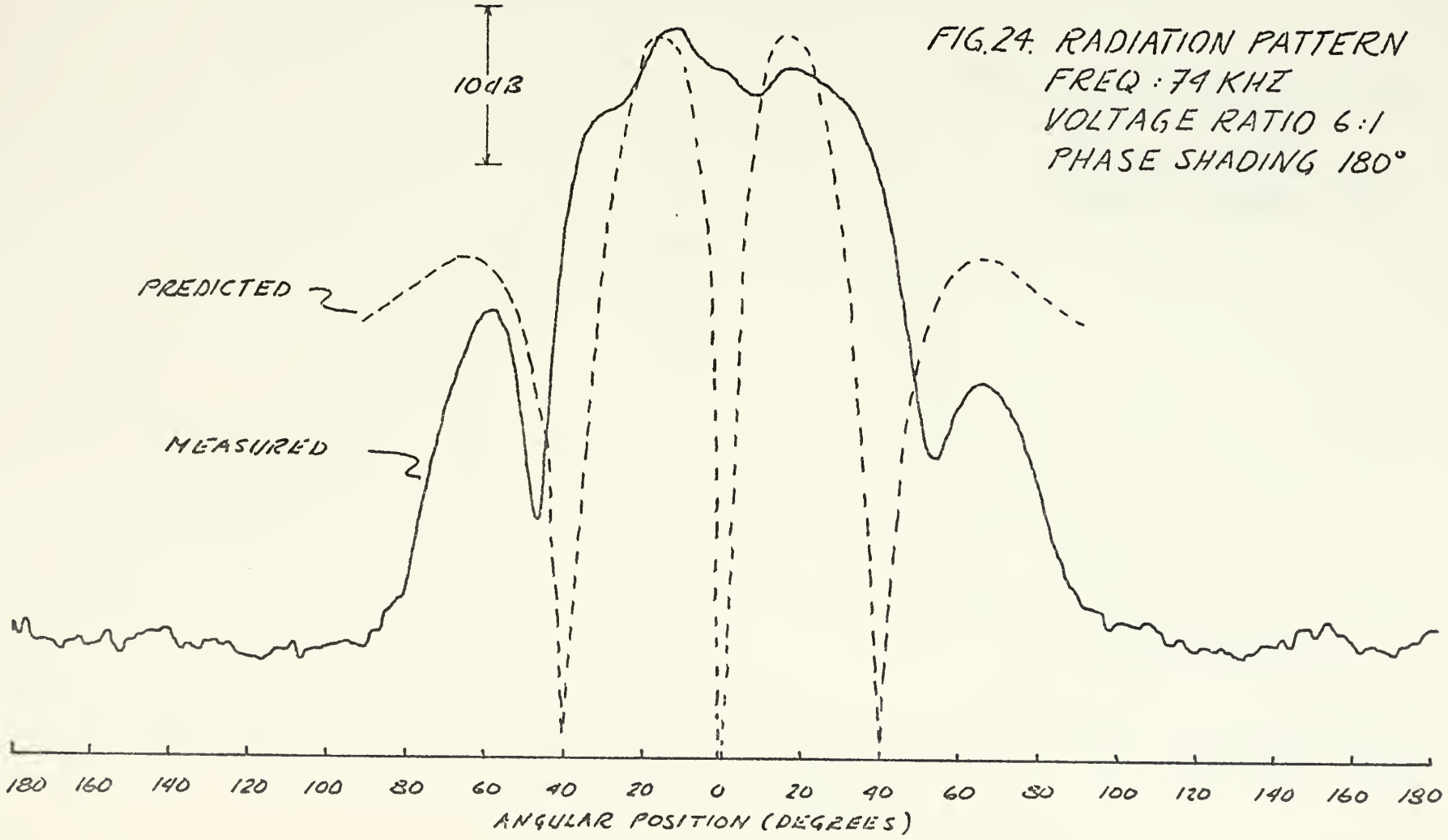

FIG. 24. RADIATION PATTERN
FREQ : 74 KHZ
VOLTAGE RATIO 6:1
PHASE SHADING 180°

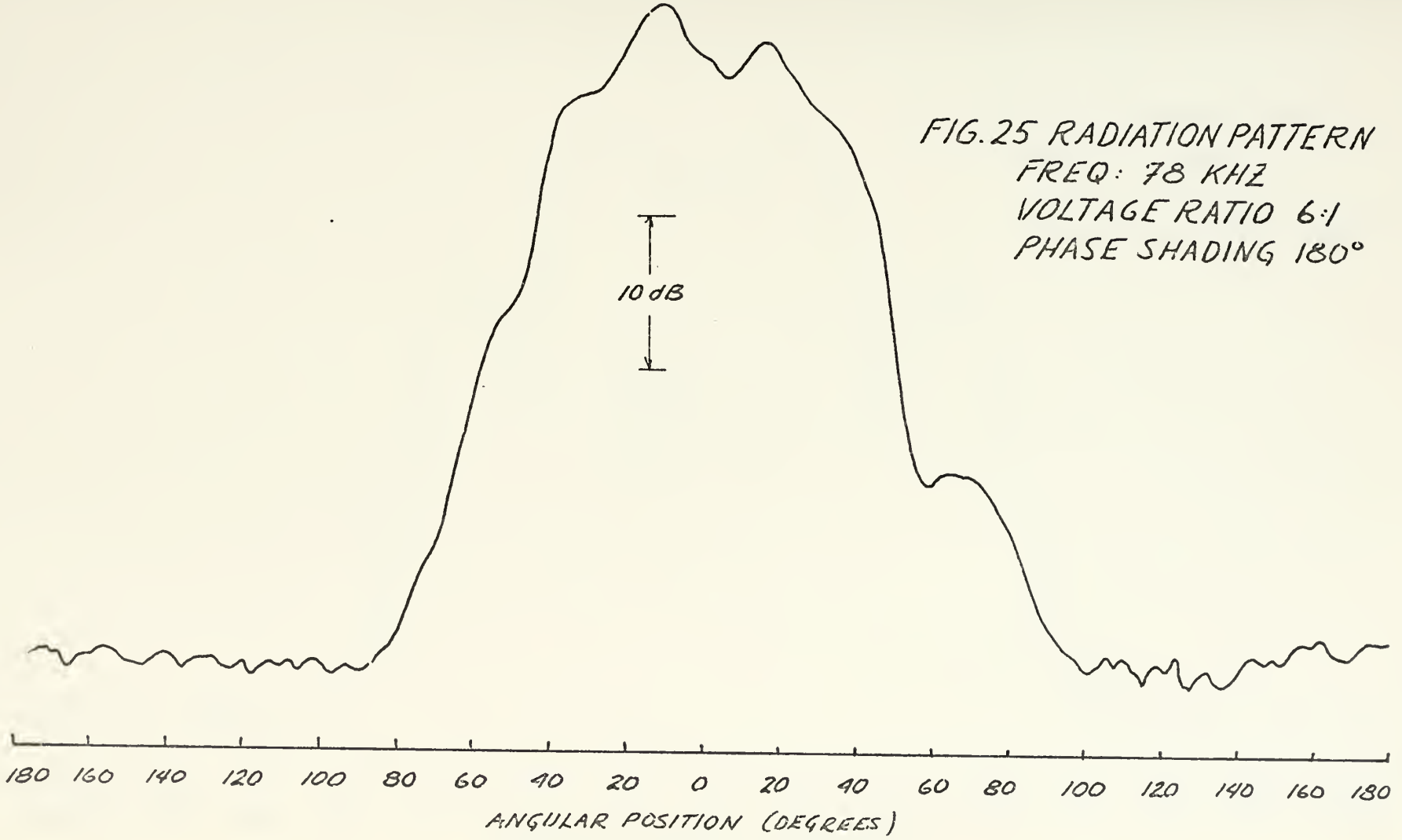

FIG. 25 RADIATION PATTERN
FREQ: 78 KHZ
VOLTAGE RATIO 6:1
PHASE SHADING 180°

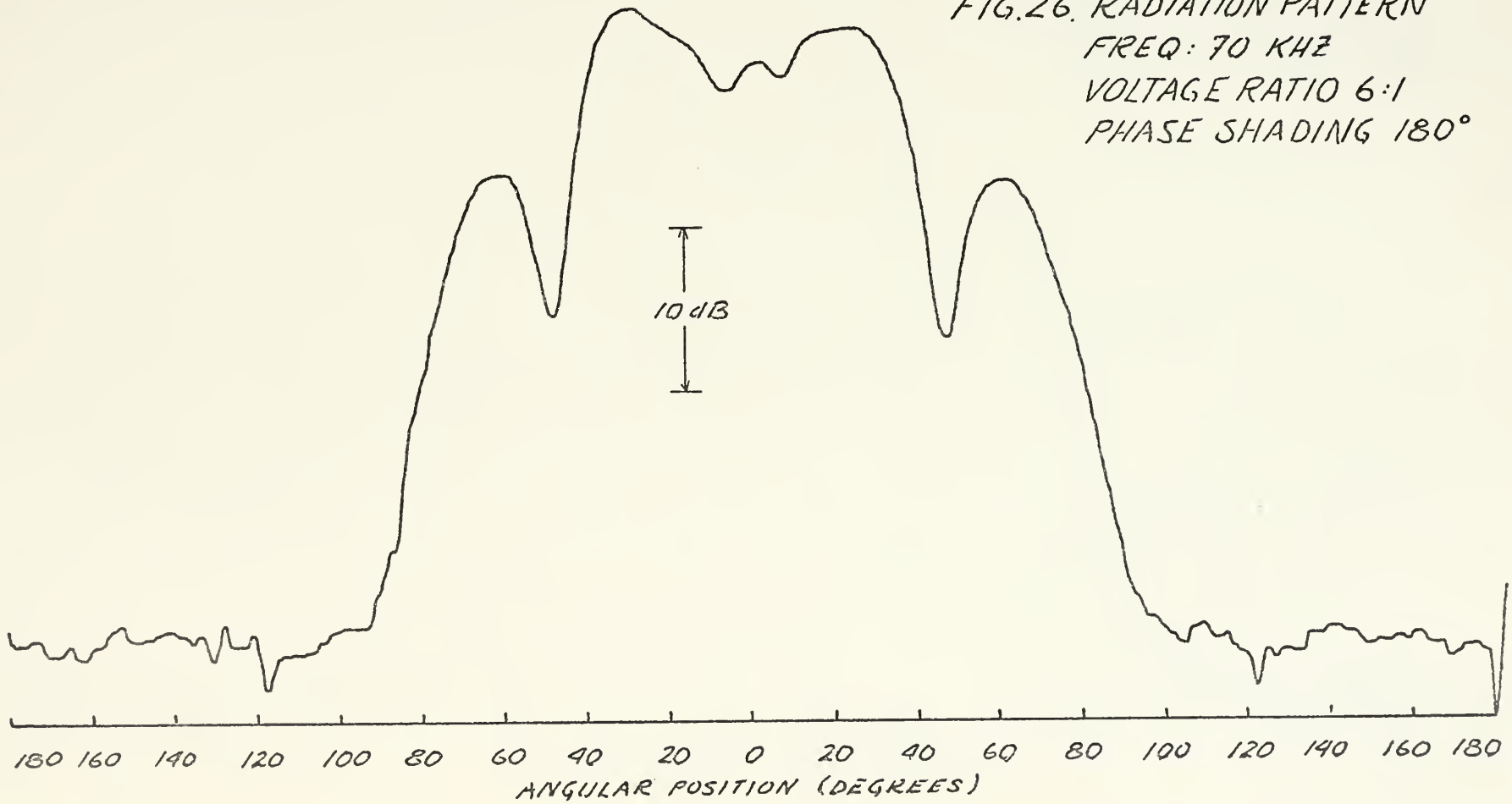

FIG. 26. RADIATION PATTERN
FREQ: 70 KHZ
VOLTAGE RATIO 6:1
PHASE SHADING 180°

FIG. 27. RADIATION PATTERN
FREQ : 68 KHZ
VOLTAGE RATIO 6:1
PHASE SHADING 180°

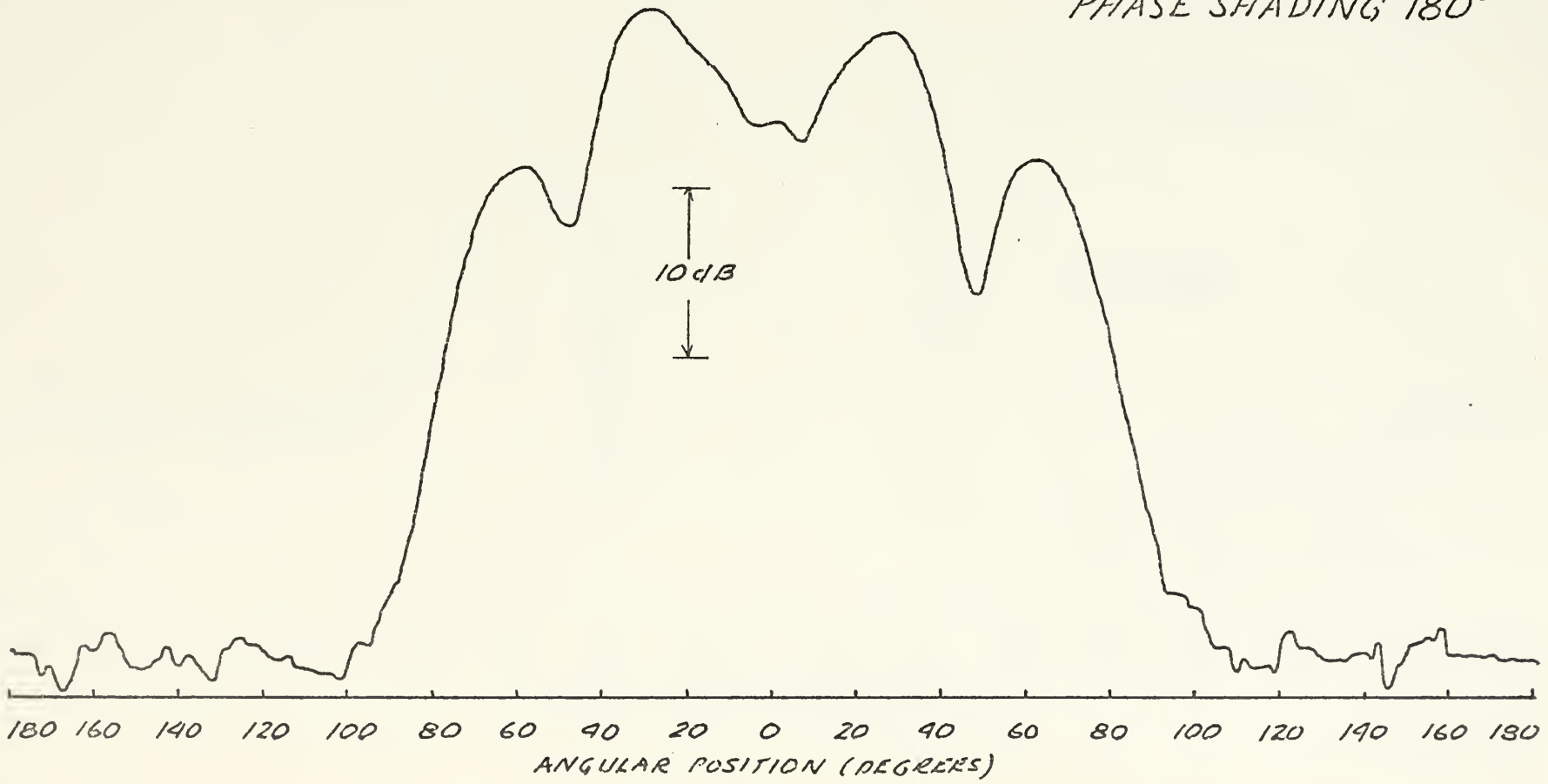

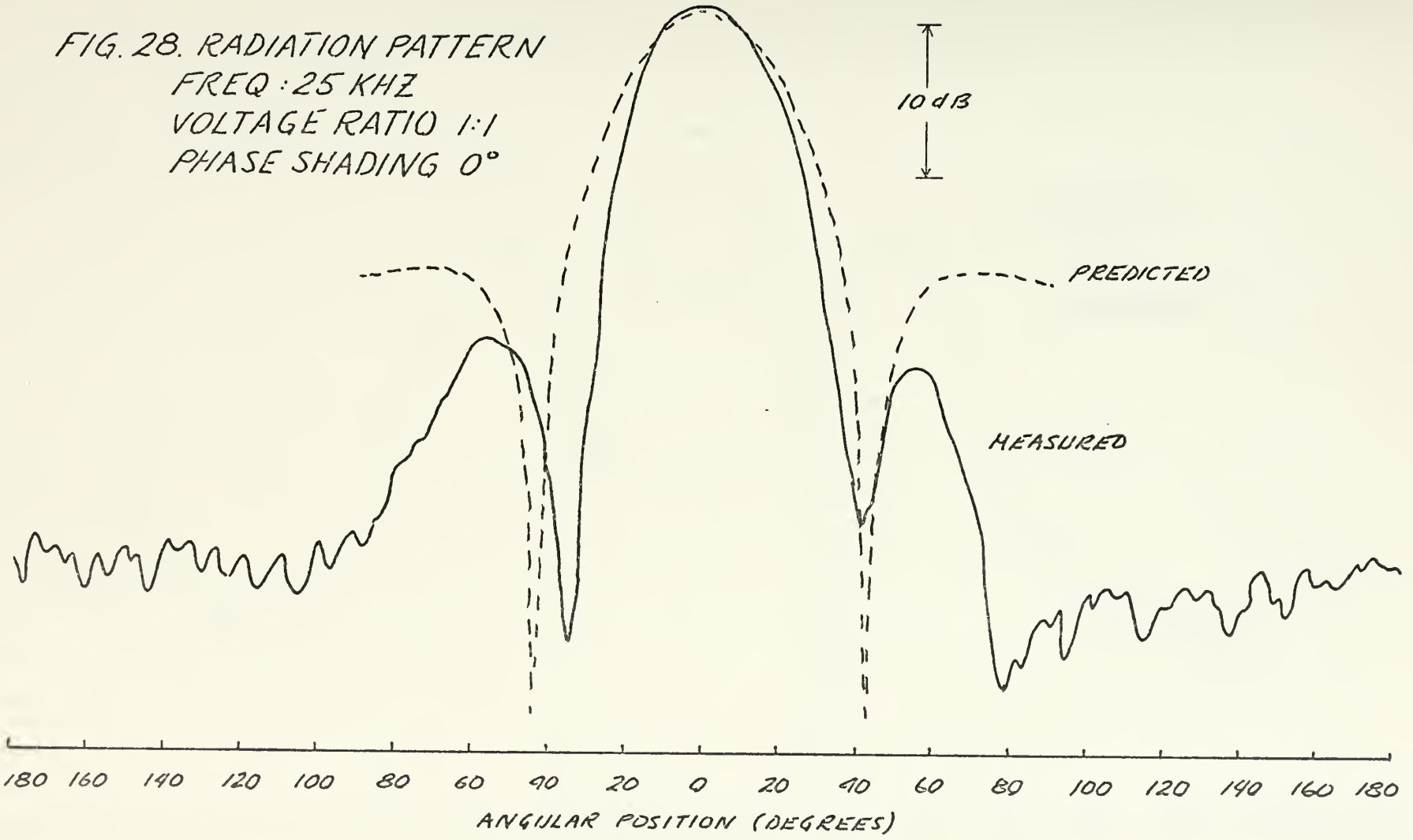
FIG. 28. RADIATION PATTERN
FREQ : 25 KHZ
VOLTAGE RATIO 1:1
PHASE SHADING 0°
10 dB
PREDICTED
MEASURED
180 160 140 120 100 80 60 40 20 0 20 40 60 80 100 120 140 160 180
ANGULAR POSITION (DEGREES)

FIG. 29. RADIATION PATTERN
FREQ : 25 KHZ
VOLTAGE RATIO 1:1
PHASE SHADING 180°

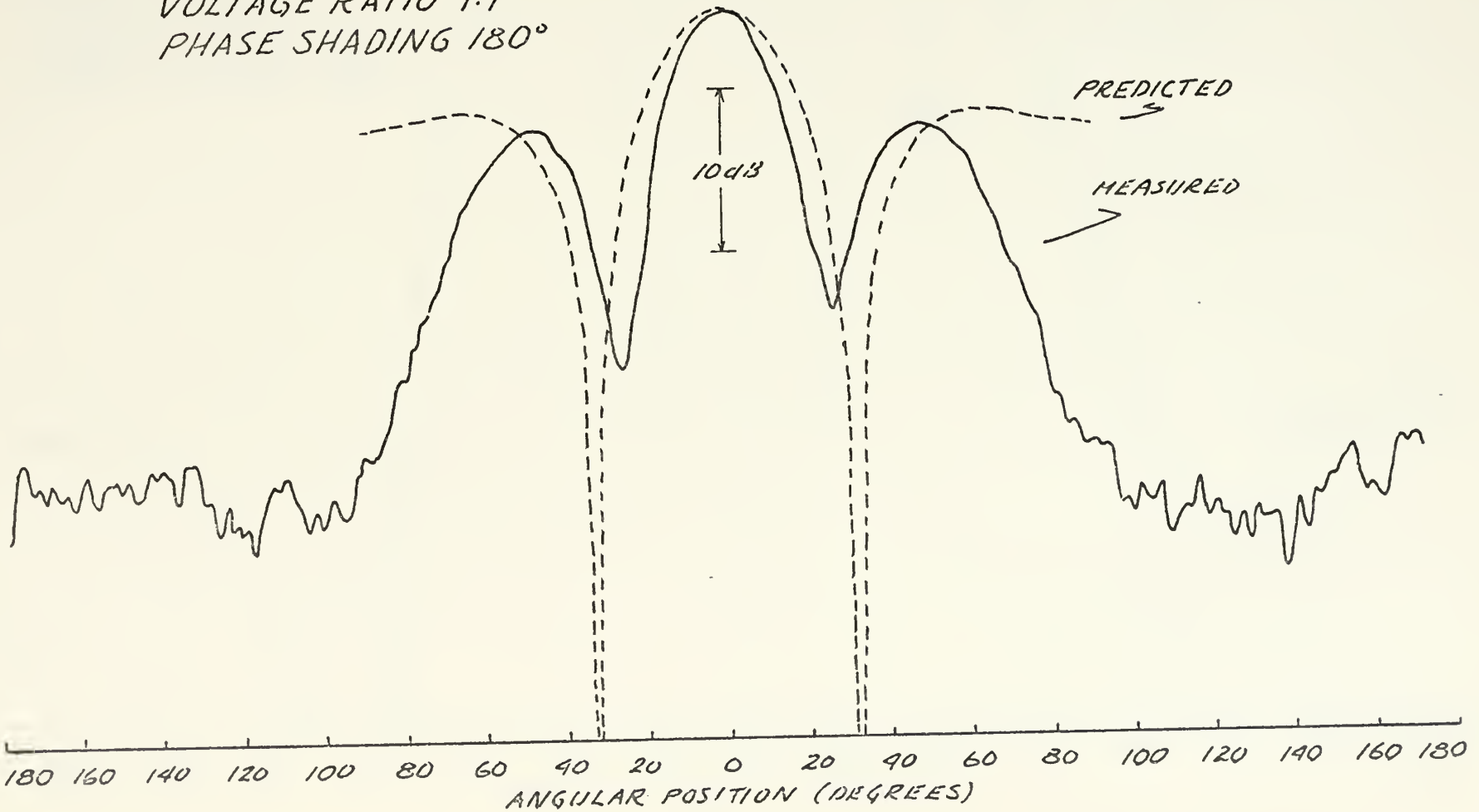

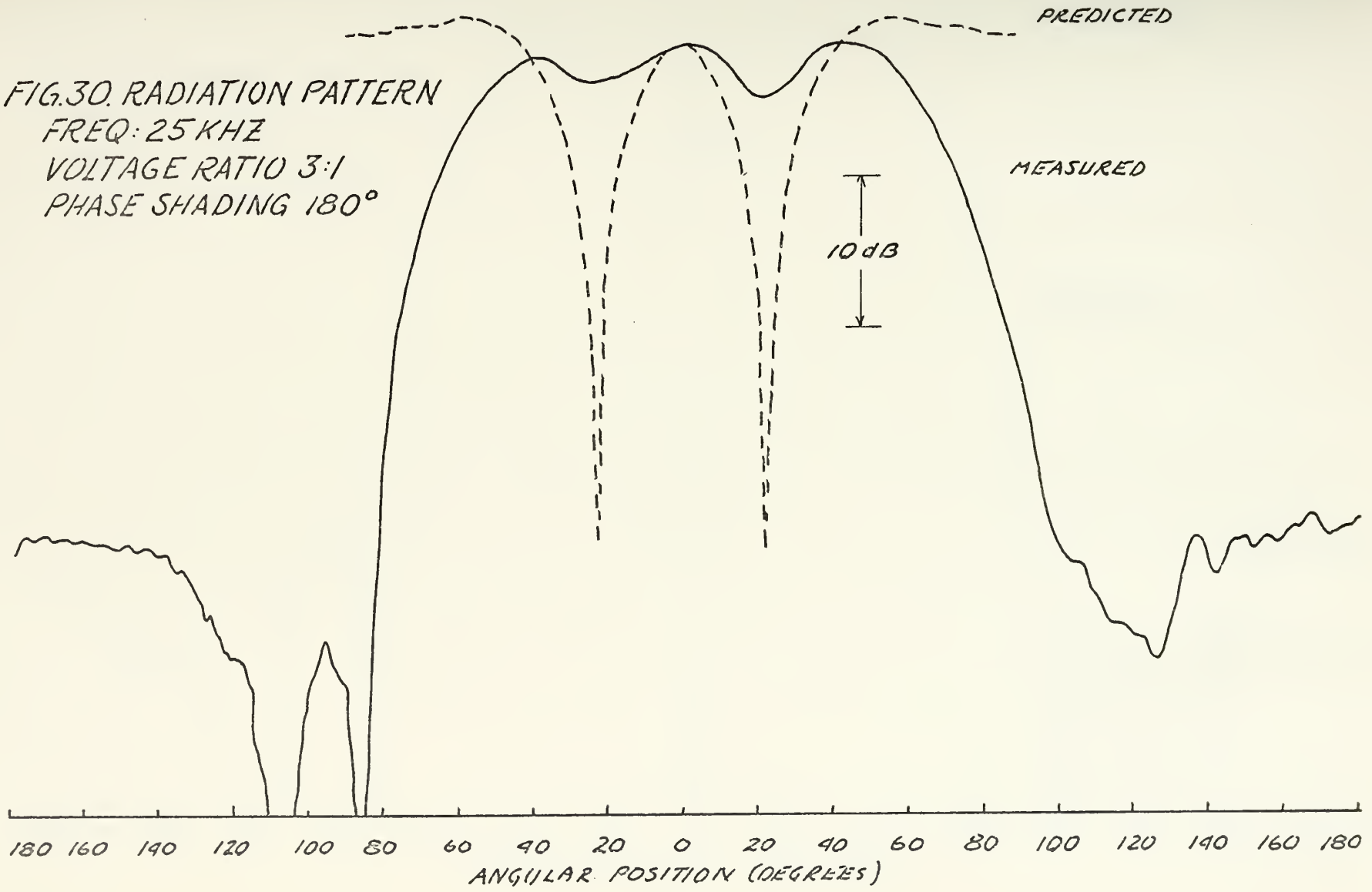

FIG. 30. RADIATION PATTERN
FREQ: 25 KHZ
VOLTAGE RATIO 3:1
PHASE SHADING 180°

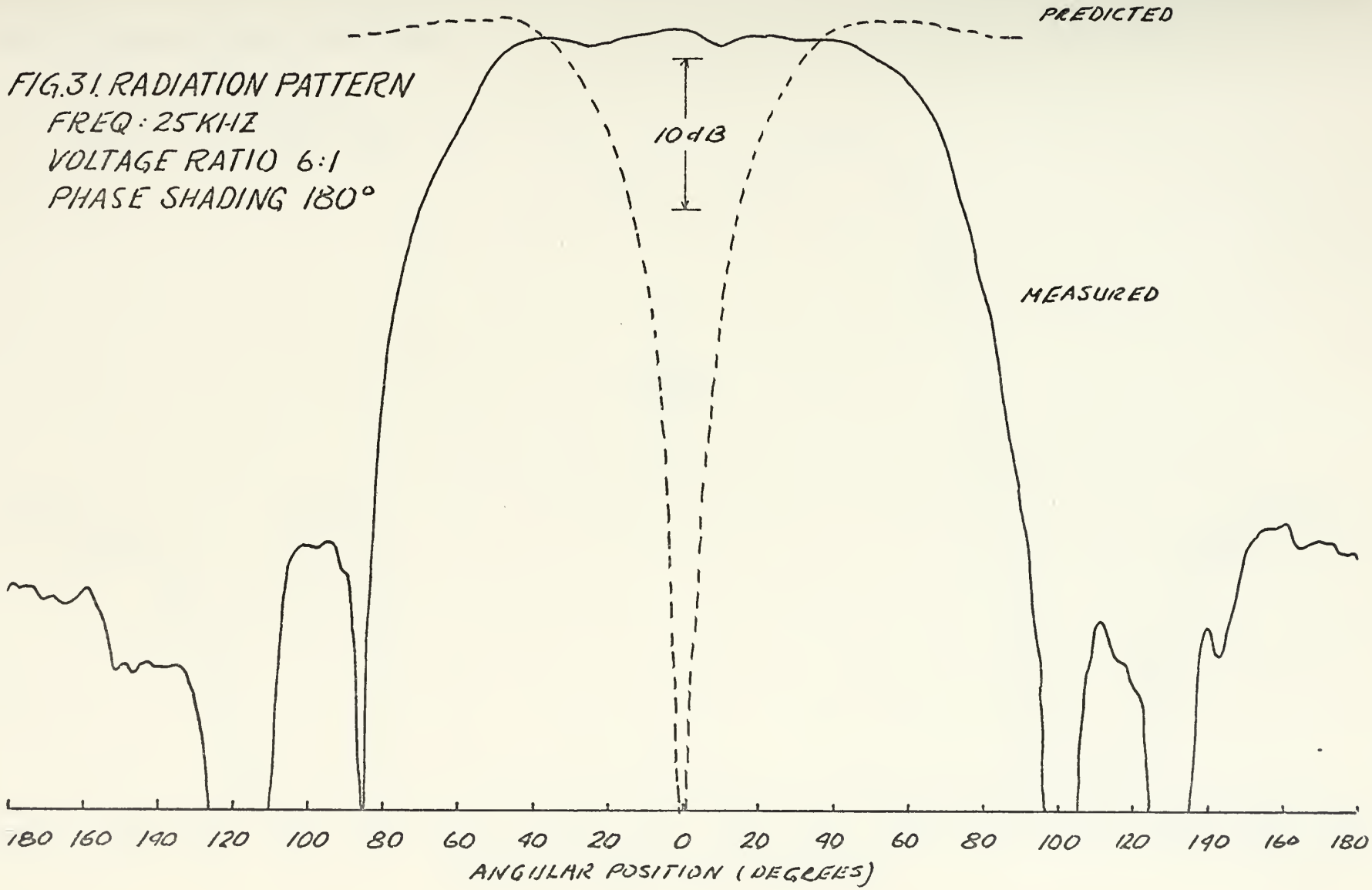
FIG.31. RADIATION PATTERN
FREQ: 25 KHZ
VOLTAGE RATIO 6:1
PHASE SHADING 180°
PREDICTED
10 dB
MEASURED
180 160 140 120 100 80 60 40 20 0 20 40 60 80 100 120 140 160 180
ANGULAR POSITION (DEGREES)

FIG.32. RADIATION PATTERNS
FREQ : 27.5 KHZ
VOLTAGE RATIO 3:1
PHASE SHADING 180°

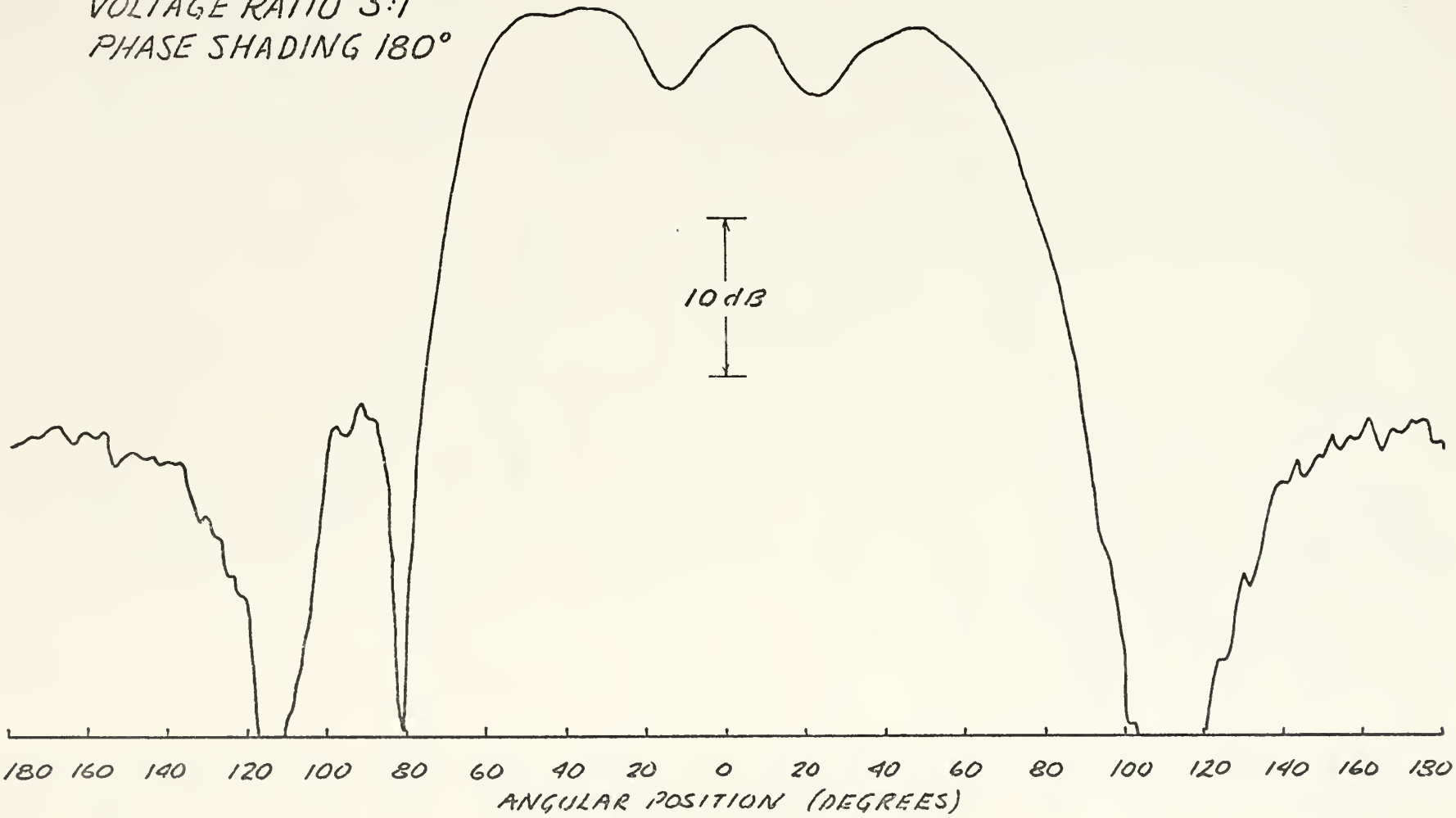

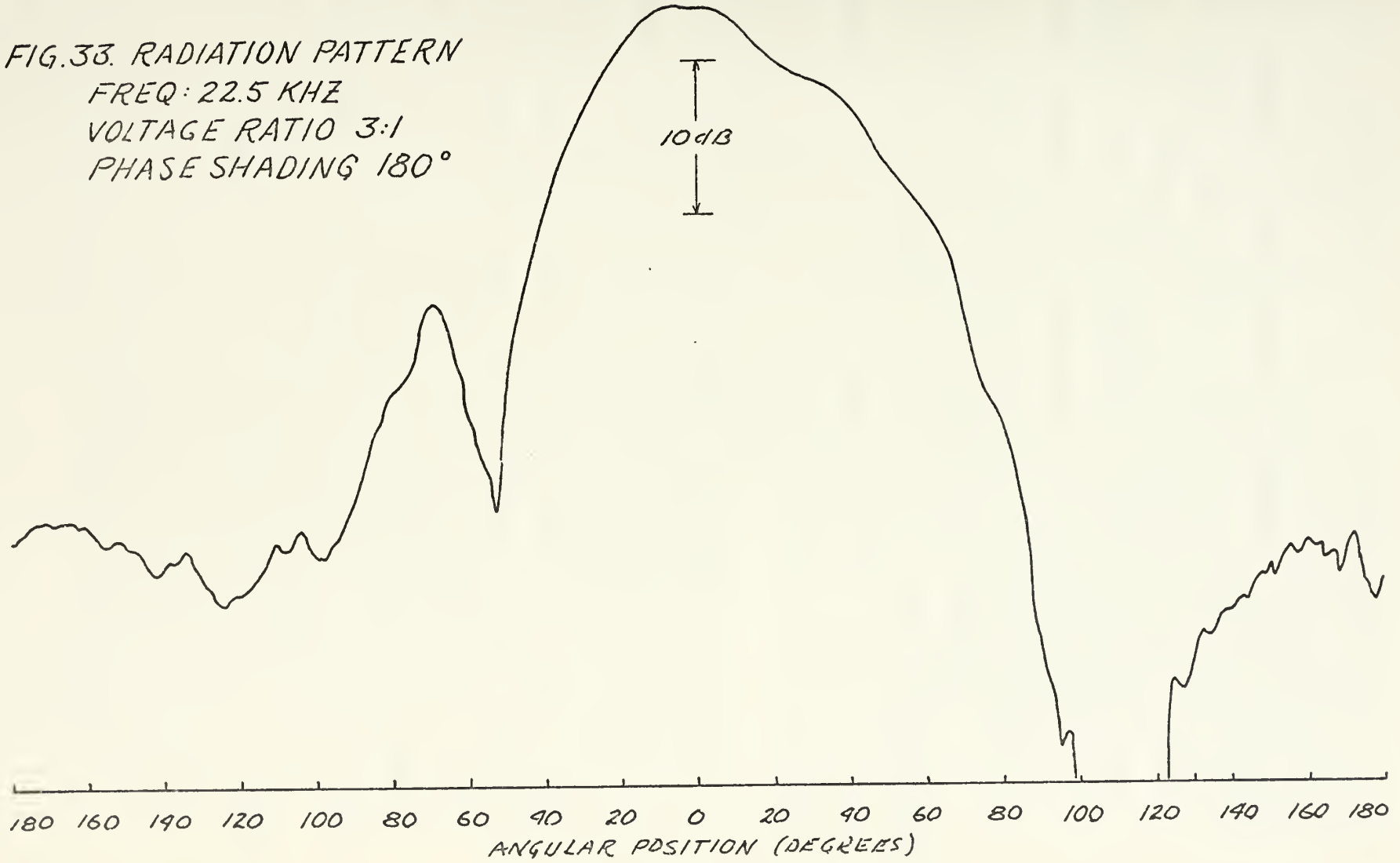
FIG. 33. RADIATION PATTERN
FREQ: 22.5 KHZ
VOLTAGE RATIO 3:1
PHASE SHADING 180°
10 dB
180 160 140 120 100 80 60 40 20 0 20 40 60 80 100 120 140 160 180
ANGULAR POSITION (DEGREES)

The interpretation of the transducer three port is illustrated in Fig. 34. Ports one and two are the electrical terminals to the transducer elements in the inner and outer rings, respectively. Port three is the acoustical port. The impedances Z_o, Z_1, Z_2 and Z_m are the internal equivalent electrical impedances for each radiator. The backing impedance Z_B represents the mechanical impedance which couples the back side of each transducer element and depends in part on the action of all elements. Similarly the radiation impedance Z_R has both self and mutual components. No attempt was made to evaluate each of these impedances since only an estimate of their gross magnitude and interrelationship was required.

Ten volts rms were applied to the input electrical terminal and the voltage at the output electrical port measured. The results obtained are summarized in Table II.

The data reveal that the inner ring is strongly influenced by the outer ring. This confirms the same conclusion reached as a result of the admittance measurement. It is apparent that there is strong coupling through the common backing plate of the radiation elements, so strong, in fact, that the effects of the mutual radiation impedance are quite overshadowed. It is concluded from these measurements that the operation of the transducer was very likely not in accordance with the assumptions of the model and that actual displacement measurements ought to be made to quantify the non-uniformity.

TABLE II

MUTUAL EFFECTS

Frequency (kHz)	Medium	Driven Port	Output Port	Voltage (Volts)
25	Air	1 (Inner)	2 (Outer)	.027
74	Air	1 (Inner)	2 (Outer)	.950
25	Water	1 (Inner)	2 (Outer)	.021
74	Water	1 (Inner)	2 (Outer)	.720
25	Air	2 (Outer)	1 (Inner)	.096
74	Air	2 (Outer)	1 (Inner)	3.60
25	Water	2 (Outer)	1 (Inner)	.062
74	Water	2 (Outer)	1 (Inner)	2.77

FIG. 34. TRANSDUCER EQUIVALENT CIRCUIT

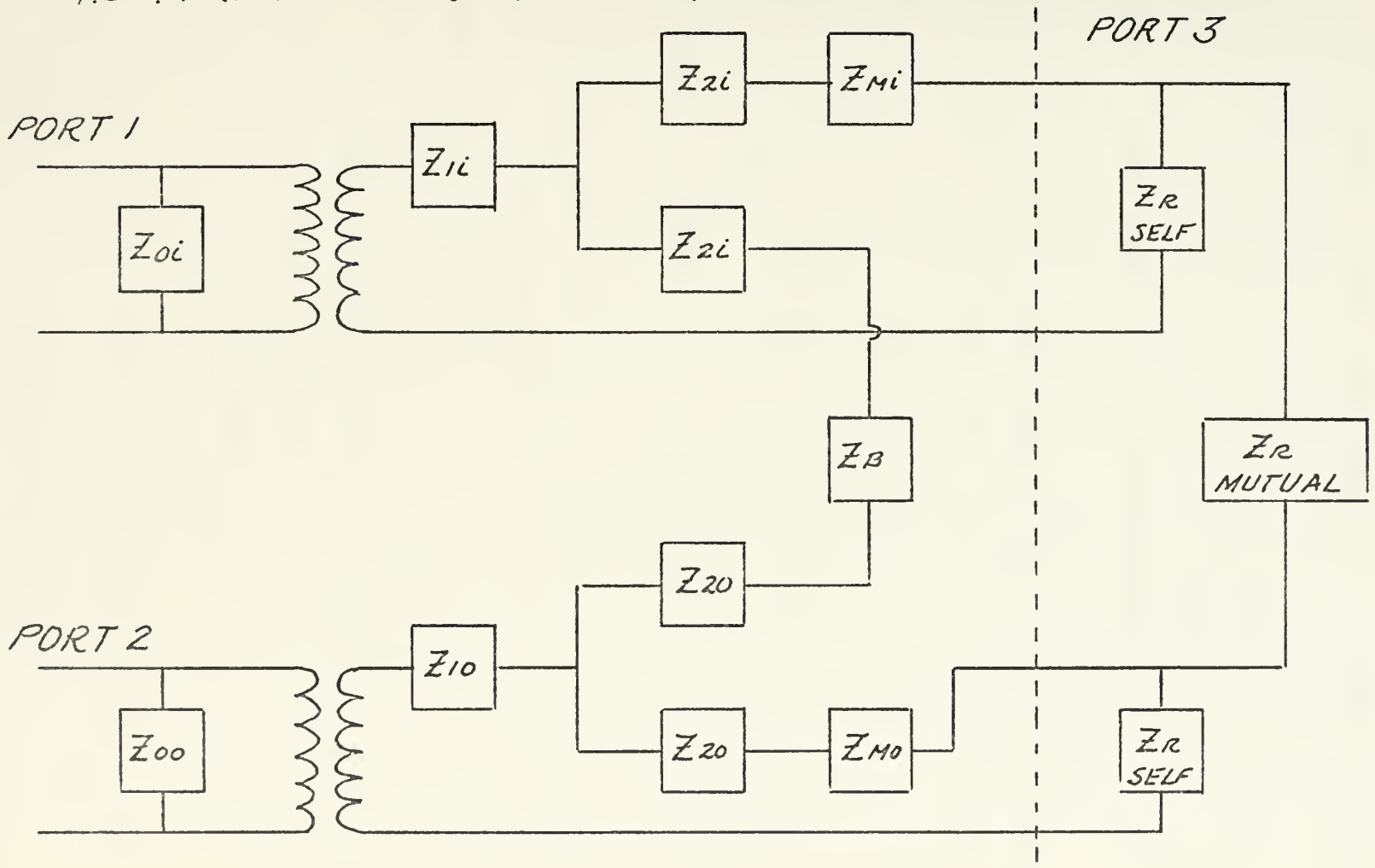

E. DISPLACEMENT MEASUREMENTS

The objective of this experiment was to obtain displacement amplitude and phase information as a function of position on the radiating faces of the transducer. While it would have been desirable to obtain such information for operation in water and in air, instrumentation availability precluded measurements in water. The air measurements necessitated removal of the neoprene cover of the transducer.

Measurements were made using a capacitive displacement probe similar to that described in Ref. 4. The probe dimensions are shown in Fig. 35 and are seen not to be small relative to the dimensions of the radiating faces. This limited the fineness of detail to which the displacement field could be measured since fringe effects near the edges of the faces strongly affected the probe readings. To obtain displacement data, the probe was placed on the transducer face. A resilient gasket 0.2 mm thick, attached to the outer ring of the probe, served to control the spacing between the transducer and the other electrode of the probe. The gasket provided sufficient mechanical isolation so as not to load the transducer faces. No attempt was made to calibrate the probe since only relative motion was of concern.

In addition to the probe, the following items of test equipment were used:

Hewlett Packard 3590A Wave Analyzer

Hewlett Packard 3594A Sweeping Local Oscillator

Hewlett Packard 467A Power Amplifier

Krohn-Hite DCA50R Power Amplifier

Altec 526 B Power Supply

Altec 526 Microphone Preamplifier

Hewlett Packard 450A Voltage Amplifier

Krohn Hite 3202R Band Pass Filter

Dranetz Series 305 Phase Meter

Hewlett Packard 120B Oscilloscope

The equipment was set up in accordance with the block diagram in Fig. 37.

Relative displacement amplitude and phase for the positions identified in Fig. 36 are shown in Figs. 38 through 43 for varying amplitude and phase shadings at the frequency of interest. The results are summarized in Table III.

It can be seen clearly that, especially for the outer annulus, the motion was not uniform. It can also be seen that the assumed amplitude and phase shading was not being achieved although at the higher amplitude shading ratios the control was better. As the measurements were made in air with the transducer unloaded, it is assumed that these problems were due largely to the coupling effects through the transducer structure and flexural resonances in the outer annulus. The position of the securing bolts is seen to have also affected the displacement data. A strong symmetry existed at resonance which was not present at

TABLE III

DISPLACEMENT AMPLITUDE AND PHASE

Freq. (kHz)	Voltage Ratio	Phase Shading (Degrees)	Amplitude		Phase	
			Range of Values (dB)	Mean Inner Ring re Mean Outer Ring (dB)	Range of Values (°)	Mean Inner Ring re Mean Outer Ring (°)
25	1:1	0	10 - 15	0	100	-170
25	1:1	180	15 - 20	-3	150	-180
25	6:1	180	15 - 20	+9	150	-150
74	1:1	0	15 - 20	0	200	0
74	1:1	180	15 - 20	0	200	+65
74	6:1	180	15 - 20	+9	200	-180

25 kHz. This suggests that the motions of the transducer will be more uniform and more easily controlled when operated at a longitudinal resonance. From these data, it is apparent that for a production transducer design steps should be taken in order to reduce coupling between the inner and outer vibrators and to minimize the effects of flexural resonances in the outer annulus.

While data were only obtained in air, it has been assumed that had it been possible to make measurements in water a similarly non-uniform displacement field would have been noted. Failure to achieve uniform motion was likely the single greatest contributing factor to the disagreement between the predicted and measured radiation patterns. The finite baffle size also may have affected the secondary lobe structure as may have transient effects in the pulsed mode which were not investigated as displacement data could only be obtained in a continuous mode of excitation.

F. NEAR FIELD PRESSURE MEASUREMENTS

As a final test of the performance of the transducer, it was decided to obtain near field pressure amplitude and phase data which would be used in two ways. It would be indicative of the effectiveness of the amplitude and phase shading of the input voltages in controlling the aperture function, and, using a program developed by Crawford [Ref. 5], the far field radiation pattern would be predicted using actual near field pressure data.

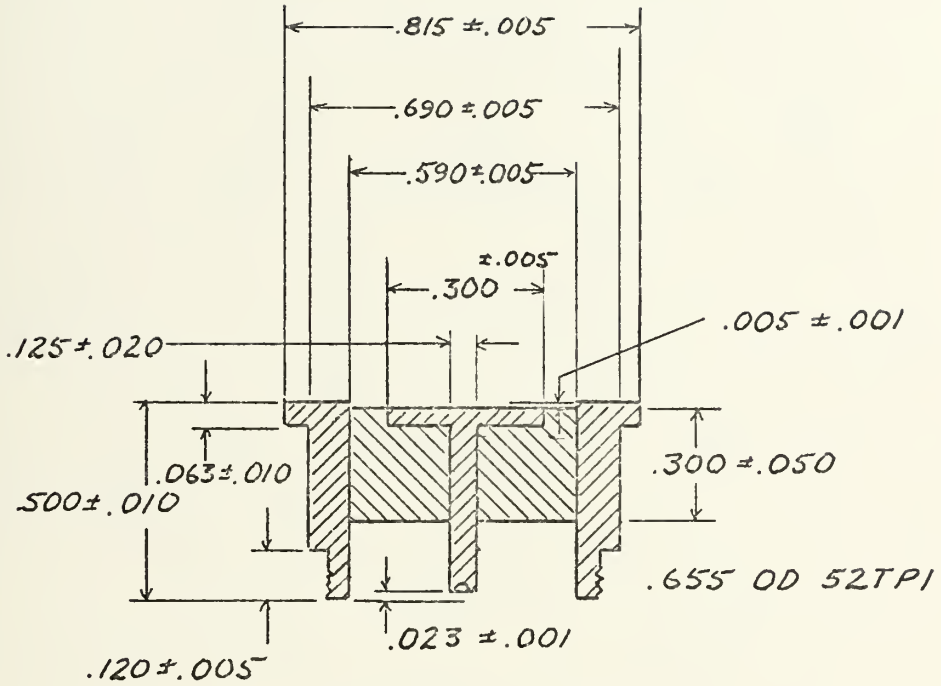

FIG.35. CAPACITIVE DISPLACEMENT PROBE

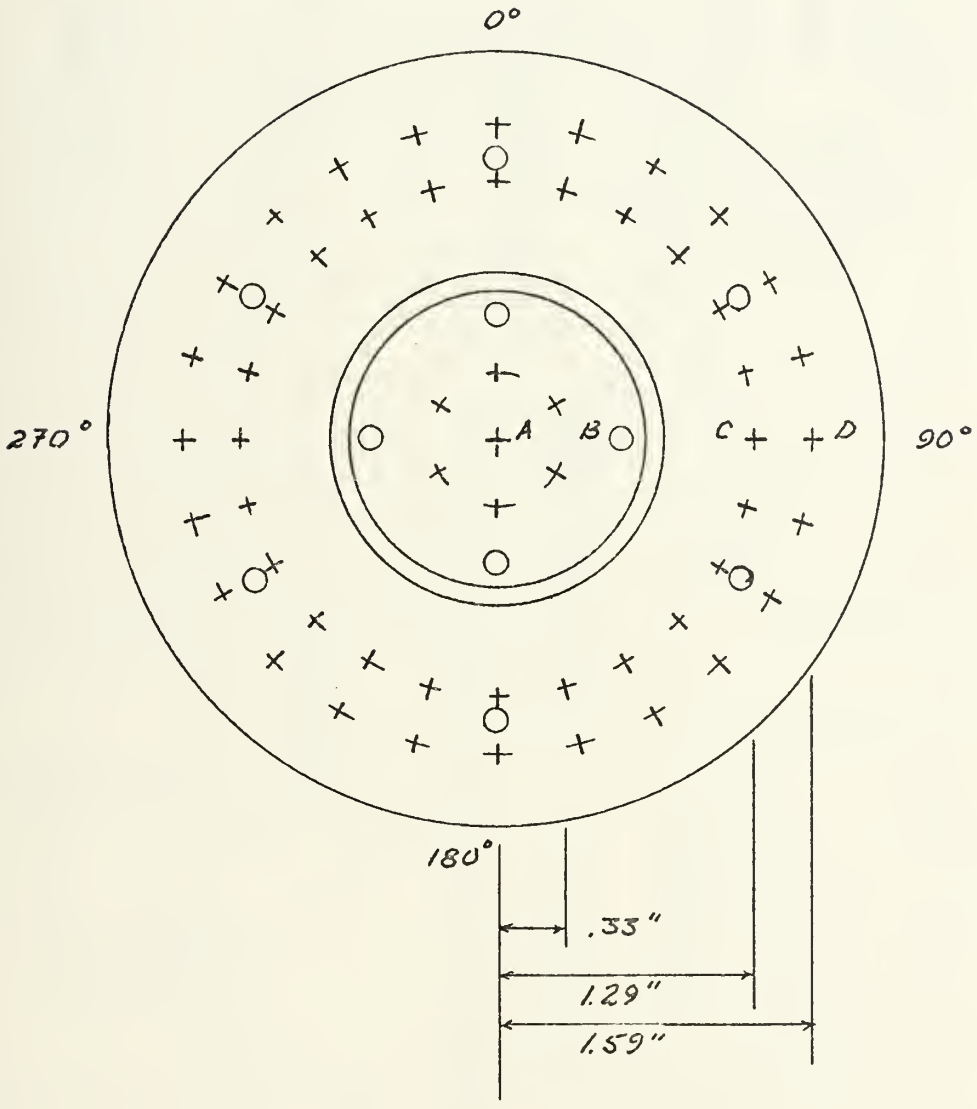

FIG 36 DISPLACEMENT
MEASUREMENT POSITIONS

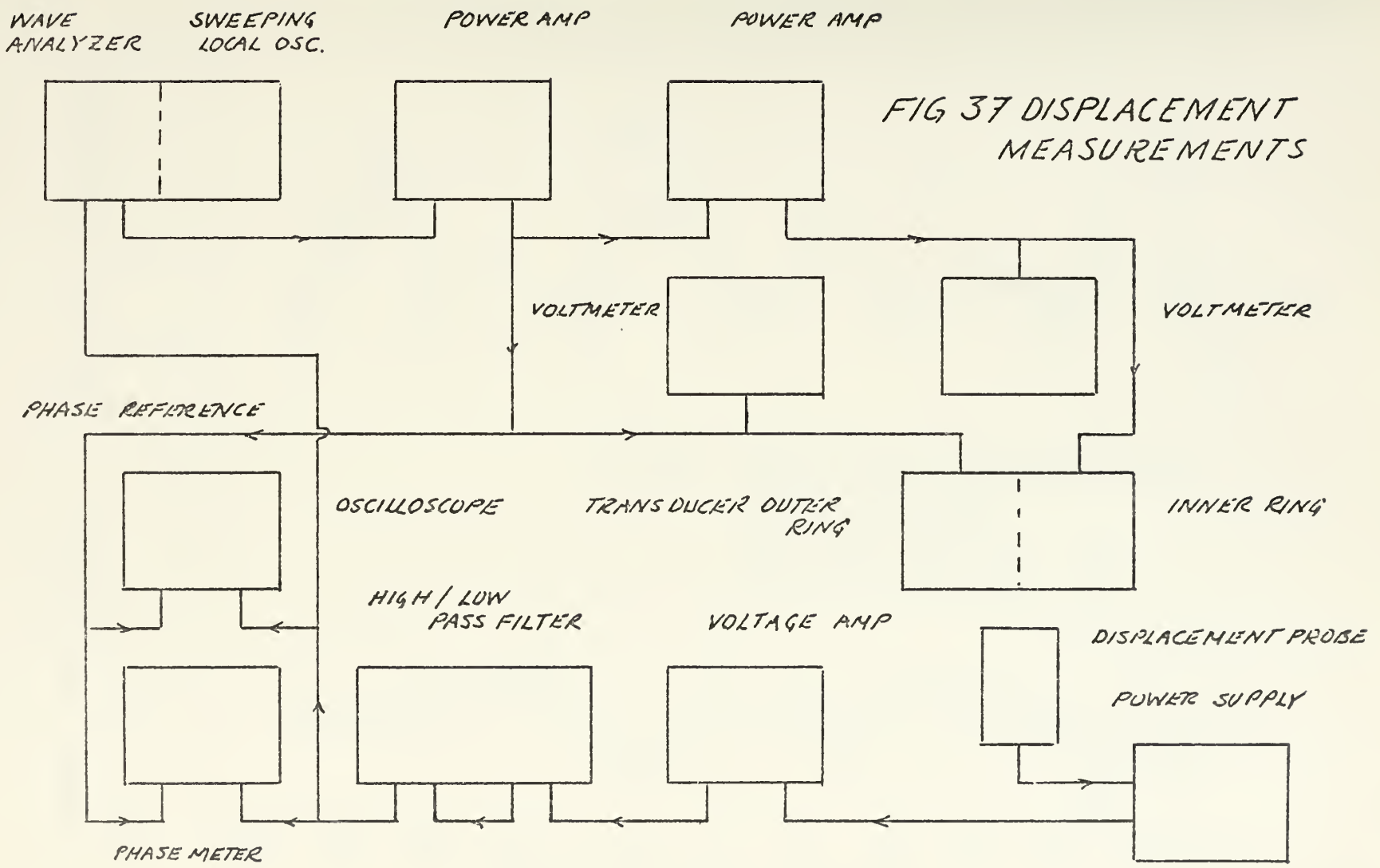

FIG 37 DISPLACEMENT MEASUREMENTS

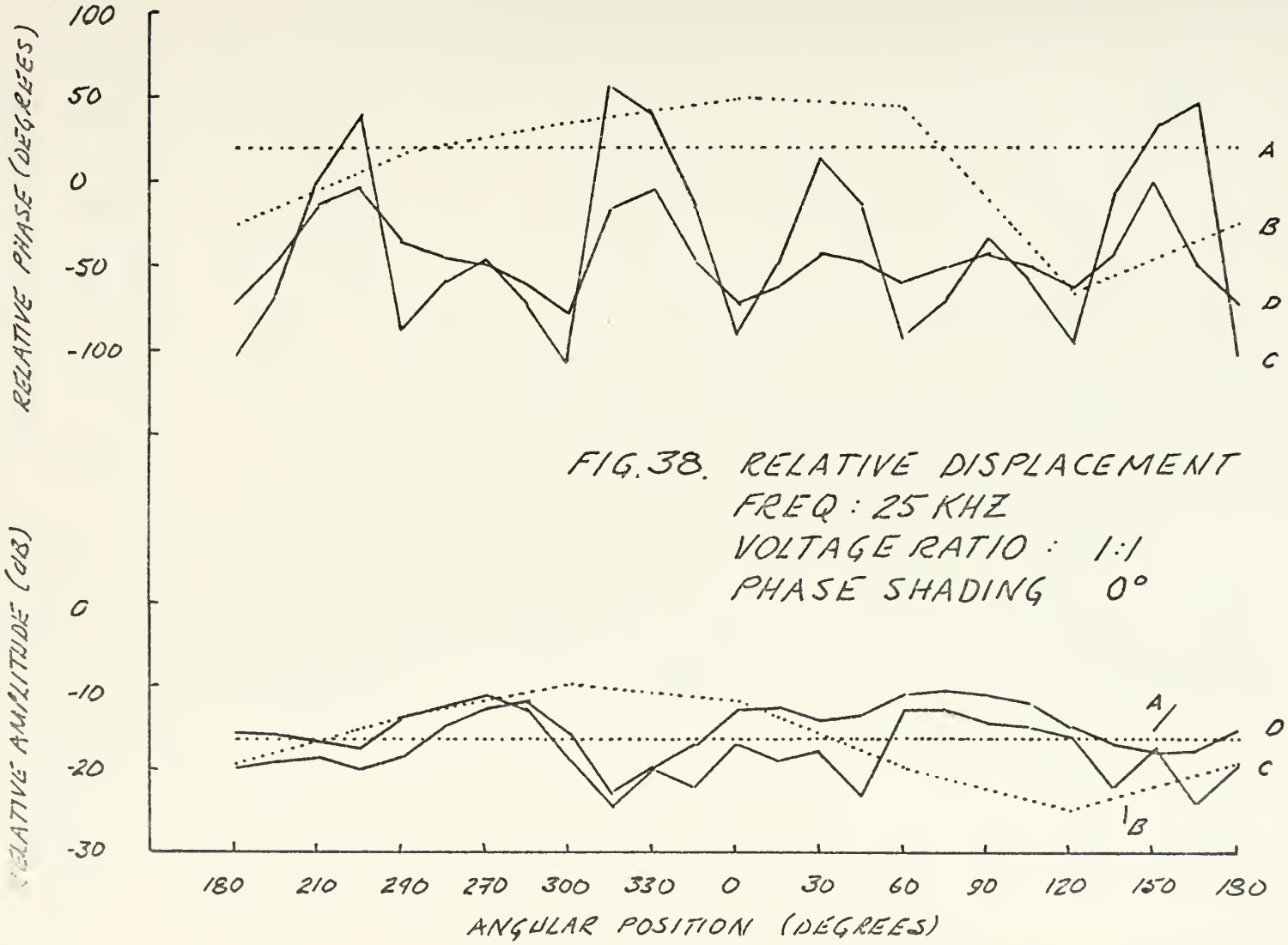

FIG. 38. RELATIVE DISPLACEMENT
FREQ : 25 KHZ
VOLTAGE RATIO : 1:1
PHASE SHADING 0°

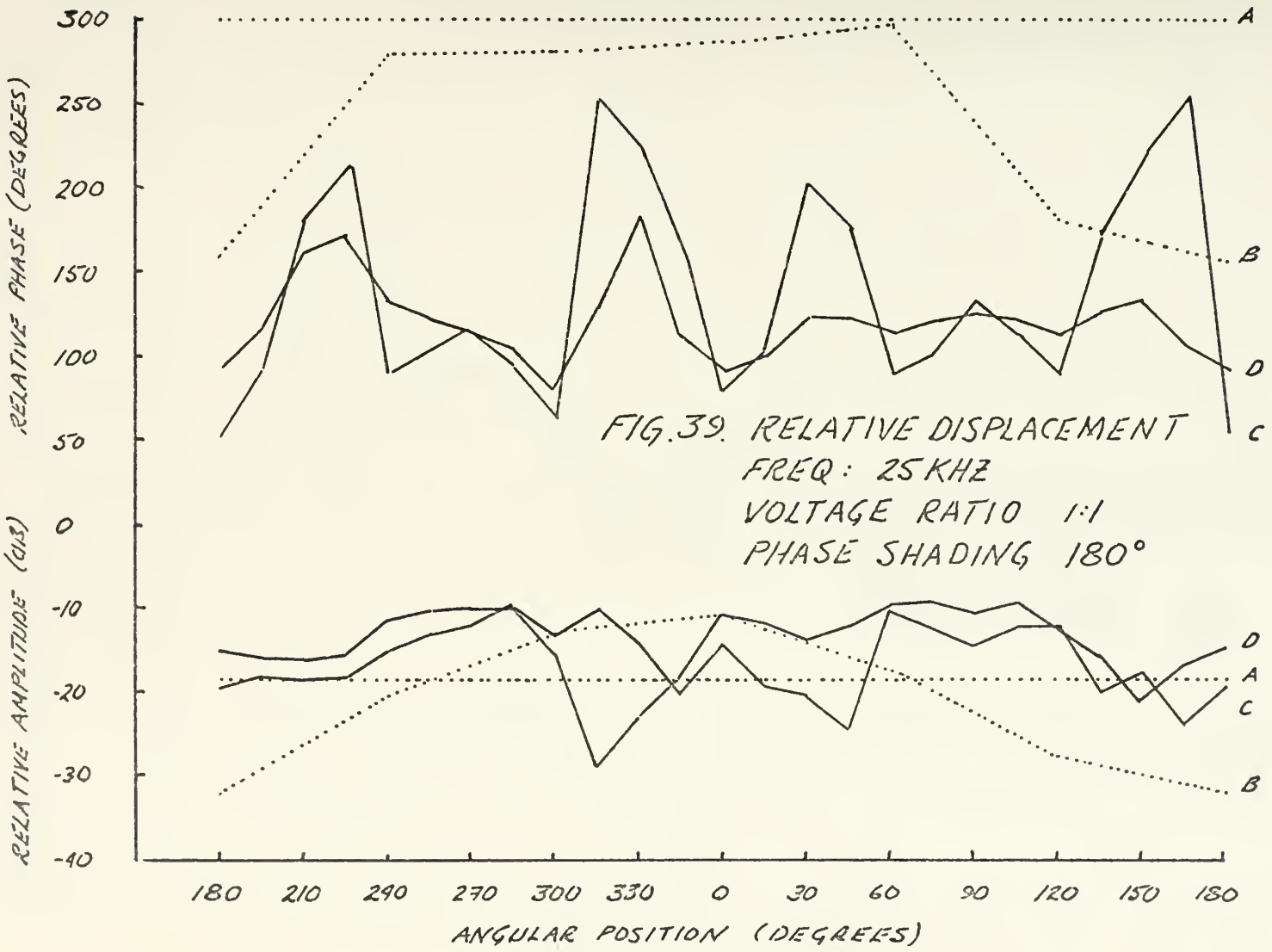

FIG. 39. RELATIVE DISPLACEMENT
FREQ: 25 KHZ
VOLTAGE RATIO 1:1
PHASE SHADING 180°

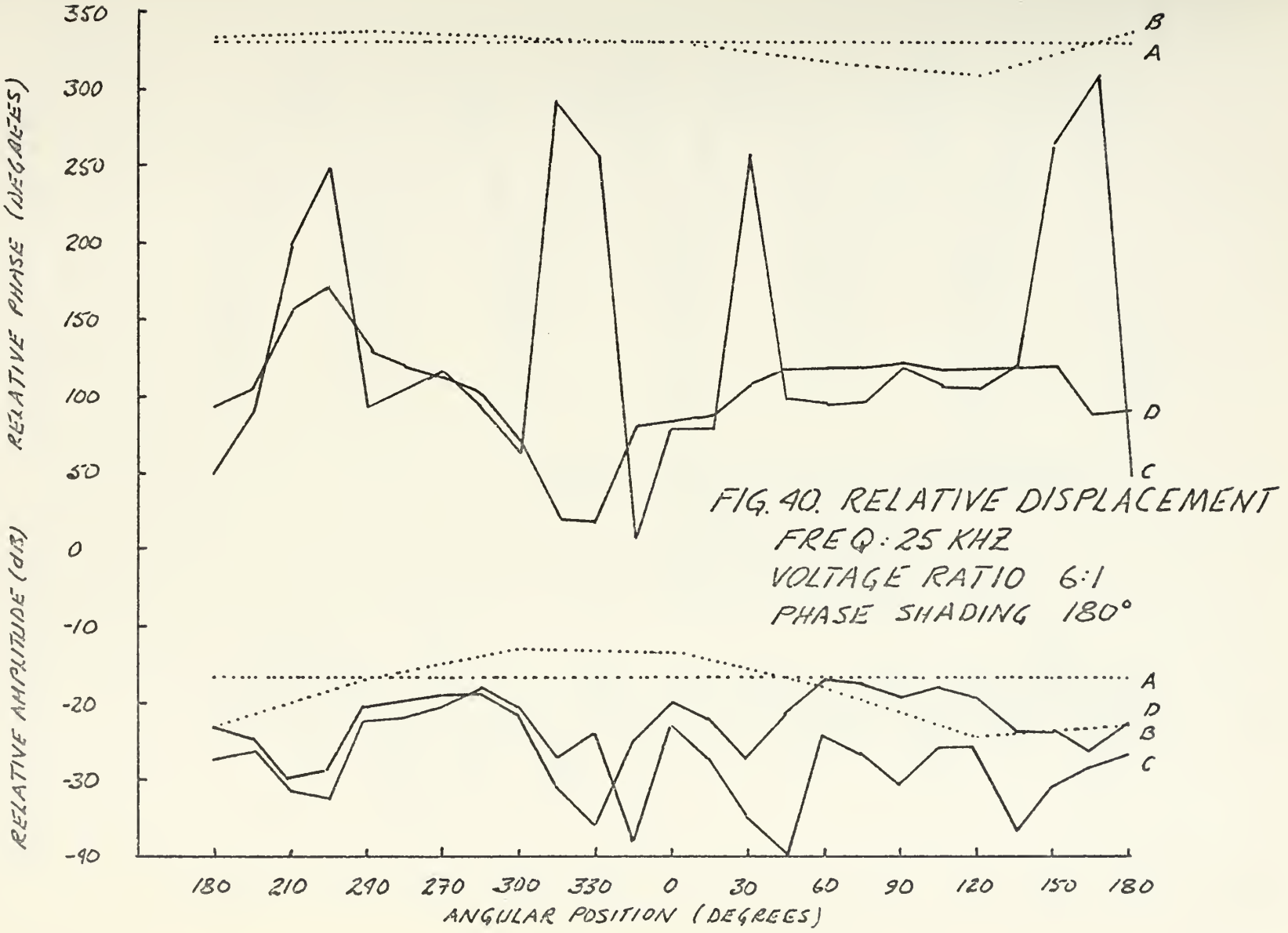

FIG. 40. RELATIVE DISPLACEMENT
FREQ: 25 KHZ
VOLTAGE RATIO 6:1
PHASE SHADING 180°

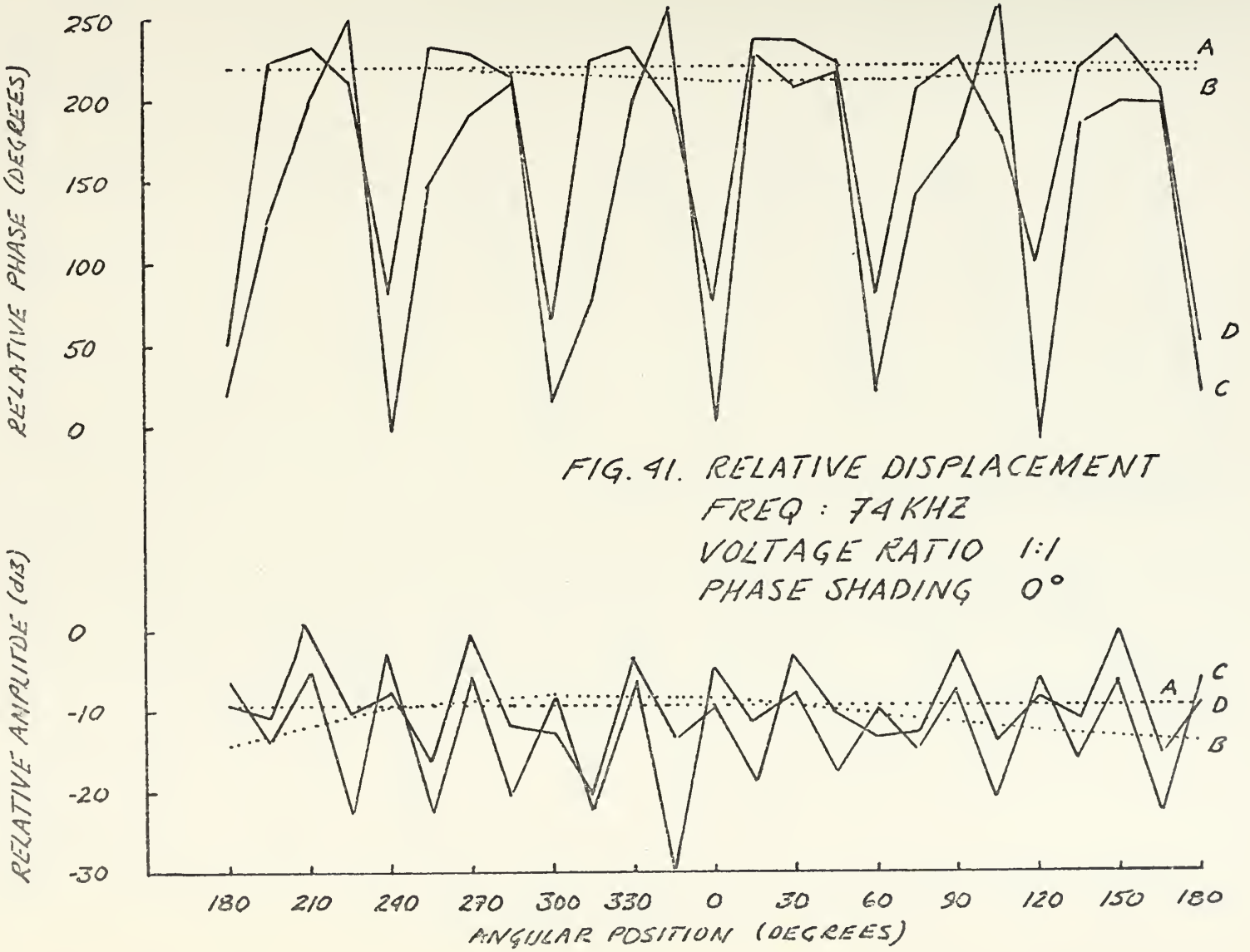

FIG. 41. RELATIVE DISPLACEMENT
FREQ : 74 KHZ
VOLTAGE RATIO 1:1
PHASE SHADING 0°

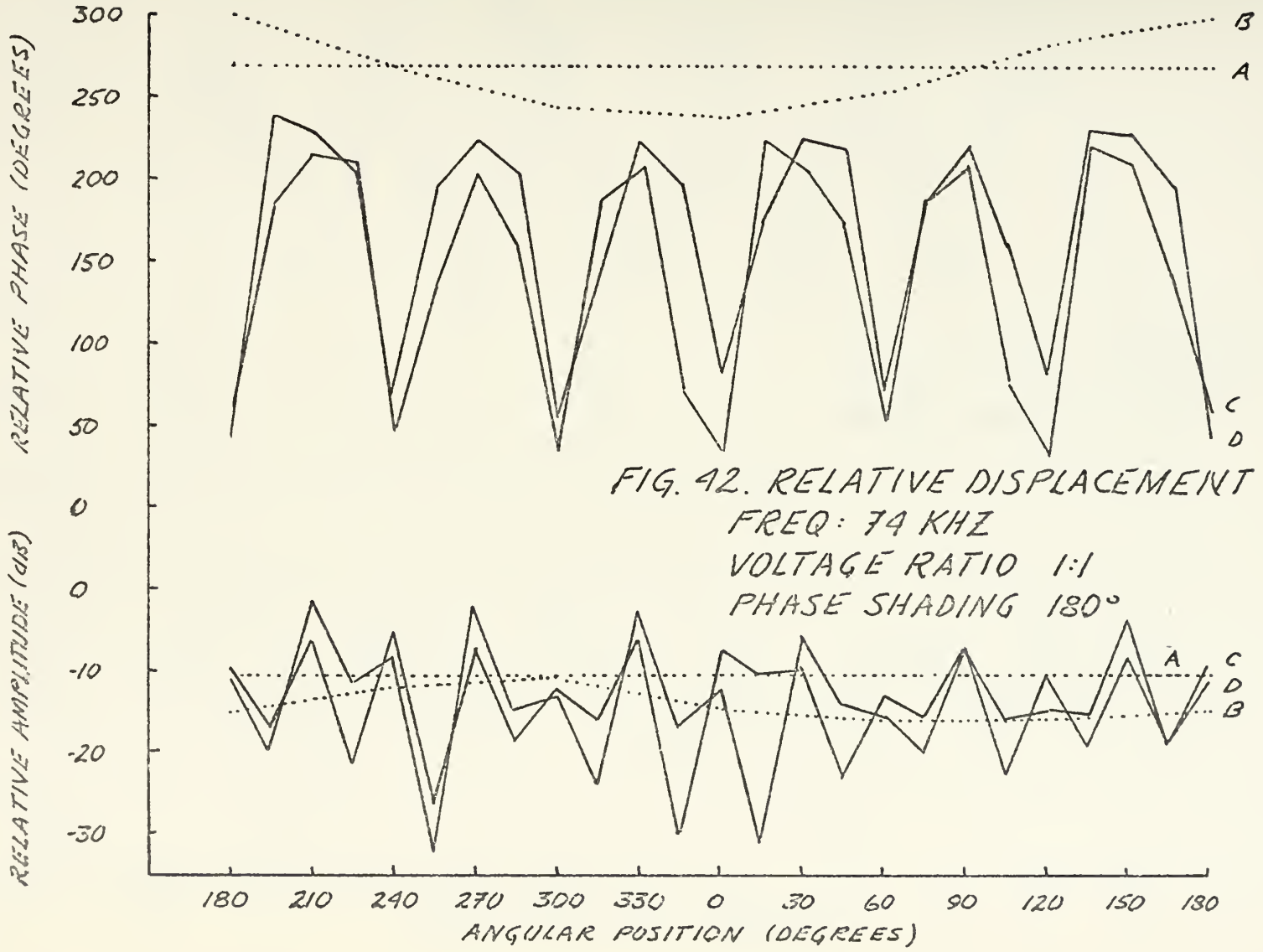

FIG. 42. RELATIVE DISPLACEMENT
FREQ: 74 KHZ
VOLTAGE RATIO 1:1
PHASE SHADING 180°

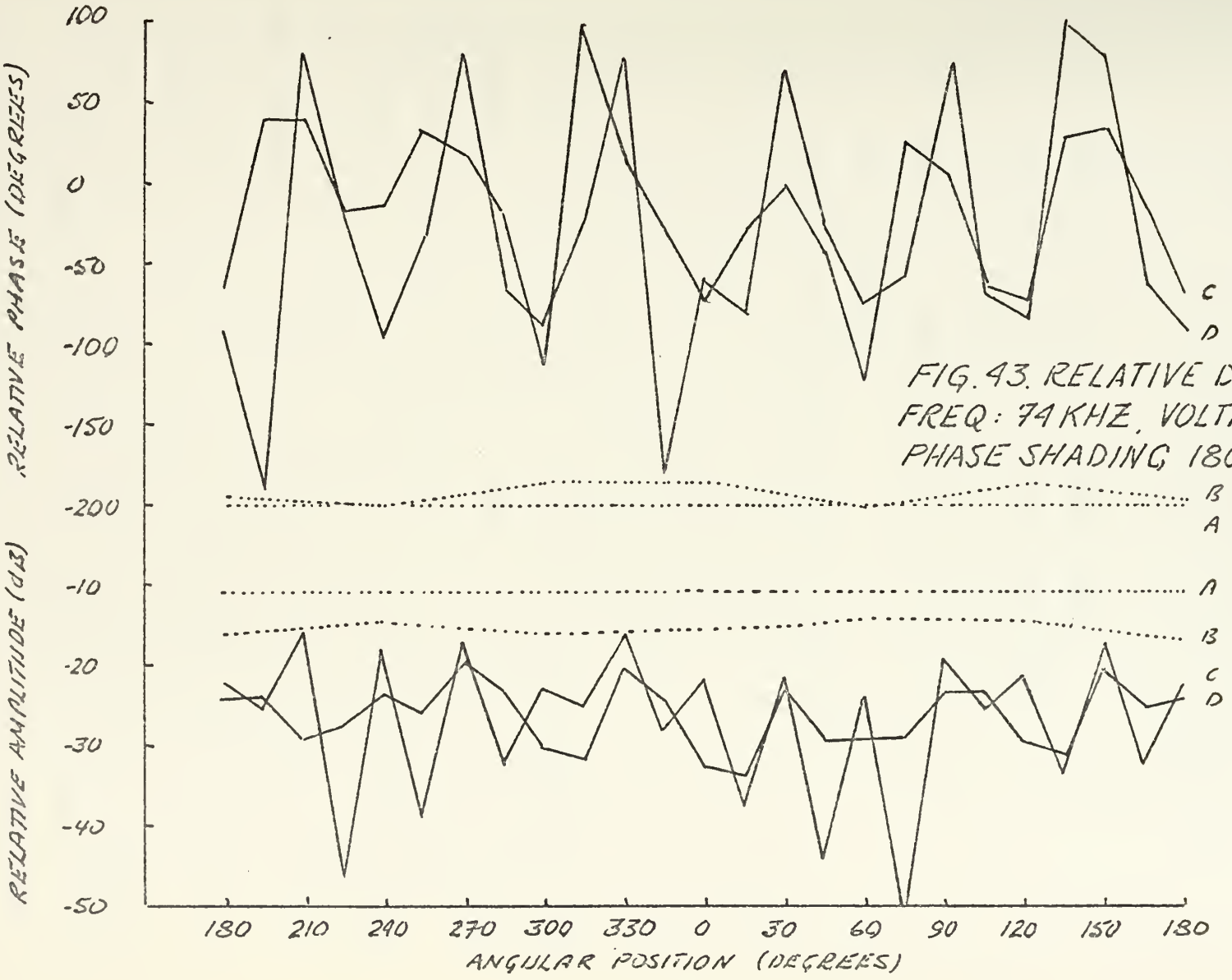

FIG. 43. RELATIVE DISPLACEMENT
FREQ: 74 KHZ, VOLTAGE RATIO 6:1
PHASE SHADING 180°

Utilizing the following items of test equipment the experiment was set up as shown in Fig. 44.

Hewlett Packard 204C Oscillator

General Radio 1192B Frequency Counter

General Radio Type 1396A Tone Burst Generator

40 dB Gate

Harrison 6205B D.C. Power Supply

Hewlett Packard 467A Power Amplifier

Krohn Hite DCA 50R Power Amplifier

Tektronix RM45A Oscilloscope (Dual Trace)

LC5 Hydrophone

Hewlett Packard 465A Voltage Amplifier

Krohn Hite 3202R Band Pass Filter

Dranetz Phase Meter Series 305

Hewlett Packard 120B Oscilloscope

Hewlett Packard 403B Voltmeter

Since the phase meter responded to only continuous wave excitation, data taking was limited to this mode. Relative phase and amplitude were obtained at points one cm apart a distance of 0.5 cm from the face of the transducer along the horizontal diameter. The transducer face was directed away from the air-water surface in order to reduce effects of surface reflections. For various amplitude and phase shadings the results obtained at 74 kHz and 25 kHz are shown in Figs. 45 through 50 and are summarized in Table IV.

The results showed good axial symmetry at least across the principal horizontal diameter. At 74 kHz, although

TABLE IV

NEAR FIELD PRESSURE

Freq. (kHz)	Voltage Ratio	Phase Shading (Degrees)	Mean Amplitude Inner Ring re Outer Ring (dB)	Mean Phase Inner Ring re Outer Ring (Degrees)
25	1:1	0	+4	+90
25	1:1	180	+9	-90
25	3:1	180	+12	-200
75	1:1	0	0	0
75	1:1	180	0	+65
75	3:1	180	+9	-180

voltage amplitude shading led to similar pressure amplitude shadings, relative voltage phase shading did not produce the same mean pressure phase shading except at the higher voltage ratios. This result was similar to that noted for the displacement measurements in air. The increase in relative pressure amplitude of the center radiator at 25 kHz was attributed to constructive interference due to the approximate half wave length spacing between the centers of the radiating faces.

Using Crawford's program, the far field radiation pattern was produced for one set of data at 74 kHz. On the main lobe, the pattern agreed well with that obtained experimentally. Secondary lobe structure, however, agreed more closely with that also predicted by the author's program model. As this tended to cast some doubt on the validity of the measured radiation patterns, these were rerun. Both in pulsed and C.W. modes the patterns obtained were essentially identical with those measured earlier. An assumption of Crawford's model that the pressure be measured at a sufficient distance from the face of the transducer so that plane wave motion may be approximated was not entirely valid in this case. An additional condition that pressure amplitude be measured radially until the value dropped by 10 dB was not fully met. Failure to meet these criteria might explain the discrepancies. It is also feasible that radiation from the baffle was still a problem. In any subsequent work using the baffle, this possibility should be eliminated.

While the response of the aperture function to the electrical control was not completely linear, it was shown to be controllable. The near field pressure data confirm that the transducer can be manipulated to obtain a desired aperture function. This effectively validates the design concept used.

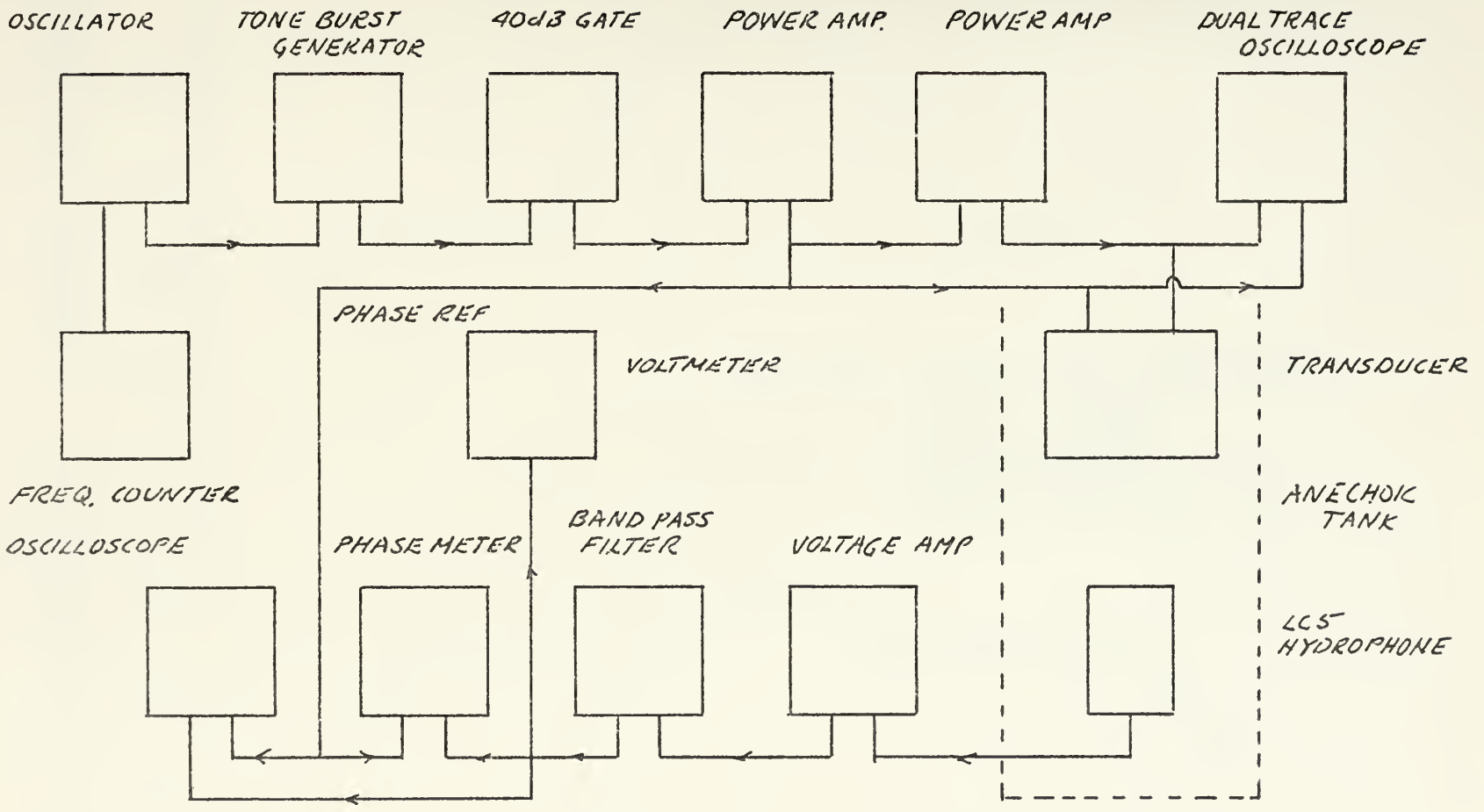

FIG. 44. NEAR FIELD PRESSURE MEASUREMENTS

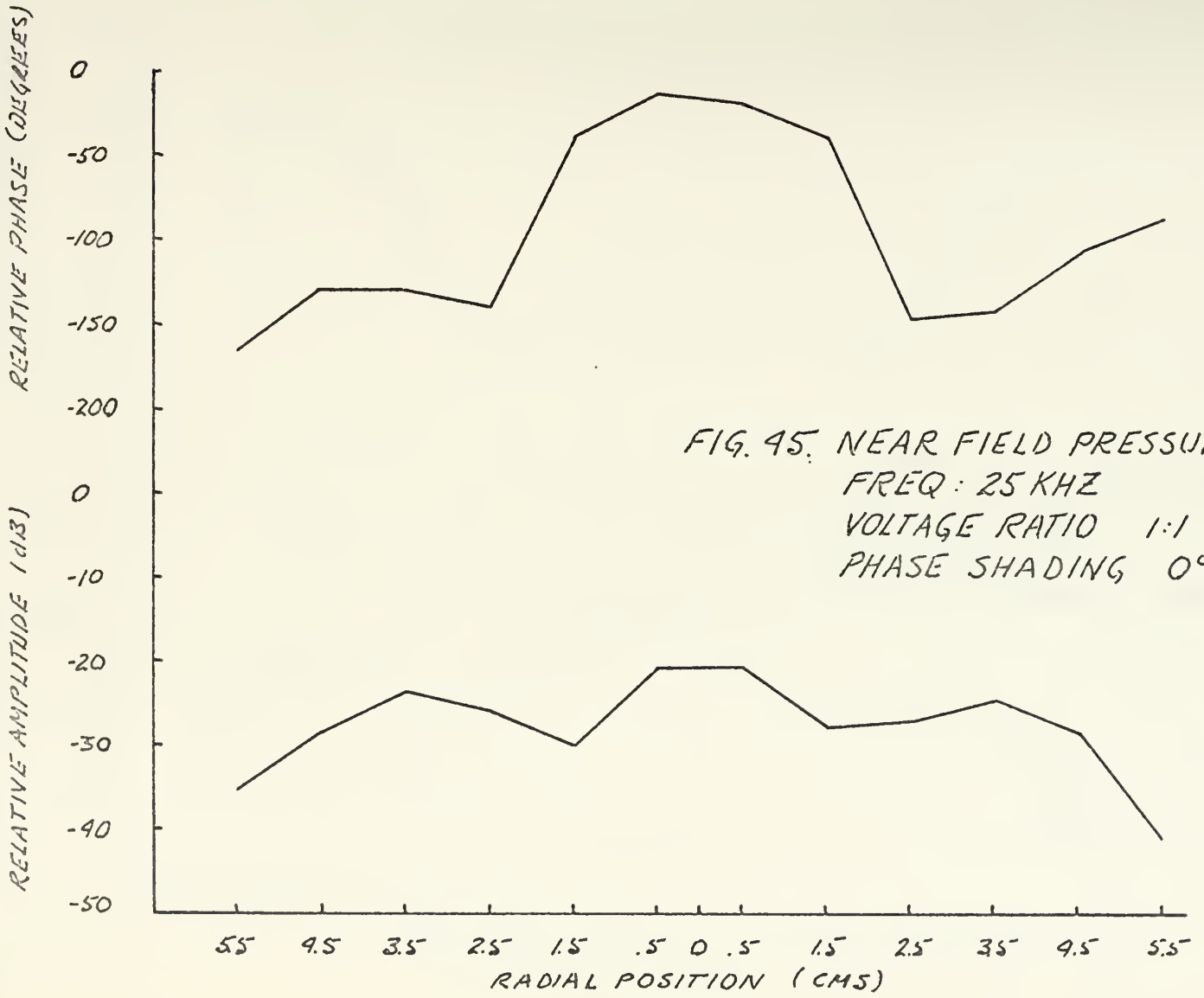

FIG. 45. NEAR FIELD PRESSURE
FREQ: 25 KHZ
VOLTAGE RATIO 1:1
PHASE SHADING 0°

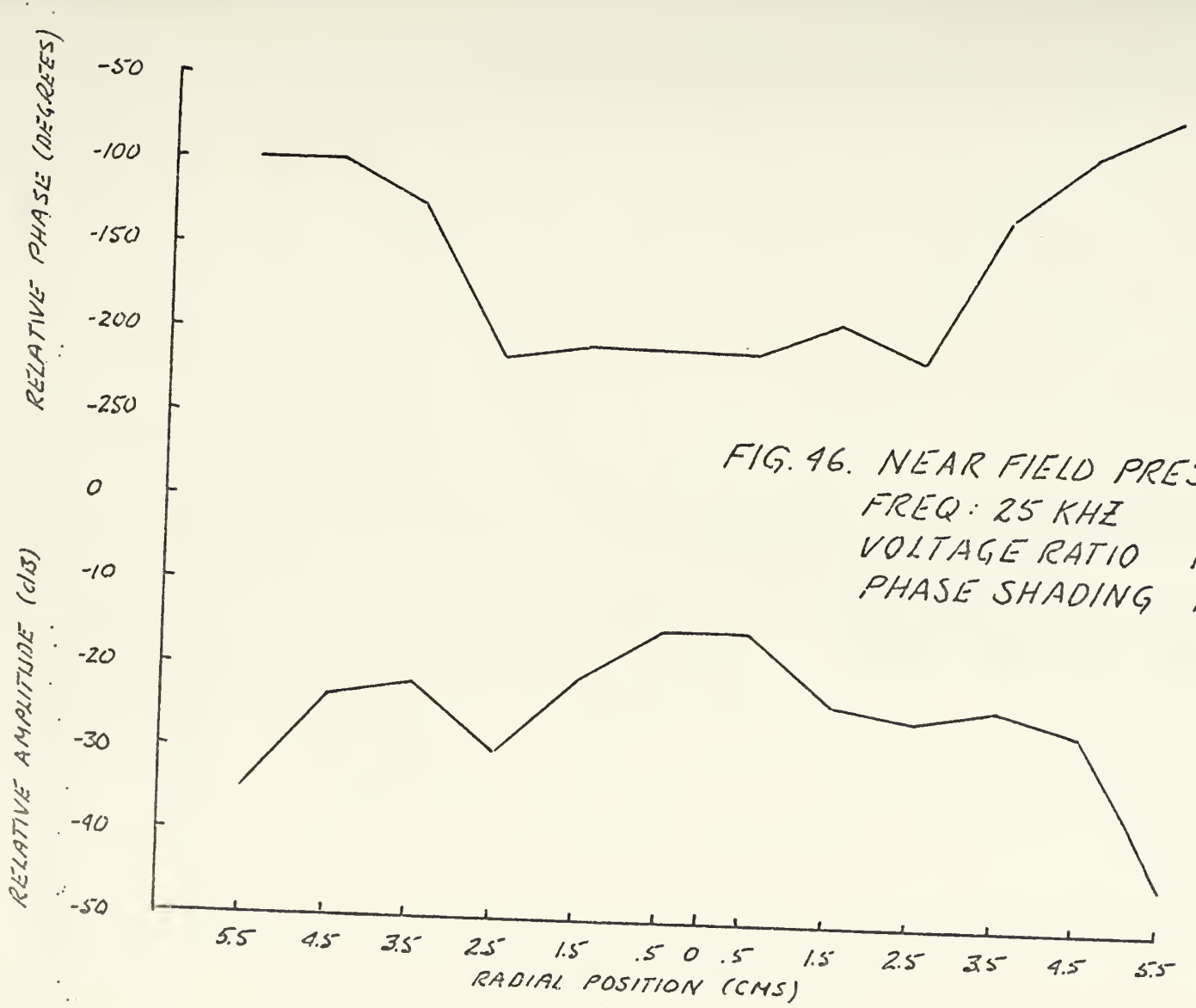

FIG. 46. NEAR FIELD PRESSURE
FREQ: 25 KHZ
VOLTAGE RATIO 1:1
PHASE SHADING 180°

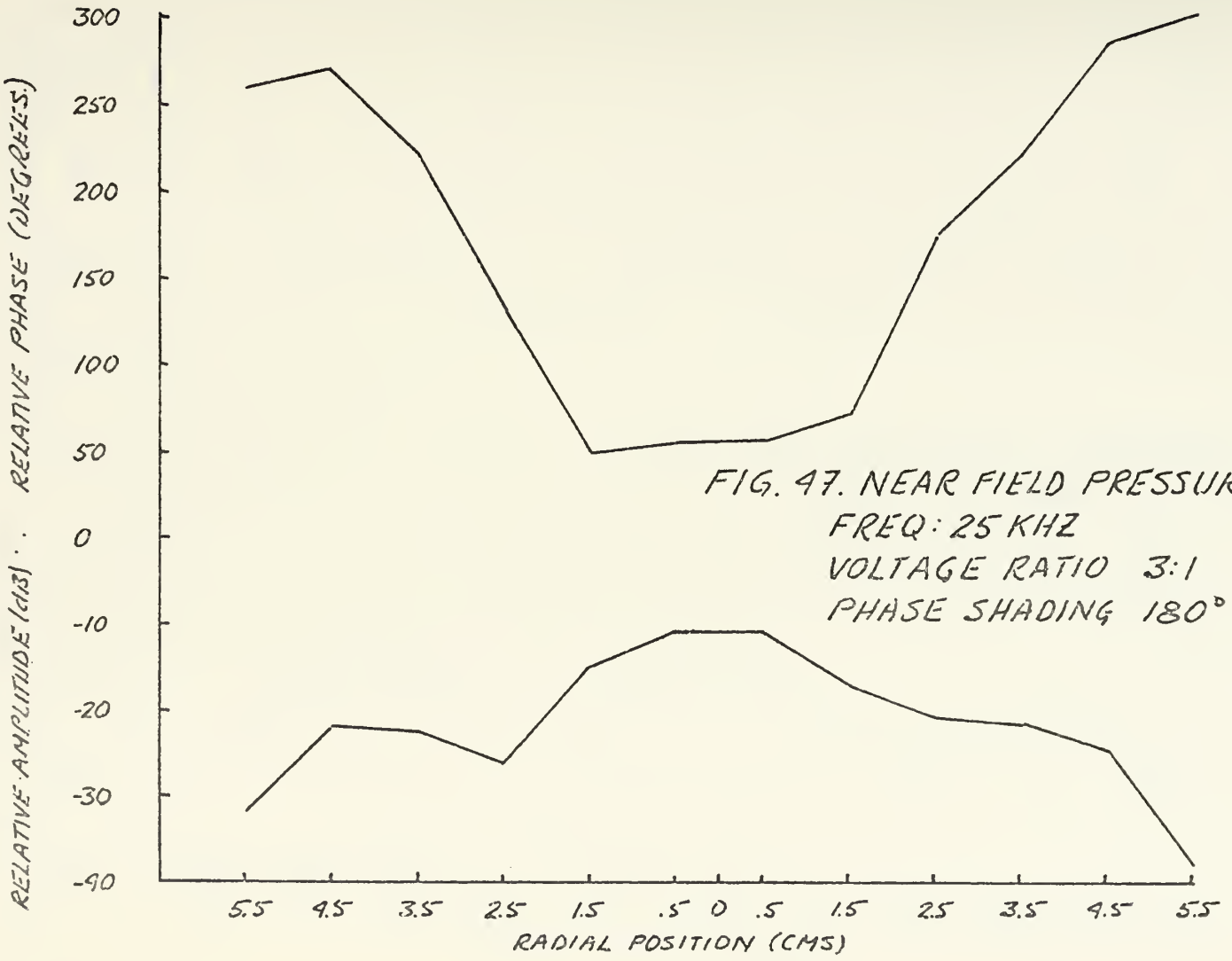

FIG. 47. NEAR FIELD PRESSURE
FREQ: 25 KHZ
VOLTAGE RATIO 3:1
PHASE SHADING 180°

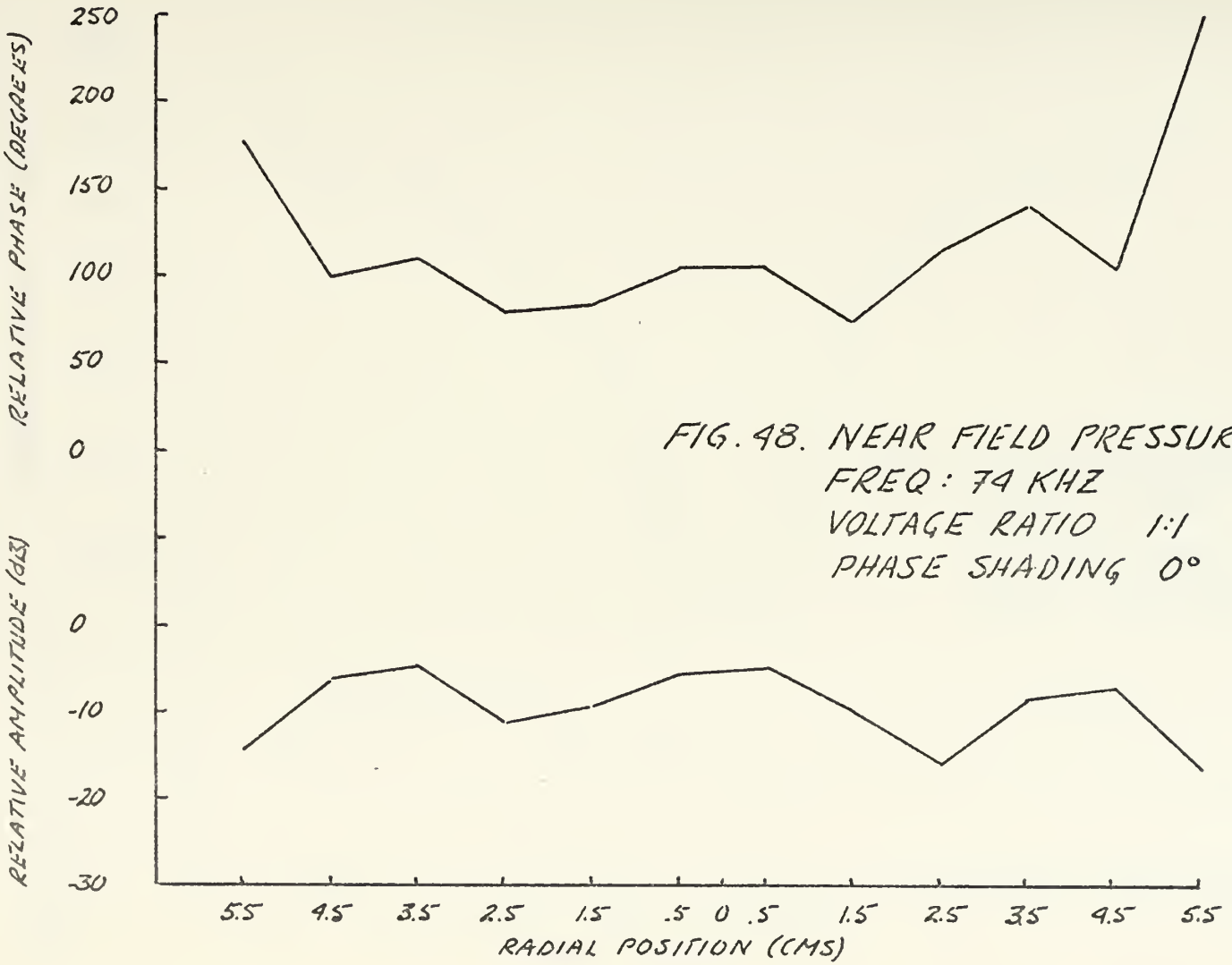

FIG. 48. NEAR FIELD PRESSURE
FREQ: 74 KHZ
VOLTAGE RATIO 1:1
PHASE SHADING 0°

FIG. 49. NEAR FIELD PRESSURE
FREQ : 74 KHZ
VOLTAGE RATIO 1:1
PHASE SHADING 180°

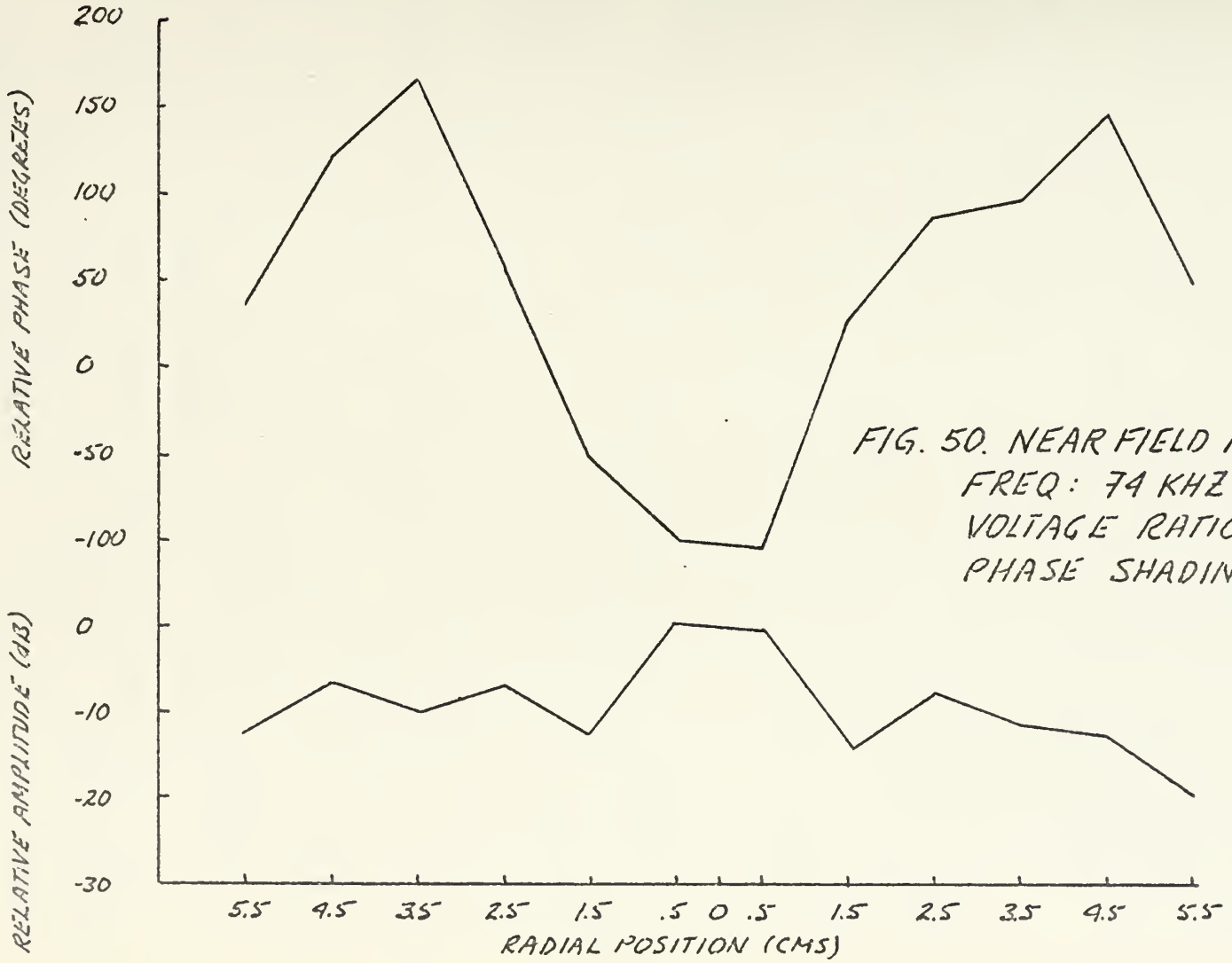

FIG. 50. NEAR FIELD PRESSURE
FREQ: 74 KHZ
VOLTAGE RATIO 3:1
PHASE SHADING 180°

V. CONCLUSIONS AND RECOMMENDATIONS

As a result of this investigation, it has been shown that the proposed approach to the design problem posed by the underwater acoustic ranges is a viable one. Simple phase and amplitude shading of a transducer constructed of two radiating elements, an inner circular piston and an outer concentric annulus, has been used to generate a desirable radiation pattern. At the scaled frequency of 25 kHz using 180° phase shading and amplitude shading of 3:1, a pattern with a 10 dB down beam width of 152° was obtained. This was achieved in spite of a non-optimum radiating face geometry.

Problems associated with the prototype transducer contributed to the failure of the program model to accurately predict fine scale details of the beam patterns obtained. It is likely that this was due in large part to the non-uniform motion of the radiating faces and the difficulty in obtaining a uniform phase shading. The non-uniform motion has been shown to be primarily a result of the strong coupling between the inner and outer radiating faces resulting from the use of a common backing place. The necessity of using a number of ceramic disks to drive the outer ring also contributed to the problems encountered. Baffle difficulties possibly further compounded the issue. The detrimental

effects of mutual radiation impedances could not be investigated and remain unknown.

Since the design approach appears to be promising, further developmental work is recommended. Several simple fixes suggest themselves to alleviate some of the problems of the prototype. It is suggested that in addition to being designed for 75 kHz operation, subsequent transducer designs incorporate the following modifications:

(1) For mechanical simplicity each radiating face should be driven by only one piezoelectric ceramic element.

(2) Commensurate with the power requirements, minimal radiating face areas should be used to minimize flexural motions, especially in the outer annulus.

(3) Each ceramic radiator element should be designed to operate independently in a half wave length longitudinal resonance mode. The use of a common backing plate should be avoided for experimental units.

(4) The use of a pressure release material such as "Sonite" to surround the non-radiating surfaces of the transducer elements should be investigated. Such a material could reduce coupling between elements of the transducer and, in addition, effectively decouple the transducer itself from the target vehicle.

(5) The use of variable phase shading of the input voltages should also be investigated. This should allow for optimum control of the near field pressure phase shading.

A transducer embodying these modifications should suffer fewer problems of the type so far encountered and should, hopefully, provide essentially predictable, in addition to controllable, radiation patterns.

```
C      DETERMINATION OF BEAM PATTERN FOR TWO CONCENTRIC TRANDUCERS
C      OF RADII RI AND RO WHERE RO.GT.RI
C      RCI IS INNER RADIUS OF OUTER RING
C
    1 READ(5,100,END=3)RI,ROI,RO
      WRITE(6,200)RI,ROI,RO
  100 FORMAT(3F10.5)
  200 FORMAT(//,2X,'RI=',2X,F10.5,2X,'ROI=',2X,F10.5,2X,'RO=',2X,F10.5)
      PI=3.14159
C
CC   CALC PROPAGATION CONSTANT FOR 74 KHZ
C
      PK=2.*PI*74000./1480.
      AKI=PK*RI
      AKOI=PK*ROI
      AKO=PK*RO
C
CCC   CALC AXIS PRESSURE
C
      PTZI=RI**2
      PTZOI=ROI**2
      PTZO=RO**2
      PTZ=ABS(PTZO-PTZOI+PTZI)
      WRITE(6,300)PTZ
      WRITE(6,500)
  300 FORMAT(//,2X,'AXIS PRESSURE',2X,E12.5)
  500 FORMAT(//,3X,'ANGLE',10X,'PRESSURE',14X,'DECIBEL')
C
CCC   CALC PRESSURES FROM AXIS TO 90 DEGREES
C
      DO 2 I=1,90
      AI=I
      TH=AI/57.29578
      ARGO=PK*RO*SIN(TH)
      CALL BESJ(ARGO,1,BJ,.1,IER)
      TERMO=PTZO*(2.*BJ/ARGO)
      ARGOI=PK*ROI*SIN(TH)
      CALL BESJ(ARGOI,1,BJ,.1,IER)
      TERMOI=PTZOI*(2.*BJ/ARGOI)
      ARGI=PK*RI*SIN(TH)
      CALL BESJ(ARGI,1,BJ,.1,IER)
      TERMI=PTZI*(2.*BJ/ARGI)
      PTI=TERMO-TERMOI+TERMI
      PDB=20.*ALOG10(ABS(PTI/PTZ))
      WRITE(6,400)I,PTI,PDB
  400 FORMAT(4X,I3,8X,E12.5,8X,F10.2)
    2 CONTINUE
      GO TO 1
```

```
      3 STOP
        END
C
C       SUBROUTINE BESJ                                                      3
C                                                                            4
C       PURPOSE                                                              5
C          COMPUTE THE J BESSEL FUNCTION FOR A GIVEN ARGUMENT AND ORDER      6
C                                                                            7
C       USAGE                                                                8
C          CALL BESJ(X,N,BJ,D,IER)                                           9
C                                                                           10
C       DESCRIPTION OF PARAMETERS                                           11
C          X   -THE ARGUMENT OF THE J BESSEL FUNCTION DESIRED               12
C          N   -THE ORDER OF THE J BESSEL FUNCTION DESIRED                  13
C          BJ  -THE RESULTANT J BESSEL FUNCTION                             14
C          D   -REQUIRED ACCURACY                                           15
C          IER-RESULTANT ERROR CODE WHERE                                   16
C              IER=0  NO ERROR                                              17
C              IER=1  N IS NEGATIVE                                         18
C              IER=2  X IS NEGATIVE OR ZERO                                 19
C              IER=3  REQUIRED ACCURACY NOT OBTAINED                        20
C              IER=4  RANGE OF N COMPARED TO X NOT CORRECT (SEE REMARKS)    21
C                                                                           22
C       REMARKS                                                             23
C          N MUST BE GREATER THAN OR EQUAL TO ZERO, BUT IT MUST BE           24
C          LESS THAN                                                        25
C             20+10*X-X** 2/3    FOR X LESS THAN OR EQUAL TO 15             26
C             90+X/2             FOR X GREATER THAN 15                      27
C                                                                           28
C       SUBROUTINES AND FUNCTION SUBPROGRAMS REQUIRED                       29
C          NONE                                                             30
C                                                                           31
C       METHOD                                                              32
C          RECURRENCE RELATION TECHNIQUE DESCRIBED BY H. GOLDSTEIN AND      33
C          R.M. THALER,'RECURRENCE TECHNIQUES FOR THE CALCULATION OF        34
C          BESSEL FUNCTIONS',M.T.A.C.,V.13,PP.102-108 AND I.A. STEGUN       35
C          AND M. ABRAMOWITZ,'GENERATION OF BESSEL FUNCTIONS ON HIGH        36
C          SPEED COMPUTERS',M.T.A.C.,V.11,1957,PP.255-257                   37
C                                                                           38
C  ..........................................................               39
C                                                                           40
      SUBROUTINE BESJ (X,N,BJ,D,IER)                                        41
C                                                                           42
      BJ = .0                                                               43
      IF (N) 1,2,2                                                          44
    1 IER = 1                                                               45
      RETURN                                                                46
    2 IF (X) 3,3,4                                                          47
```

```
      3 IER = 2                                                          48
        RETURN                                                           49
      4 IF (X-15.) 5,5,6                                                 50
      5 NTEST = 20.+10.*X-X**2/3                                         51
        GO TO 7                                                          52
      6 NTEST = 90.+X/2.                                                 53
      7 IF (N-NTEST) 9,8,8                                               54
      8 IER = 4                                                          55
        RETURN                                                           56
      9 IER = 0                                                          57
        N1 = N+1                                                         58
        BPREV = .0                                                       59
C                                                                        60
CC      COMPUTE STARTING VALUE OF M                                      61
C                                                                        62
        IF (X-5.) 10,11,11                                               63
     10 MA = X+6.                                                        64
        GO TO 12                                                         65
     11 MA = 1.4*X+60./X                                                 66
     12 MB = N+IFIX(X)/4+2                                               67
        MZERO = MAX0(MA,MB)                                              68
C                                                                        69
CC      SET UPPER LIMIT OF M                                             70
C                                                                        71
        MMAX = NTEST                                                     72
C                                                                        73
        DO 21 M=MZERO,MMAX,3                                             74
C                                                                        75
CC      SET F(M),F(M-1)                                                  76
C                                                                        77
        FM1 = 1.0E-28                                                    78
        FM = .0                                                          79
        ALPHA = .0                                                       80
        IF (M-(M/2)*2) 14,13,14                                          81
     13 JT = -1                                                          82
        GO TO 15                                                         83
     14 JT = 1                                                           84
     15 M2 = M-2                                                         85
C                                                                        86
        DO 18 K=1,M2                                                     87
        MK = M-K                                                         88
        BMK = 2.*FLOAT(MK)*FM1/X-FM                                      89
        FM = FM1                                                         90
        FM1 = BMK                                                        91
        IF (MK-N-1) 17,16,17                                             92
     16 BJ = BMK                                                         93
     17 JT = -JT                                                         94
        S = 1+JT                                                         95
```

```
   18 ALPHA = ALPHA+BMK*S                                                96
C                                                                        97
      BMK = 2.*FM1/X-FM                                                  98
      IF (N) 20,19,20                                                    99
   19 BJ = BMK                                                          100
   20 ALPHA = ALPHA+BMK                                                 101
      BJ = BJ/ALPHA                                                     102
      IF (ABS(BJ-BPREV)-ABS(D*BJ)) 22,22,21                             103
   21 BPREV = BJ                                                        104
C                                                                       105
      IER = 3                                                           106
   22 RETURN                                                            107
      END                                                               108
```

LIST OF REFERENCES

1. Kinsler, L. E. and Frey, A. R., Fundamentals of Acoustics, 2d ed., John Wiley and Sons, 1962.

2. Bracewell, R., The Fourier Transform and its Applications, McGraw Hill, 1965.

3. Johnson, R. R., Models for Computing the Directional Radiation of Sound from Sources on a Rigid Cylindrical Baffle, M.Sc. Thesis, Naval Postgraduate School, Monterey, California, 1974.

4. Shattuck, R. A., "Capacitive-Type Displacement Probe," Journal of the Acoustical Society of America, v. 31(10), p. 1297-1299.

5. Crawford, F. R., Submarine Radiated Noise Far-Field Beam Patterns for Discrete Frequencies from Near-Field Measurements, M.Sc. Thesis, Naval Postgraduate School, Monterey, California, 1975.

INITIAL DISTRIBUTION LIST

		No. Copies
1.	Defense Documentation Center Cameron Station Alexandria, Virginia 22314	2
2.	Library, Code 0212 Naval Postgraduate School Monterey, California 93940	2
3.	Department Chairman, Code 61 Department of Physics and Chemistry Naval Postgraduate School Monterey, California 93940	1
4.	Professor O. B. Wilson, Code 61 W1 Department of Physics and Chemistry Naval Postgraduate School Monterey, California 93940	5
5.	Department Library, Code 61 Department of Physics and Chemistry Naval Postgraduate School Monterey, California 93940	1
6.	Professor G. L. Sackman, Code 52 Sa Department of Electrical Engineering Naval Postgraduate School Monterey, California 93940	1
7.	Dr. W. A. Middleton, Code 7002 Naval Torpedo Station Keyport, Washington 98345	1
8.	Director, Maritime Combat Systems National Defence Headquarters Ottawa, KIA OK2, Canada	2
9.	LCDR A. H. P. Shaw, Canadian Forces 1702 Amberdale Cres. Ottawa, KIH 7B3, Canada	1

103516

Thesis
S43722 Shaw
c.1

Radiation pattern shaping of a two-element, concentric ring transducer using phase and amplitude shading.